博士論文

Numerical Simulation of Failure of RC Beam-Column Joint by 3D RBSM

（三次元離散解析手法による鉄筋コンクリート柱梁接合部の破壊シミュレーション）

リャント　エディ

Liyanto Eddy

A dissertation submitted to
University of Tokyo
In partial fulfillment on the requirements for
The Degree of Doctor Philosophy

Supervisor
Associate Professor Kohei Nagai

Department of Civil Engineering
University of Tokyo
Tokyo, Japan

August 2015

ABSTRACT

Because of the demand of the current specification, reinforcement congestion occurs in the beam column joint that causes difficulties during compaction and increases the construction time. As the result, poor quality of concrete is obtained. However, the specification of anchorages has not been changed for many years and was developed based on the simple arrangement of reinforcement bars so that there is a possibility to reduce the reinforcement congestion based on the mechanical behavior in the congested joint. Meanwhile, based on the experimental works, it is not easy to understand the behavior because complex cracks occur due to the complex arrangement of reinforcement bars and the loading history.

Meanwhile, mechanical anchorage can be one way to reduce the reinforcement congestion. However, the use of mechanical anchorages is still limited because the behavior has not been well understood. If the mechanical anchorages are placed near the surface of the beam column joint, anchorage failure occurs in the beam column joint. To avoid this failure, additional reinforcement should be placed along the anchorages. However, the best or rational way to strengthen this anchorage system has not been found yet because the internal condition has not been well understood. Many experiments were necessary. It is inefficient and takes time.

Simulation can be a beneficial tool to understand the behavior through the study of the internal stress and internal cracks. In this study, meso-scale analysis by 3D RBSM is proposed. The study by 3D meso-scale discrete analysis is useful since the reinforcement can be modeled in an accurate manner, i.e. ribs of a reinforcement bar and 3D shape of a reinforcement bar, local failure can be predicted precisely as the result of the discontinuous deformation of concrete and the interaction of concrete and the reinforcement at meso-scale level, and cracks can be simulated directly as the displacement between two elements. Based on the previous study, the simulation can simulate the local failure at the anchorages of beam column joints. However, the simulation system was not enough to simulate the beam column joint with complex arrangement of reinforcement bars, the meshing of a reinforcement bar was complex, and the constitutive models have not fixed yet.

In RBSM, a little attention to the mesh size is necessary. The mesh size of simulation models should be selected in an appropriate way to represent the real cracking pattern of

concrete. Since in the normal concrete, microcracks occur at the interface between the mortar and aggregate or at the mortar between two aggregates, 10x10x10 – 20x20x20 mm^3 of mesh size is selected to represent the real cracking pattern in the normal concrete that is determined by the aggregate size and location. Based on this selected mesh size, the constitutive models will be decided. For other types of concrete, different mesh size and constitutive models should be decided to represent the real cracking pattern.

In this study, the simulation system is developed by introducing a simple meshing of a reinforcement bar so that the computational time can be reduced. Furthermore, various shapes of reinforcement bars can be modeled, so that at this time the same model and reinforcement bars arrangement as the real condition can be modeled.

A unified constutive models of RBSM is proposed based on the simulations in the material scale. Simulations of concrete under uniaxial compressive and tensile loading, and biaxial compressive loading are conducted to upgrade the constitutive models. A bi-linear model is introduced for the tension softening of normal springs of concrete elements. A new failure criterion of concrete is introduced. Furthermore, strain hardening region is also introduced for the normal springs of steel elements. Parametric studies are conducted to investigate the effect of each constitutive model on the macroscale behavior of the material.

In order to investigate the applicability of RBSM in modeling bond between concrete and a reinforcement bar, simulations of tension stiffening model are conducted. Two numerical models having different yield strength of reinforcement are simulated. Based on the simulation results, as the load increases, cracks can propagate gradually because of the bond between concrete and the reinforcement bar. Furthemore, simulation results show a good agreement with the experimental results.

By using the well-developed simulation system, some achievements have been obtained. First, by this simulation system, it can be understood how the loading position and the local shape of the reinforcement affect the local cracks in the corbel because the local shape of the reinforcement is modeled directly. Furthermore, a simple method to repair the damage corbel can be proposed. Second, by the simulation system, it can be understood how complicated cracks occur in the beam column joint with complex arrangement of reinforcement bars since three dimensional shape of reinforcement bars

is modeled directly. And last, by the simulation system, it can be understood how each reinforcement bar contributes to the failure behavior of the beam column joint with the mechanical anchorages. Furthemore, a failure process of the beam column joint with the mechanical anchorages is proposed through the study of the internal stress and cracks of simulation results.

Some bearing pads of corbels were designed at the wrong position, at the edge of the corbel. Consequently, local failure, anchorage splitting failure occurs in the corbel because of this wrong detailing. This condition does not satisfy the specification code. By simulation, the cause of this local failure can be understood because the local shape of reinforcement bars is modeled directly. Different loading positions show different capacities. Local cracking in the edge causes the significant drop in capacity. By simulating the existing damage in the corbel, a simple method to repair the damage corbel can be proposed. Based on the simulation results, just by changing the loading position can be the simplest way to recover the capacity of the damage corbel. This kind of residucal capacity simulation can be conducted.

Based on the simulation of a beam column joint with complex arrangement of reinforcement bars, since the complex arrangement of reinforcement bars is modeled as the same as the experimental specimen, the same cracking pattern as the experimental specimen can be simulated. Cracks parallel to the bending portion of anchorages can be simulated due to a moment that tends to open the beam column joint, since the bending shape of the reinforcement bar is modeled directly. Compression strut occurs due to a moment that tends to close the beam column joint. Simulation results show the same tendency as the experimental results.

Based on the past researches of beam column joints with mechanical anchorages, since the internal stress condition and cracks have not been understood, many experiments were necessary to find a rational reinforcement arrangement in the beam column joint with mechanical anchorages. Based on experiments, there are two possible ways to strengthen this anchorage system, i.e. by placing stirrups along the anchorages, and by adding concrete block at the top surface of the beam column joint. Simulations are conducted based on the past experiments. Simulation results show the same tendency as experimental results. Furthemore, the surface cracks of numerical models are roughly the same as those of experimental specimens. Through the study of the internal stress and cracks of simulation results, the failure process of the beam column joint with

mechanical anchorages is proposed. First, bond works along the development length of anchorages. Second, diagonal cracks occur in the beam column joint. Third, cracks propagate to the surface of the beam column joint. Final Step is the opening of diagonal cracks. Furthermore, based on the simulation results, the meaning of stirrups along the development length has been understood, i.e. stirrups increase the bond performance along the development length of anchorages and restrict the opening of diagonal cracks. Meanwhile, the meaning of additional concrete block at the top surface of the beam column joint and reinforcement inside the concrete block is to increase the bond performance along the development length of anchorages and to restrict the crack penetration to the surface of the beam column joint.

ACKNOWLEDGEMENTS

First and foremost I wish to thank my advisor, Associate Professor Kohei NAGAI who with open arms received me as a member of Nagai Laboratory. I was privileged and fortunate to be under his supervision. I appreciate all his contributions of time, ideas, marvelous guidance, great motivation, and continuous support. This dissertation could not be completed without his motivation and support since the days I began working in Nagai Laboratory. I will always remember his encouragement to improve myself.

I would like to extend my gratitude to all my committee members, Professor Koichi MAEKAWA, Professor Muneo HORI, Professor Toshiharu KISHI, and Associate Professor Koichi KUSUNOKI for their willing participation to me amidst their busy schedules. This dissertation could not be completed without their all valuable comments, great advices in conducting researches.

I would extend my gratitude to Mr. IGUCHI, East Japan Railway Company, for his invitation during experiments of beam column joints in Japan Railway Research Center, Saitama, and thoughtful discussion for the beam column joint simulations. I would extend my gratitude to Dr. Yuya SAKAI and Dr. Koji MATSUMOTO for their thoughtful discussions and advices during the laboratory meetings. I like to extend gratitude also to my seniors, Mr. Daisuke HAYASHI and Mr. Koichiro Ikuta, who help me in understanding simulations, RBSM and FEM, and also for their willing discussions amidst their busy schedules. I believe these two brilliant men are the key of this study.

I would thank also to my tutor, Mr. Yoshiyuki Takano, who is the first nice and kind person that I met when I first arrived in Japan. Adaptation and living in Japan became easier by his guidance. I extend a word to thanks to current and former Nagai and Kishi Laboratory members: Mr. Hayato IKOMA, Mr. VU Viet Hung, Mr. Masato SHIMURA, Mr. Shunya KIMURA, Mr. Ram Chandra NEUPANE, Mr. Umair BAIG, Mr. Mato KOIKE, Ms. Rieko KOJIMA, Ms. Mari NAKASHIMA, Mr. Muzafalu KAYONDO, Mr. Tomohisa KAMADA, Ms. Tarakegne BIRUKTAWIT Taye, Mr. Shigeki YAMAZAKI, Mr. Tao WANG, Mr. Punyawut JIRADILOK, and Mr. Hirofumi YAMAGUCHI.

Lastly but not least, I would thank to my parents, sister, and brother for their encouragement support and attention.

TABLE OF CONTENTS

LIST OF FIGURES

Chapter One

Chapter Two

Chapter Three

Chapter Four

Chapter Five

Chapter Six

Chapter Seven

Chapter Eight

Appendix A

LIST OF TABLES

Chapter One

INTRODUCTION

1.1 BACKGROUND AND PROBLEM STATEMENT

The Japanese seismic design code is gradually becoming more stringent. Satisfying the latest demands of the code means placing a large amount of reinforcement which results in reinforcement congestion. Such congestion is a particular problem in beam column joints, where reinforcement bars from many directions come together. As the space between reinforcement bars becomes smaller, it becomes difficult to ensure proper compaction of concrete and adequate anchoring of reinforcement (**Fig.1.1**). One of the reasons for the reinforcement congestion is that the design specification detailing the reinforcement does not specify anchorage performance in consideration of the precise of the multidirectional reinforcement arrangement. Furthermore, the design specifications (JSCE 2007 and ACI 318-11) were developed based on the simple arrangement of reinforcement bars and have not been changed for many years (**Fig.1.2**). The behaviors of anchorages in a congested beam column joint have not been studied. The reduction of reinforcement congestion is possible based on the mechanical behavior. However, based on the experimental works done by Japan Railway (2012), the behaviors of beam column joint with multidirectional reinforcement arrangement are not easy to be understood because complex cracks occur depending on reinforcement arrangement and loading history (**Fig.1.3**).

Meanwhile, mechanical anchorage can be one way to reduce the reinforcement congestion in the beam column joint by introducing simpler detail of anchorages and shorter length of anchorages, compared with conventional 90 or 180 degree hooked bars (**Fig.1.4**). However, the use of mechanical anchorages is still limited in the concrete

Fig. 1.1 Reinforcement congestion at beam column joint

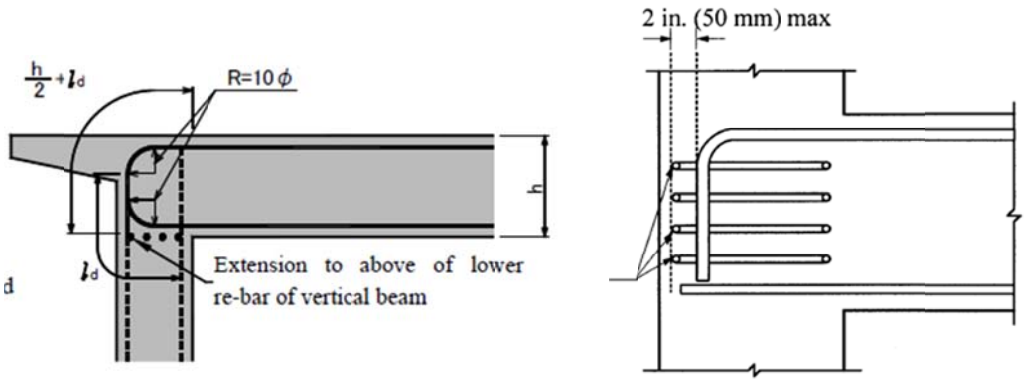

(a) JSCE specification of beam anchorages **(b)** ACI specification of beam anchorages

Fig. 1.2 Design specification detailing reinforcement

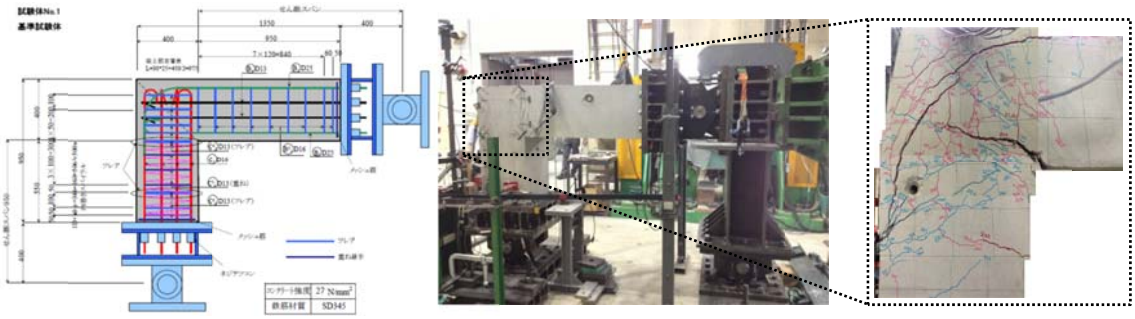

Fig. 1.3 Experiment of beam column joint with complex arrangement of reinforcement bars (Japan Railway 2012)

members with thin concrete cover (JSCE 2007) because the bond performance and the stress transfer between concrete and reinforcement bars have not been well understood.

When this new technology is applied, just by changing from the conventional 90 or 180 degree hooked bars to the mechanical anchorages, the reinforcement arrangement becomes simpler, but local failure occurs in the beam column joint due to the local stresses from the anchorage plates, that cause brittle failure (**Fig.1.5.a)**. To avoid this condition, additional local reinforcement bars, i.e. stirrups, should be placed along the anchorages (**Fig.1.5.b**). Many experiments of beam column joints with mechanical anchorages were necessary to be conducted in order to study the potential of using mechanical anchorages in a beam column joint, the behaviors of mechanical anchorages,

Fig. 1.4 Mechanical anchorage

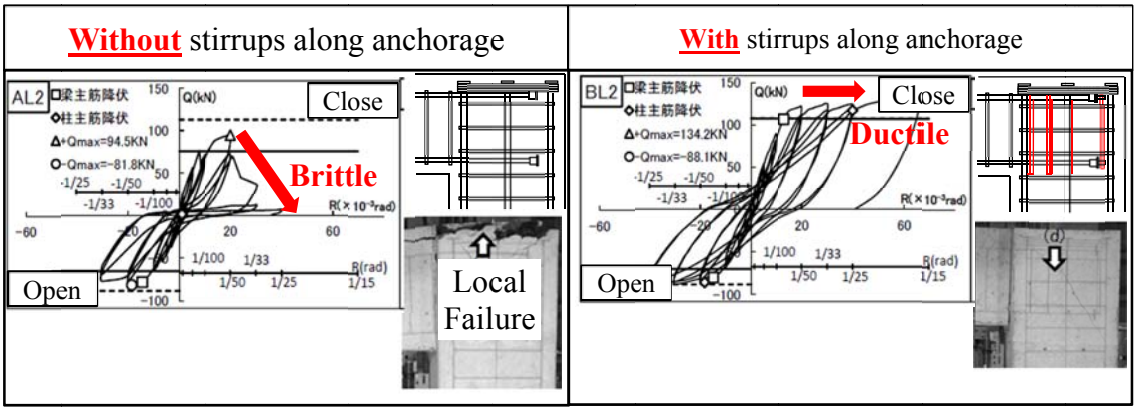

(a) Without stirrups (b) With stirrups

Fig. 1.5 Experiments of beam column joint with mechanical anchorages (Yoshimura *et al.* 2012)

and to make the reinforcement arrangement in the beam column joint with mechanical anchorages as simple as possible (Wallace *et al.* 1998, Chen *et al.* 2007, Kato *et al.* 2011, and Yoshimura *et al.* 2012).

Wallace *et al.* (1998) conducted experiment tests of beam column joints in order to investigate the potential of using mechanical anchorages as the anchorage system in exterior and corner beam column joints. Two exterior joint specimens and five corner joint specimens were investigated in this study through the comparison between conventional bending anchorages and mechanical anchorages. They concluded that through the experimental studies, the use of headed reinforcement in place of standard hooks within exterior or corner beam column joints is a viable option. However, additional transverse reinforcement is required to ensure that the heads are adequately restrained and additional studies are needed to identify how much concrete cover is needed as the replacement of the additional transverse reinforcement bars in case of corner beam column joints.

Chun *et al.* (2007) conducted further studies to investigate the influence of some parameters, i.e. the anchorage type, the size and arrangement of the beam bars and the heads, and the detailing provided for the roof joints. A total of 14 specimens of exterior and corner joint specimens were tested under cyclic loading. First conclusion of their studies is that locating the heads of the column reinforcement bars above the location of top flexural reinforcement bars of beam leads to the improvement of load-displacement relationship because of the confinement provided by an additional horizontal layer of transverse reinforcement. Furthermore, they also concluded that U-shape bars were effective to restrain the bar.

In Japan, Yokohama National University conducted extensive investigations on the performance of mechanical anchorage in exterior and corner beam column joints. Kato *et al.* (2011) carried out experimental investigations on eight corner joint specimens, i.e. one specimen of corner joint with conventional bending anchorages and seven specimens of corner joints with mechanical anchorages. Seven specimens of corner joints with mechanical anchorages consist of four specimens with additional concrete block at the top surface of the beam column joint and three specimens in which the tails of the conventional bending anchorages were replaced with the mechanical anchorages. Just by replacing the tails of the conventional bending anchorages with mechanical anchorages caused brittle failure in the beam column joints. Meanwhile, a good performance was obtained if additional concrete block was placed at the top surface of beam column joints with mechanical anchorages.

Yoshimura *et al.* (2012) carried out experimental investigations on six corner joint specimens in order to find the rational method or the best way to strengthen corner joint with mechanical anchorages. The same result as the previous researches was obtained that additional transverse reinforcement should be placed along the anchorages.

However, since the internal stress condition, the internal cracking pattern, and the meaning of each reinforcement bar to the cracking patterns have not been well understood, a rational method to strengthen the mechanical anchorage system has not been obtained, so that numerical simulation can be a beneficial tool to reveal the internal conditions. Over the past few decades, the Finite Element Analysis (FEA) has been known as the powerful simulation method not only in civil engineering but also in other disciplines. Simulations of beam-column connections by Finite Element Analysis have been started since 2000 which were conducted by Baglin *et al.* (2000).

Baglin *et al.* (2000) used SBETA, a nonlinear finite element analysis that was developed for the analysis of reinforced concrete structures under plane stress conditions in order to investigate the applicability of finite element analysis in modeling reinforced concrete beam-column connections. Reinforcement bars were modeled as line elements, called discrete bars, where an element representing the discrete bar is constraint at the boundary of the concrete element. A total of 19 simulations were conducted. The simulation results showed the same tendency as the experimental results and global failure could be predicted. However, the simulations were limited in 2D analysis so that cracks propagated in lateral direction could not be simulated. Furthermore, they

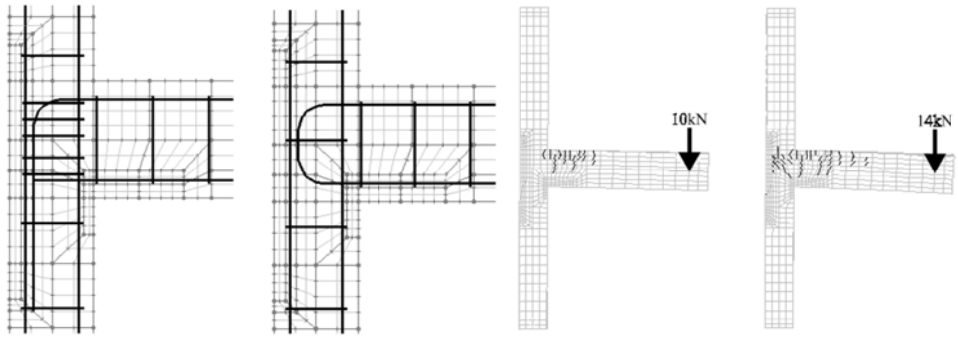

Fig. 1.6 Finite element model and crack propagations of simulation results (Baglin *et al.* 2000)

concluded that "modeling of the deformation due to crack growth and dislocation was inhibited by the smeared crack approach" (**Fig. 1.6**).

Hegger *et al.* (2004) used ATENA, a nonlinear finite analysis that also was developed for the analysis of reinforced concrete structures under plane stress condition in order to examine the effects of different parameters on the behavior and strength of beam column joints. 10 x 10 mm of element size was used for modeling the beam column joints and a coarser mesh was used for modeling the beams and the columns. Reinforcement bars were also modeled as discrete bar model in which full bond was assumed between the reinforcement bar and the concrete. A total of 15 simulations of exterior beam column joints and interior beam column joints were simulated. The simulation results showed that there is a good agreement of load-deflection curves with experimental results, but the simulations were limited in 2D analysis and local failures were difficult to be observed (**Fig. 1.7**).

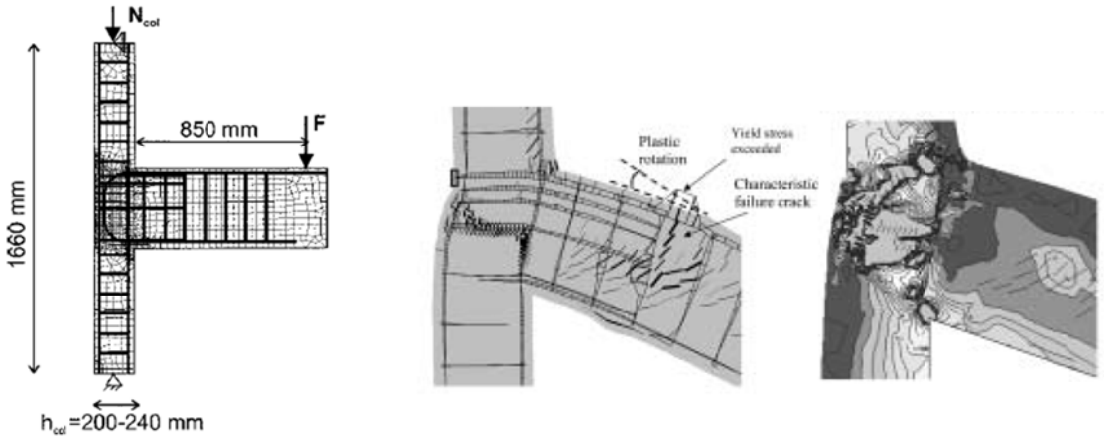

Fig. 1.7 Finite element model and failure types of simulation results (Hegger *et al.* 2004)

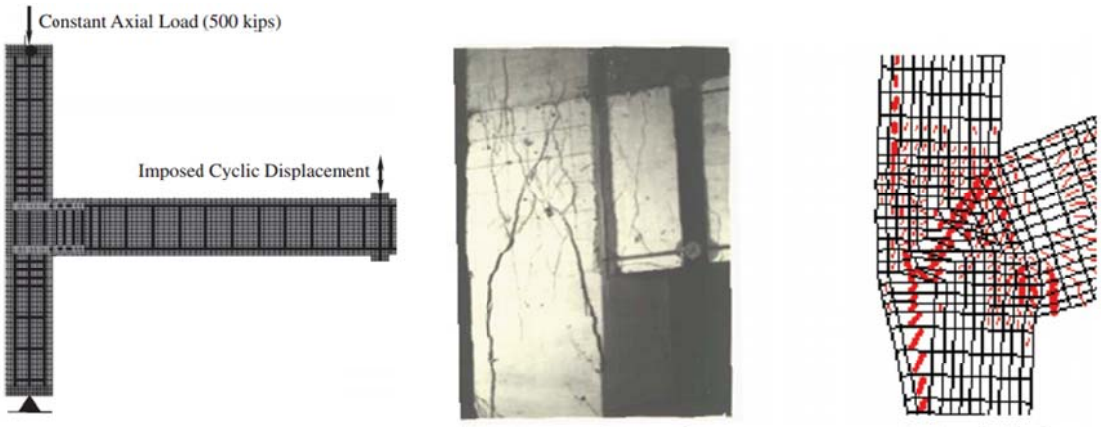

Fig. 1.8 Finite element model and final failure modes of simulation results (Sagbas *et al.* 2004)

Sagbas *et al.* (2011) used Vector2 which was developed by The University of Toronto in order to investigate the effectiveness of finite element modeling procedures in accurately capturing the nonlinear cyclic response of beam-column subassemblies. However, the same limitations were encountered in this study, i.e. the simulations were limited in 2D analysis and local failures were difficult to be observed (**Fig. 1.8**).

Eligenhausen *et al.* (2008) and Sasmal *et al.* (2011) used finite element analysis in three-dimensional modeling of beam column joints. However, reinforcement bars were limited as the line elements.

Based on the previous explanations, there are some limitations to model a beam column joint by using finite element analysis:

- Some simulations were limited in two-dimensional modeling
- Smeared crack approach inhibited the crack growth and dislocation
- Complex local failures that usually occurs in a beam column joint were difficult to be observed.

Author *et al.* (2013) has also used program Com3, a three-dimensional finite element analysis program that was developed by The University of Tokyo, in order to simulate a beam column joint with complex arrangement of reinforcement bar. Three-dimensional modeling of beam column joint including the three-dimensional shape of a reinforcement bar was simulated. Perfect bond between a reinforcement bar and concrete was assumed in this study. The same tendency of load-displacement relationship as experimental result was predicted. When the displacement is relatively small, the same cracks as experimental results can be simulated. However, as the

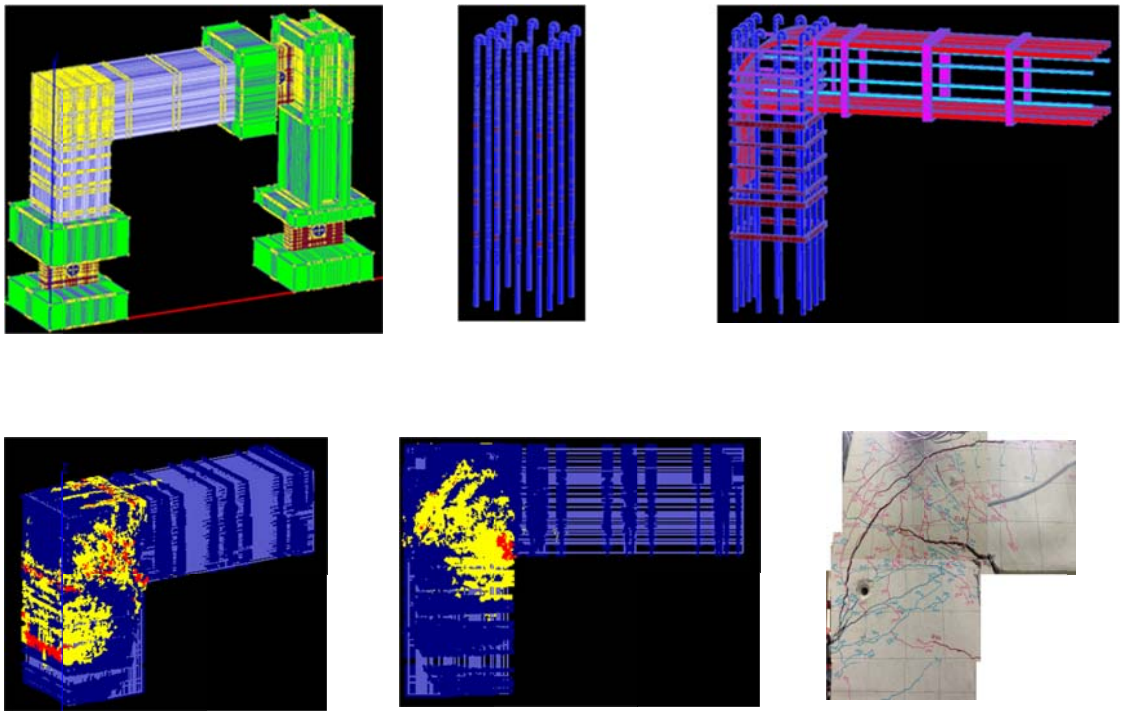

Fig. 1.9 Finite element model and final failure modes of simulation results (Eddy *et al.* 2013)

displacement increases, complex cracks occur in the beam column joint. As the result, global failure can be predicted, but local cracks were difficult to be observed (**Fig. 1.9**).

Meanwhile, discrete analysis method might be a suitable simulation since cracks can be modeled directly as the displacement between two elements. Cundal *et al.* (1971, 1974, and 1979) is the first among all who proposed a discrete numerical model, called Distinct Element Method, in order to analysis rock mechanics problems and behavior of granular assemblies. Williams and Mostoe (1987) continued more study on Distinct Element Method. Furthermore, various discrete analysis methods were applied in other fields.

In concrete field, as transpired from their recent researches that failure due to distributed cracking could not be simulated adequately in a continuum manner (Bazant 1986), Zubelewicz and Bazant (1987) proposed a discrete approach which directly simulated from the microstructure. Concrete in two dimensions was modeled as a random arrangement of perfectly rigid particles separated by interface elements. In 1990, Bazant *et al.* introduced a modification and refinement of the previous approach, called random particle model. In this model, two adjacent particles were assumed to interact only in the axial direction in which shear and moment interactions in the contact zone are neglected

and a particle was assumed to be elastic rather than rigid.

Schalangen and Van Mier (1992) proposed a triangular latticed model which consists of bar elements that can transfer normal force and bending moment. Once the combination of normal force and bending moment exceeds the capacity, the bar element is removed.

Meguro and Hakuno (1989) upgraded Distinct Element Method that was proposed by Cundal *et al.* (1971), called Modified Distinct Element Method (MDEM). In this model, concrete is represented as circular particle elements and non-linear springs.

In this study, the simulation is carried out by meso-scale analysis of reinforced concrete members by a 3D discrete element analysis, called Rigid Body Spring Model (RBSM), which was proposed by Kawai *et al.* (1978). In RBSM, each rigid body connects with another rigid by springs. This approach has been applied by some researchers in order to study the behavior of reinforced concrete members.

Bolander *et al.* (1998, 1999, 2000, and 2002) applied 2D RBSM not only to reinforced concrete members but also to prestressed concrete members. Reinforced bars were assumed as line elements. Furthermore, the application of RBSM was extended to the simulation of fiber reinforced concrete and shrinkage phenomena by using 3D RBSM (Bolander *et.al.* 2004, 2006, 2008, and 2010). Line elements were adopted for modeling the fiber.

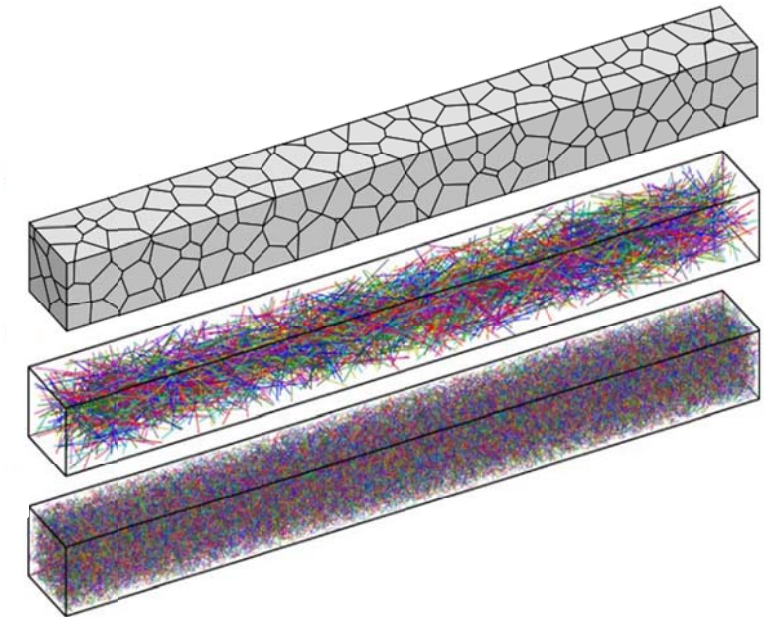

Fig. 1.10 Fiber reinforced concrete model by 3D RBSM (Bohlander *et al.* 2008)

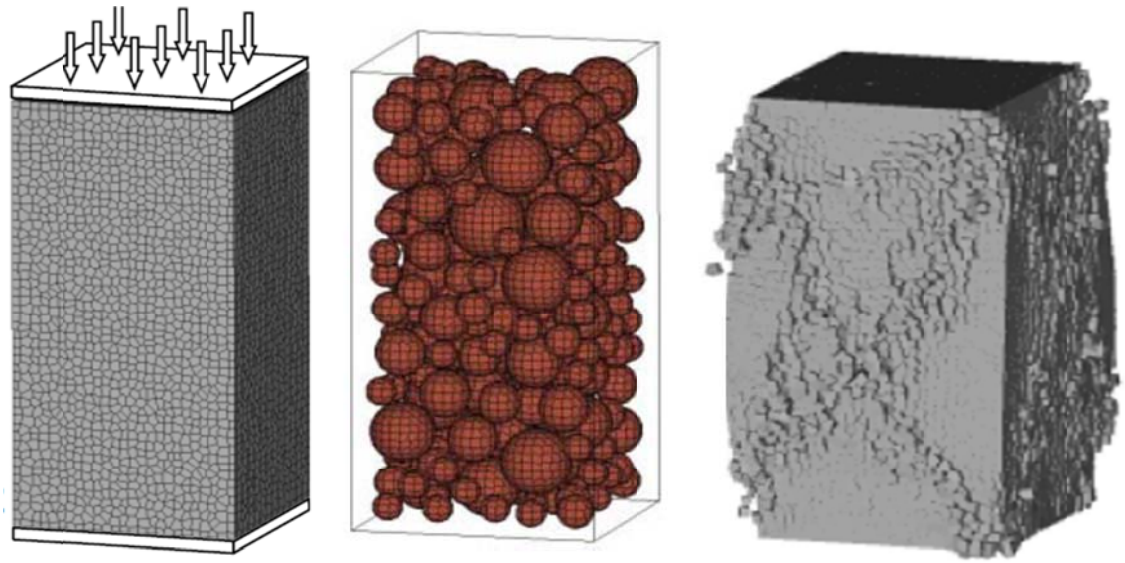

Fig. 1.11 3D meso scale analysis of mortar and concrete by RBSM (Nagai *et al.* 2005)

Our research group has used 3D RBSM to simulate various kinds of reinforced concrete members (Nagai *et al.* 2005, Inoue *et al.* 2011, Ikuta *et al.* 2012, and Hayashi *et al.* 2014).

Nagai *et al.* (2005) were the first that carried out the 3D meso scale analysis of mortar and concrete by RBSM in order to evaluate the behavior of concrete quantitatively. It was concluded that the analysis predicts well the uniaxial compressive and tensile strength relationship of both mortar and concrete. Furthermore, the analysis could simulate the failure crack pattern of concrete under uniaxial compressive stress condition, uniaxial tensile stress condition, and biaxial compressive stress condition (**Fig. 1.11**).

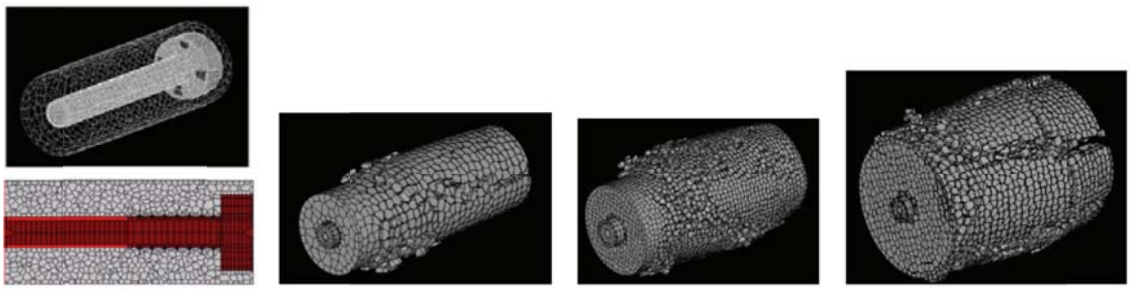

Fig. 1.12 3D meso scale analysis of T-headed bar of anchorage in a reinforced concrete member with thin concrete cover by RBSM (Inoue *et al.* 2011)

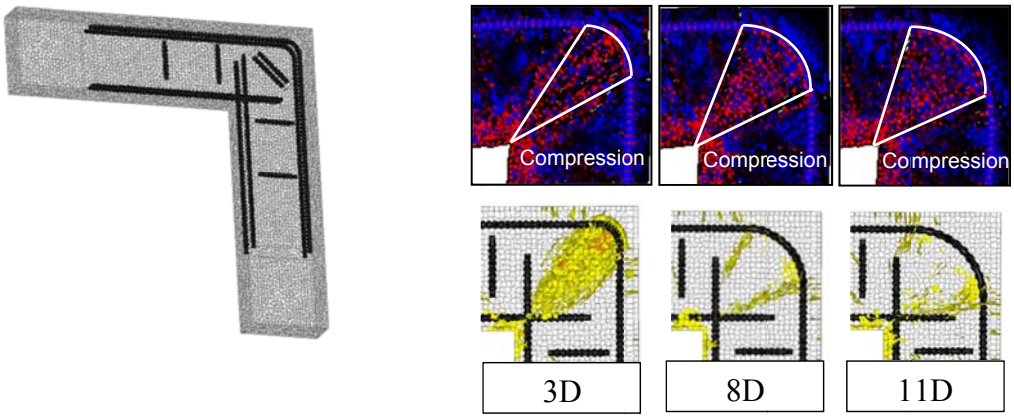

Fig. 1.13 3D meso scale analysis of beam column joints with different bending radius of anchorage bars by RBSM (Ikuta *et al.* 2012)

Inoue *et al.* (2011) were the first in our research group that conducted 3D meso scale analysis by RBSM in order to investigate the behavior of reinforced concrete members. Furthermore, the simulations were carried out in order to study the mechanical behavior of a T-headed bar of anchorage which was used in a reinforced concrete member with thin concrete cover. It was showed that 3D RBSM can simulate the splitting cracks and different failure patterns depending on the concrete cover thickness which are the same as the experimental observations (**Fig. 1.12**).

Ikuta *et al.* (2012) were the first in our research group that used 3D meso scale analysis by RBSM in order to investigate the behavior of beam column joints with simple arrangement of reinforcement bars. Different internal stress conditions and failure patterns can be simulated due to different bending radius of anchorage bars (**Fig. 1.13**).

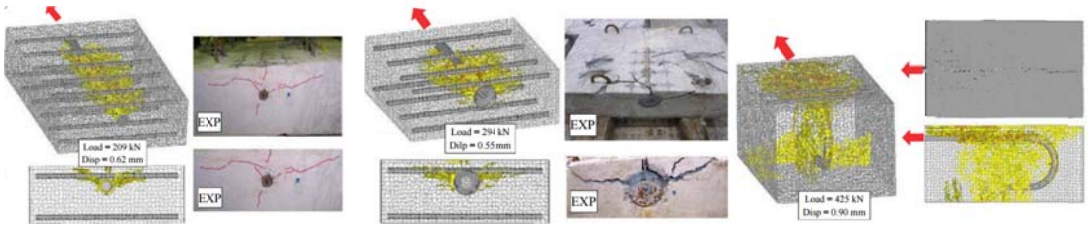

Fig. 1.14 3D meso scale analysis of reinforced concrete members by different types of anchorages by RBSM (Hayashi *et al.* 2012)

Hayashi *et al.* (2014) used 3D meso scale analysis by 3D RBSM in order to investigate the anchorage performance in a reinforced concrete. The simulations were done for reinforced concrete members with different types of anchorages, i.e. straight bar, mechanical anchorage, and conventional 180 degrees hooked bar. It was shown that different failure patterns can be predicted due to different anchorage systems (**Fig. 1.14**).

However, the simulation system was limited in which the model and the arrangement of reinforcement bars were simple, the meshing of a reinforcement bar was complex, and the constitutive models were not fixed yet. In this study, the target of the simulation is the beam column joint with complex arrangement of reinforcement bars and the complicated stress occurred in the beam column joint. Thus, the previous simulation system was not enough to simulate these complex behaviors. So at the first stage of this research, the simulation system must be improved.

1.2 RESEARCH SIGNIFICANCE

In using discrete analysis, RBSM, a good understanding in the heterogeneous properties of concrete must be obtained to be reflected in the simulation models. A little attention to the mesh size is necessary in RBSM. The mesh size of the simulation models should be selected in an appropriate way to represent the actual cracking pattern of concrete. Based on this mesh size, the constitutive models of simulation will be decided. The meaning of meso-scale analysis and element size will be explained in this study. So that, the first contribution of the present study is to gain the knowledge of the importance of the mesh size in the simulation models of 3D RBSM, in order to represent the real cracking pattern in the concrete.

By using this 3D RBSM in the general applications, there is interest in obtaining of complete understanding on the structural behavior when local failure, local arrangement, or local loading conditions affect macroscopic behavior significantly. Through the study of the internal cracks and internal stress conditions, it can reveal details of the local responses of concrete and reinforcement and their interactions with cracking that were difficult to be investigated by the experimental works.

By revealing the behavior of a reinforced concrete element through the study of internal cracks and internal stress condition, the mechanism of strengthening mechanical anchorages, particularly in a beam column joint, can be proposed. Furthermore, in the

future, a rational method to strengthen the beam column joint with mechanical anchorages can be achieved. Further implications of this study are to provide a tool for assessing the deteriorated structures relating to the anchorage parts and joints of structures, to retrofit deteriorated structure, and to predict the life span of the retrofitted structure.

1.3 OBJECTIVE AND SCOPE OF STUDY

The first objective of this research is to improve the simulation system of RBSM. A brief review on the relative task is given follows:

1. Develop the algorithm of simple meshing of a reinforcement bar. The meshing technique of a reinforcement bar used by the previous researchers was very complex. As the result, a lot number of elements were necessary to model a beam column joint with complex arrangement of reinforcement bars. It will not be efficient for the simulation.
2. Develop the algorithm to model any shapes of reinforcement bars. It is necessary because various shapes of reinforcement bars are used to simulate a beam column joint with complex arrangement of reinforcement bars.
3. Improve the number of elements in the simulation system. In the past, the simulation system was limited with less than 300000 elements.

Ultimately, the simulation system should be able to model the same model and the same reinforcement arrangement as the real condition of reinforced concrete members.

The second objective of this research is to upgrade the constitutive models in the simulation system of RBSM. The improvements were done based on the simulations in the material scale. Here, the following simulations were conducted:

1. Concrete element
    a. Compressive uniaxial simulation
    b. Tensile uniaxial simulation
    c. Biaxial simulation
2. Concrete-steel interface: Tension stiffening stimulation

The applicability of RBSM in material scale simulation was verified through the comparison with the experimental results.

The third objective of this research is to reveal the behavior of reinforced concrete structures, i.e. corbels, a beam column joint with complex arrangement of reinforcement bars, and beam column joints with mechanical anchorages. The applicability of RBSM

to model in the structural scale will also be investigated through the comparison with the experimental results. The simulation must able to simulate its strong points. Those are:

1. 3D RBSM should be able to simulate different failure pattern due to different loading position and the local reinforcement bars arrangement.
2. 3D RBSM should be able to simulate different failure pattern due to different loading condition. In this case, cyclic load was applied to the numerical models.
3. 3D RBSM should be able to simulate complex cracks in a beam column joint with complex arrangement of reinforcement bars.
4. 3D RBSM should be able to simulate different behaviors due different local arrangements of reinforcement bars.

The forth objective is to suggest an efficient method of retrofitting the damage structure members.

The fifth objective is to propose the mechanism how to strengthen the beam column joint with mechanical anchorages through the study of internal stress condition and internal cracking pattern.

1.4 RESEARCH STRATEGY

Step 1: The first step of this research is to select an appropriate element size to represent the real cracking pattern, especially in the normal concrete. *Step 2*: Based on the selected element size, the simulation system was improved and the constitutive models of RBSM were upgraded. The applicability of the constitutive models was verified trough the comparison with the experimental results in material scale. *Step 3:* The simulation system was used to understand the behavior of reinforced concrete structures under different loading position, different local reinforcement bar arrangement and different loading condition. *Step 4:* Based on the study of the internal stress condition and crack propagations, a proposed retrofitting method and a proposed failure mechanism in a beam column joint with mechanical anchorages were raised.

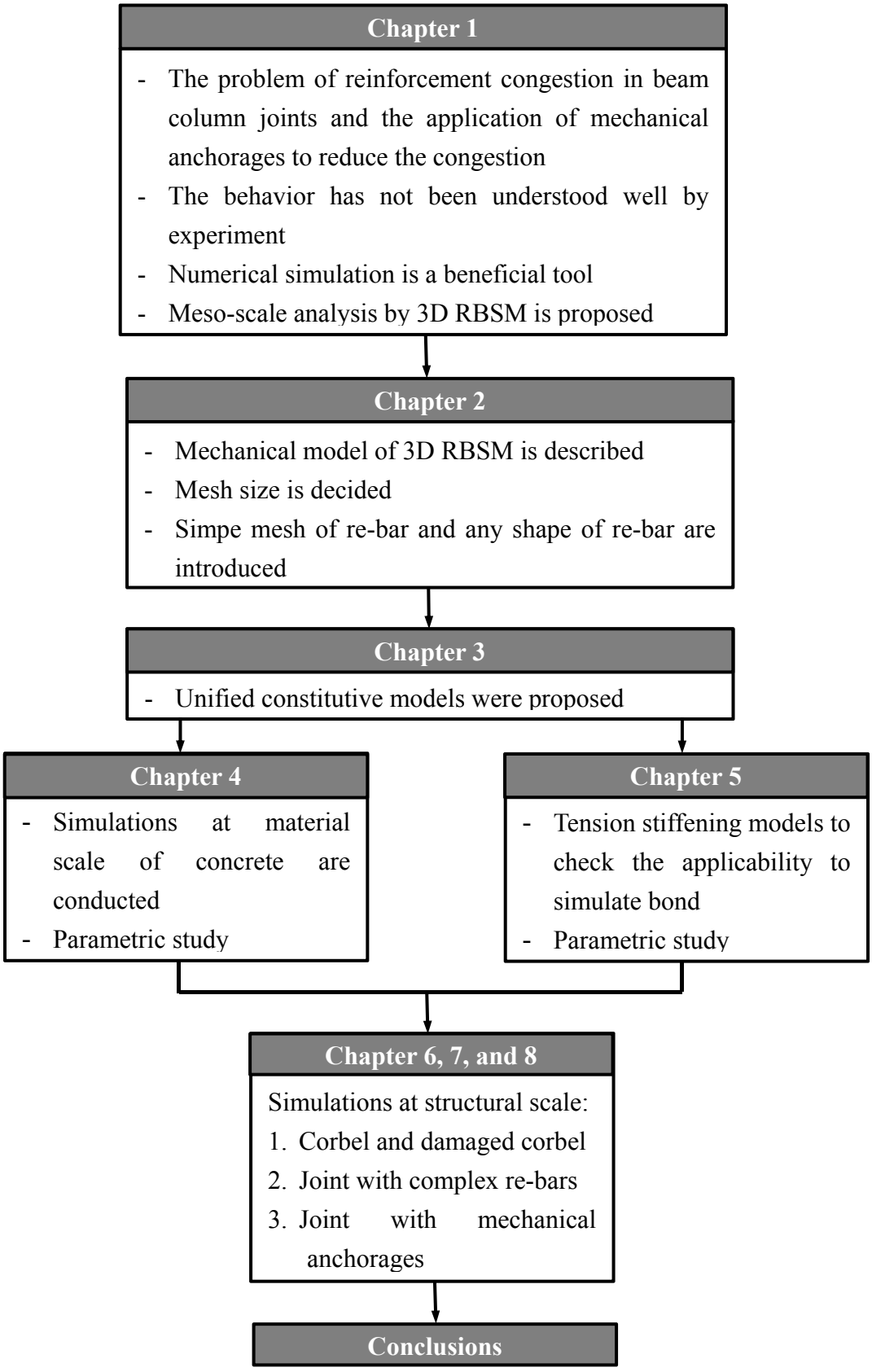

Fig. 1.15 Organization of contents

1.5 ORGANIZATION OF CONTENTS

Chapter 1 explains the background and problem of reinforcement congestion in the beam column joint that caused by the demanding in the current specification. By experimental works, it is not easy to understand the behaviors of beam column joints with complex arrangement of reinforcement bars because of complex cracks behavior in the beam column joints. Meanwhile, mechanical anchorage can be a beneficial tool to reduce the reinforcement congestion. However, to strengthen this system, many experimental works are necessary. It is inefficient and it takes time. Thus, in this study, numerical simulation can be a beneficial tool to understand the behavior. Literature reviews of numerical simulation are presented and meso-scale analysis by 3D RBSM is proposed. In this chapter, the significances of this research have been represented. In order to achieve the objective and scope in this study, some research strategies are presented.

Chapter 2 describes the mechanical model of the three-dimensional RBSM in detail. Equations that are used to make local stiffness matrix and global stiffness matrix will be described, including the equilibrium equation of RBSM. As described above, a little attention to the mesh size is necessary to represent the cracking pattern in the concrete. In this chapter, the heterogeneous property of concrete will also be explained, and based on this property, an appropriate size of meshing will be determined. In other words, the reason in determining the mesh size will be described. The concept of the mesh arrangement of concrete elements and steel elements is provided, including the improvement of the simulation system that has been achieved so that the simulation can model the same model and the same reinforcement arrangement with the real condition.

Chapter 3 mentions the constitutive models of all elements that will be used in this study, i.e. concrete elements, steel elements, and interface interface-concrete elements. Constitutive models were developed based on the simulations in material scale.

Chapter 4 shows the simulation results of concrete in the material scale to confirm the constitutive models that will be used in the simulation. Results of simulations of uniaxial compressive test, uniaxial tensile test, and biaxial compressive stress will be shown in this chapter. The results are compared with those of equations in the specification code and the experimental results. Furthermore, the effect of various types of failure criterion of concrete on the behavior of concrete material will be revealed in this chapter. The applicability of RBSM to simulate Poisson's Ratio effect will be

checked.

Chapter 5 shows the reliability of RBSM in modeling the bond between the concrete and a reinforcement bar. In this chapter, tension stiffening simulations were conducted to confirm the applicability of RBSM in modeling the bond behavior. 2 simulations were conducted based on the experiment done by Shima *et al*. (1987), i.e. low yield strength of reinforcement bar and normal yield strength of reinforcement bar. Macroscopic responses, microscopic responses, and strain distributions along the reinforcement bar of simulation results will be compared with those of experimental results. In addition, the effect of tensile strength reduction of normal springs at the interface between concrete elements and steel elements, and modeling strain hardening region in the constitutive model of springs of steel elements on the tension stiffening behavior of a reinforced concrete member will be explained in this chapter.

Chapter 6 shows the simulations of corbels by 3D RBSM. By well-developed simulation system, RBSM is used to explain how the loading condition and local arrangement of reinforcement affect significantly the local cracks and furthermore affect the macroscopic response. The simulation results will be compared with the experimental results. Simulation can simulate well the damage that occurred in the field observation because of the ability of simulation to model the local arrangement of reinforcement directly. Furthermore, simulation can propose the effective way to recover the capacity of the corbel by considering directly the existing damage in the corbel.

Chapter 7 shows the simulation of a beam column joint with complex arrangement of reinforcement bars by 3D RBSM. RBSM can simulate complex cracks in the beam column joint with complex arrangement of reinforcement bars because the same arrangement of reinforcement bars as the experimental specimen was modeled. Different cracking pattern can be simulated due to different loading condition.

Chapter 8 describes the simulations of beam column joints with mechanical anchorages. Based on the experimental work, the knowledge how to arrange the reinforcement bars in beam column joint with mechanical anchorages has not been well known yet so that many experiments were done. Based on the simulation results, each reinforcement bar has contribution to the cracks formation in the beam column joint. Furthermore, the importance to place concrete block at the top of a beam column joint or stirrups along

the anchorages of a beam column joint with mechanical anchorages will be explained in this chapter. Since the opening of diagonal cracks affects the failure pattern of the beam column joints with mechanical anchorages significantly, the effect of using plain bars or deformed bars as the stirrups on the failure behavior of the beam column joint will also be explained.

REFERENCES

American Concrete Institute (ACI) Committee 318., "Building Code Requirements for Structural Concrete and Commentary," *ACI 318M-08* Farmington Hills, MI, 2008.

American Concrete Institute (ACI) Committee 352., "Building Code Requirements for Structural Concrete and Commentary," *ACI 352R-02* Farmington Hills, MI, 2002

Baglin, P.S., and Scott, R.H., "Finite Element Modeling of Reinforced Concrete Beam-Column Connections," *ACI Structural Journal*, 97(90), pp. 886-894, 2000.

Bazant, Z.P., "Mechanics of Distributed Cracking," *Applied Mechanic Rev.*," ASME, 4(5), pp.675-705, 1986.

Bazant, Z.P., Tabbara, M.R., Kazemi, M.T., and Cabot, G.P., "Random Particle Model for Fracture of Aggregate of Fiber Composites," *Journal of Engineering Mechanics*, 116(8), pp.1686-1705, 1990.

Bolander, J. E., and Berton, S., "Simulation of Shrinkage Induced Cracking in Cement Composite Overlays," *Cement & Concrete Composites*, 26, pp.861-971, 2004.

Bolander, J. E., Choi, S., and Duddukuri, S. R, "Fracture of Fiber-reinforced Cement Composites: Effects of Fiber Distribution," *Internationl J. Fracture*, 154, pp.73-86, 2008.

Bolander, J. E., Hong, G. S., and Yoshitake, K., "Structural Concrete Analysis Using Rigid-Body-Spring Networks," *Computer-Aided Civil and Infrastructure Engineering*, 15, pp.120-133, 2000.

Bolander, J. E., and Hong, G. S., "Rigid-Body-Spring Network Modeling of Presetressed Concrete Members," *ACI Structural Journal*, 99(5), pp.595-603, 2002.

Bolander, J. E., Le, B. D., “Modeling Crack Development in Reinforced Concrete Structures Under Service Loading,” *Construction and Building Materials*, 13, pp.23-31, 1999.

Bolander, J. E., and Saito, S., “Fracture Analysis Using Spring Networks with Random Geometry,” *Engineering Fracture Mechanics*, 61, pp. 569-591, 1998.

Bolander, J. E., Yoshitake, K., and Thomure, J., “Stress Analysis Using Elastically Uniform Rigid-Body-Spring Networks,” *Journal of Structural Mechanics and Earthquake Engineering JSCE*, 633(I-49), pp.25-32, 1999.

Chun, S. C., Lee, S. H., Kang, T. H. K., Oh, B., and Wallace, J. W., “Mechanical Anchorage in Exterior Beam-Column Joints Subjected to Cyclic Loading,” *ACI Structural Journal* ,104(12), pp. 102-112, 2007.

Cundal, P. A., “A Computer Model for Simulating Progressive, Large-scale Movements in Blocky Rock Systems,” *Proc. Symp. Int. Soc. Rock Mech.*, Nancy 2, No.8, 1971.

Cundal, P. A., “BALL-A Program To Model Granular Media Using The Distinct Element Method,” *Technical Note*, Advanced Technology Group, Dames & Moore, London, 1978.

Cundal, P. A., Strack, O.D.L, “A Discrete Numerical Model for Granular Subassemblies,” *Geeeotechnique*, 29(1), pp. 47-65, 1979.

Eddy, L., and Nagai, K., “A Study of The Behavior of A Beam Column Joint with Complex Arrangement of Reinforcing Bars by Finite Element Enalysis,” *International Symposium on New Technologies for Urban Safety of Mega Cities in Asia (USMCA)*, Hanoi, Vietnam, 2013.

Eligehausen, R., Genesio, G., Ozboly, J., and Pampanin, S., “3D Analysis of Seismic Response of RC Beam-column Exterior Joints Before and After Retrofit,” Proc. of the International Conference on Repairing, Retrofit and Rehabilitation ICRRRR, Cape Town, South Africa, 2008.

Hayashi, D., and Nagai, K., “Investigating the Anchorage Performance of RC by Using Three-dimensional Discrete Analysis,” *Engineering Computations*, *30*(6), 815-824, 2013.

Hegger, J., Sherif, A., and Roeser, W., “Nonlinear Finite Element Analysis of Reinforced Concrete Beam-Column Connections,” *ACI Structural Journal*, 101(59), pp. 604-611, 2004.

Ikuta, K.; Nagai, K.; Hayashi, D., “Numerical Simulation of Beam-Column Joint with Simple Reinforcement Arrangement by Three-dimensional RBSM,” *International Symposium of New Technologies for Urban Safety Mega Cities in Asia (USMCA)*, 2012.

Inoue, Yu, and Nagai, K., “Numerical Simulation of Fracture Pattern and Bond Performance of Anchorage in Reinforced Concrete." *Procedia Engineering*14 (2011), 1165-1173, 2011.

Japan Society of Civil Engineers., “Recommendations for Design, Fabrication and Evaluation of Anchorages and Joints in Reinforcement Bars,” *Concrete Library 128*, 2007. (in Japanese)

Kato, F., Kiyohara, T., Tasai, A., and Kusunoki, K., ”Experimental Study of Knee Joints with Mechanical Anchorage,” *Proceedings of Japan Concrete Institute*, 33(2), 2011. (in Japanese)

Kawai, T., “New Discrete Models and Their Application to Seismic Response Analysis of Structure,” *Nuclear Engineering and Design*, 48, 207-229. 1978.

Meguro, K., Hakuno, M., “Fracture Analyses of Concrete Structures by The Modified Distinct Element Method,” *Structural Eng./Earthquake Eng. Japan Society of Civil Engineers*, 6(2), pp.113-124. 1989.

Nagai, K., Sato, Y., and Ueda, T., ”Mesoscopic Simulation of Failure of Mortar and Concrete by 3D RBSM,” *J. Adv. Conc. Technol.*, *3(3)*, 385-402, 2005.

Nam, J. W., Abell, M. P., Lim, Y. M., and Bolander. J. E., "Strength Degradation of Fiber-reinforced Cement Composites Exposed to Simulated Environments," *ACI Special Publication SP-272-10*, pp.189-204, 2010.

Sagbas, G., Vecchio, J.F., and Chsristopoulos, C., "Computational Modeling of the Seismic Performance of Beam-Column Subassemblies," *Journal of Earthquake Engineering. 15*, 640-663, 2011.

Sasmal, S., Novak, B., and Ramanjaneyulu, K., "Numerical Analysis of Fiber Composite-steel Plate Upgraded Beam-column Sub-assemblages under Cyclic Loading," *Composite Structures*, 93(2), pp.599-610, 2011.

Schalangen, E., Van Mier, J., G., M., "Simple lattice model for numerical simulation of fracture concrete materials and structutres," *Material and Structures*, 25, pp.534-542. 1992.

Wallace, J. W., McConnell, S. W., Gupta, P., and Cole, P.A., "Use of Headed Reinforcement in Beam-Column Joints Subjected to Earthquake Loads," *ACI Structural Journal*, 95(54), pp. 590-902, 1998.

Williams, J.R., Mustoe, G.G.W., "Modal Methods for The Analysis of Discrete Systems," *Computer and Geotechnics*, 4(1), pp.1-19, 1987.

Yoshimura, M., Kiyohara, T., Tasai, A., and Kusunoki, K., "Experimental Study of Performance Improvement of Knee Joints with Mechanical Anchorage," *Proceedings of Japan Concrete Institute*, 34(2), 2012. (in Japanese)

Zubelewicz, A., and Bazant, Z.P., "Interface Element Modeling of Fracture in Aggregate Composites," *Journal of Engineering Mechanics American Society of Civil Engineers* 113(11), pp.1619-1630. 1987.

Chapter TWO

METHOD OF SIMULATION

2.1 RIGID BODY SPRING MODEL

In this study, the simulations are carried out by a three dimensional RBSM, proposed by Kawai *et al.* (1978). In RBSM, a three dimensional reinforced concrete model is meshed into rigid bodies. Each rigid body consists of six degree of freedoms, i.e. three translational degrees of freedom and three rotational degrees of freedom at some points within its interior and connects with other rigid bodies by three springs, i.e. two shear springs and one normal spring.

2.2 MECHANICAL MODEL OF THREE-DIMENSIONAL RBSM

Mechanical behavior of 3D RBSM is shown in **Fig. 2.1**. In this study, the computational point (x_c, y_c, z_c) where the degrees of freedom of an element are located, is defined as follows:

$$x_c = \frac{x_1 + x_2 + \cdots + x_i + \cdots + x_m}{m}$$
$$y_c = \frac{y_1 + y_2 + \cdots + y_i + \cdots + y_m}{m} \qquad (2.1)$$
$$z_c = \frac{z_1 + z_2 + \cdots + z_i + \cdots + z_m}{m}$$

where m is the number of node composing an element and x_i, y_i, and z_i are the coordinates of the nodes in an element.

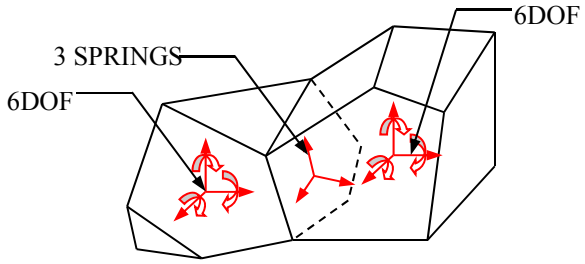

Fig.2.1 Mechanical model of 3D RBSM

Meanwhile, the point of a face of an element where springs are located, is defined as follows:

$$\begin{aligned} x_{cf} &= \frac{x_1 + x_2 + \cdots + x_j + \cdots + x_n}{n} \\ y_{cf} &= \frac{y_1 + y_2 + \cdots + y_j + \cdots + y_n}{n} \\ z_{cf} &= \frac{z_1 + z_2 + \cdots + z_j + \cdots + z_n}{n} \end{aligned} \tag{2.2}$$

where n is the number of node composing a face and x_j, y_j, and z_j are the coordinates of the nodes in a face.

When an element has small displacement [u_1, v_1, w_1, θ_{u1}, θ_{v1}, θ_{w1}], the springs at a face in an element will be displaced:

$$\begin{aligned} u &= u_1 - \theta_{w1}(y_{cf} - y_{ce1}) + \theta_{v1}(z_{cf} - z_{ce1}) \\ v &= v_1 - \theta_{u1}(z_{cf} - z_{ce1}) + \theta_{w1}(x_{cf} - x_{ce1}) \\ w &= w_1 - \theta_{v1}(x_{cf} - x_{ce1}) + \theta_{u1}(y_{cf} - y_{ce1}) \end{aligned} \tag{2.3}$$

Elongations of normal and shear spring are calculated and expressed as follows

$$d = Bu_e \tag{2.4}$$

Wehere d^T = [δ_{s1}, δ_{s2}, δ_n] and u_e^T=[u_1, v_1, w_1, θ_{u1}, θ_{v1}, θ_{w1}, u_2, v_2, w_2, θ_{u2}, θ_{v2}, θ_{w2}]. The transformation matrix B is written as:

$$B = \begin{bmatrix} K_{11}K_{12}K_{13}K_{14}K_{15}K_{16}K_{17}K_{18}K_{19}K_{110}K_{111}K_{112} \\ K_{21}K_{22}K_{23}K_{24}K_{25}K_{26}K_{27}K_{28}K_{29}K_{210}K_{211}K_{212} \\ K_{31}K_{32}K_{33}K_{34}K_{35}K_{36}K_{37}K_{38}K_{39}K_{310}K_{311}K_{312} \end{bmatrix} \tag{2.5}$$

$K_{11} = -e_{s1x}$ $K_{12} = -e_{s1y}$ $K_{13} = -e_{s1z}$

$K_{21} = -e_{s2x}$ $K_{22} = -e_{s1y}$ $K_{23} = -e_{s2z}$

$K_{31} = -e_{nx}$ $K_{32} = -e_{ny}$ $K_{33} = -e_{nz}$

$K_{14} = e_{s1y}(z_{cf}-z_{ce1})- e_{s1z}(y_{cf}-y_{ce1})$

$K_{24} = e_{s2y}(z_{cf}-z_{ce1})- e_{s2z}(y_{cf}-y_{ce1})$

$K_{34} = e_{ny}(z_{cf}-z_{ce1})- e_{nz}(y_{cf}-y_{ce1})$

$K_{15} = e_{s1z}(x_{cf}-x_{ce1})- e_{s1x}(z_{cf}-z_{ce1})$

$K_{25} = e_{s2z}(x_{cf}-x_{ce1})- e_{s2x}(z_{cf}-z_{ce1})$

$K_{35} = e_{nz}(x_{cf}-x_{ce1})- e_{nx}(z_{cf}-z_{ce1})$

$K_{16} = e_{s1x}(y_{cf}-y_{ce1})- e_{s1y}(x_{cf}-x_{ce1})$

$K_{26} = e_{s2x}(y_{cf}-y_{ce1})- e_{s2y}(x_{cf}-x_{ce1})$

$K_{36} = e_{nx}(y_{cf}-y_{ce1})- e_{ny}(x_{cf}-x_{ce1})$

$K_{17} = e_{s1x}$ $K_{18} = e_{s1y}$ $K_{19} = e_{s1z}$

$K_{27} = e_{s2x}$ $K_{28} = e_{s1y}$ $K_{29} = e_{s2z}$

$K_{37} = e_{nx}$ $K_{38} = e_{ny}$ $K_{39} = e_{nz}$

$K_{110} = e_{s1z}(y_{cf}-y_{ce2})- e_{s1y}(z_{cf}-z_{ce2})$

$K_{210} = e_{s2z}(y_{cf}-y_{ce2})- e_{s2y}(z_{cf}-z_{ce2})$

$K_{310} = e_{nz}(y_{cf}-y_{ce2})- e_{ny}(z_{cf}-z_{ce2})$

$K_{111} = e_{s1x}(z_{cf}-z_{ce2})- e_{s1z}(x_{cf}-x_{ce2})$

$K_{211} = e_{s2x}(z_{cf}-z_{ce2})- e_{s2z}(x_{cf}-x_{ce2})$

$K_{311} = e_{nx}(z_{cf}-z_{ce2})- e_{nz}(x_{cf}-x_{ce2})$

$K_{112} = e_{s1y}(x_{cf}-x_{ce2})- e_{s1x}(y_{cf}-y_{ce2})$

$K_{212} = e_{s2y}(x_{cf}-x_{ce2})- e_{s2x}(y_{cf}-y_{ce2})$

$K_{312} = e_{ny}(x_{cf}-x_{ce2})- e_{nx}(y_{cf}-y_{ce2})$

where e_{ij} is direction cosine in i axis on j axis.

By applying the principal of virtual work, the local equilibrium relation expressed in global coordinate is expressed as,

$$k_e \Delta u_e = \Delta f_e \tag{2.6}$$

where the stiffness associated with interconnected face k_e is given as

$$k_e = B^T DB \tag{2.7}$$

where

$$\mathrm{D} = \begin{bmatrix} k_{s1} & 0 & 0 \\ 0 & k_{s2} & 0 \\ 0 & 0 & k_n \end{bmatrix} \tag{2.8}$$

in which k_n, k_{s1}, and k_{s2} are the normal and shear spring stiffness, The local stiffness of k_n, k_{s1}, and ks2 can be calculated as,

$$\begin{aligned} k_n &= k_{nsp} \frac{A}{h_1 + h_2} \\ k_{s1} &= k_{ssp} \frac{A}{h_1 + h_2} \\ k_{s2} &= k_{ssp} \frac{A}{h_1 + h_2} \end{aligned} \tag{2.9}$$

where,

$$\begin{aligned} k_{nsp} &= \frac{(1 - \vartheta_{elem}) E_{elem}}{(1 + \vartheta_{elem})(1 - 2\vartheta_{elem})} \\ k_{ssp} &= \frac{E_{elem}}{(1 + \vartheta_{elem})} \end{aligned} \tag{2.10}$$

where h_1 and h_2 are length of perpendicular lines from the element computational point to the face springs are set. The A is an area of the face. E_{elem} and ν_{elem} are the modulus of elasticity and poison's ration, respectively, which are calculated as follow.

$$E_{elem} = \frac{E_{elem1} h_1 + E_{elem2} h_2}{h_1 + h_2}$$

$$\vartheta_{elem} = \frac{\vartheta_{elem1} h_1 + \vartheta_{elem2} h_2}{h_1 + h_2} \tag{2.11}$$

2.3 MEANING OF ELEMENT SIZE IN MESO-SCALE ANALYSIS

In this study, the target of simulation is for normal concrete where the target compressive strength varies from 15 MPa to around 50 MPa, and concrete is a heterogeneous material that consists of water, cement, fine aggregate, and coarse aggregate. It is well understood that in a normal concrete microcracks occur at the interface between the mortar and aggregate or at the mortar between two aggregates when a concrete is loaded because these regions are weaker than aggregates (**Fig. 2.2a**). This heterogeneous property of normal concrete is different compared with fiber reinforced mortar that cracks usually occur in the mortar (**Fig. 2.2b**).

Based on these physical behaviors of cracks, a little attention of mesh size is necessary in RBSM since in RBSM a reinforced concrete member is meshed into rigid bodies that a rigid body is not allowed to be deformed and deformation of a reinforced concrete member depends on the movements or displacements of rigid bodies. To represent the real physical behaviors of cracks in a normal concrete, it is suitable that an aggregate should be represented as a rigid body since very small deformation can be assumed in aggregates. Cracks between aggregates determine mostly the deformation of a reinforced concrete member in macro scale so that forces, i.e. normal forces and shear forces, that cause the cracks opening and cracks closing are represented by normal

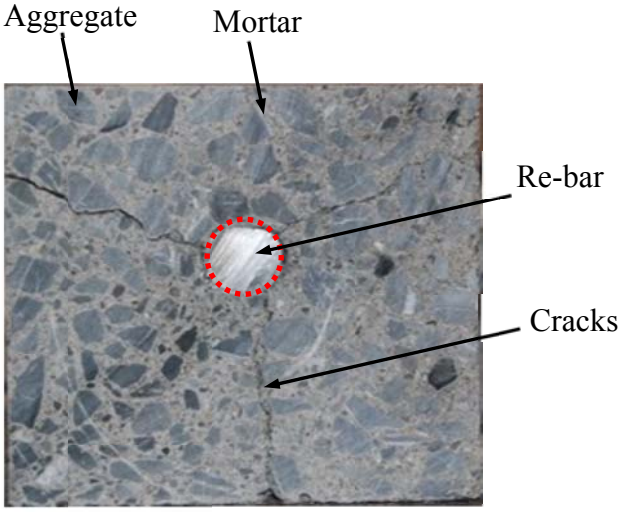

Fig.2.2a Normal concrete

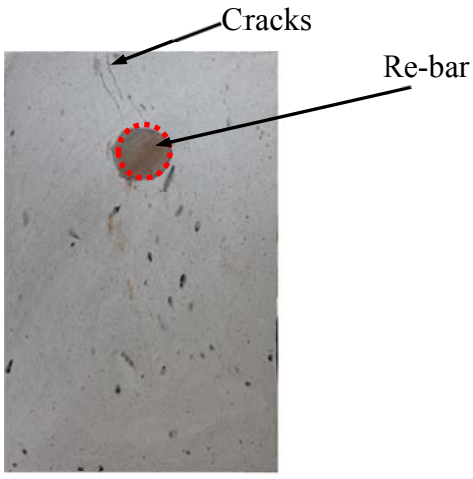

Fig.2.2b Fiber reinforced mortar

Fig.2.2 Cracks propagation of concrete

springs and shear springs in RBSM (**Fig. 2.3**). Based on this description, author decided that 10x10x10 – 20x20x20 mm^3 of mesh size is the most appropriate element size in this study to consider the aggregate size and location. After the appropriate mesh size that will be used in this study is chosen, constitutive models of springs will be decided based on the behavior at this size.

Based on the explanation above, it is well understood that in case of fiber reinforced mortar and high strength concrete, the same mesh size and constitutive models as normal concrete can't be applied. In case of fiber reinforced mortar because of the absence of aggregate, the physical behavior of cracks is straighter rather than zigzag shape found in normal concrete. Meanwhile in case of high strength concrete, cracks can penetrate into the aggregate. Furthermore, finer mesh is more appropriate in both cases and different constitutive models should be determined (**Figs. 2.4** and **2.5**).

It can be concluded that in RBSM, mesh size should be determined based on the actual cracking behavior in concrete. Furthermore, based on this mesh size, the appropriate constitutive model should be chosen.

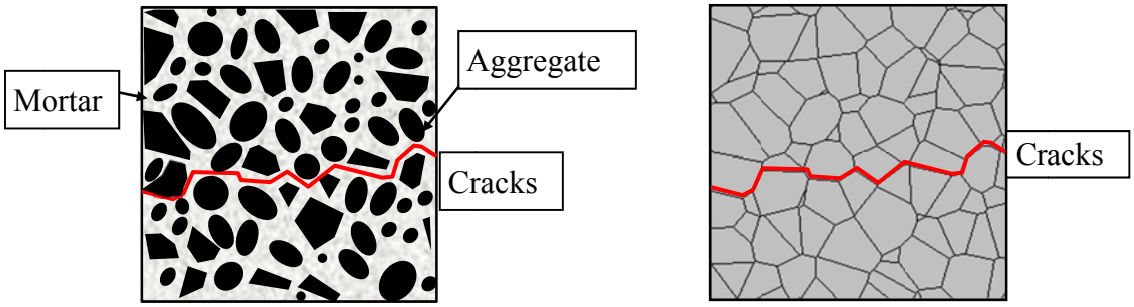

Fig.2.3 Representation of real cracks behavior of normal concrete into mesh size

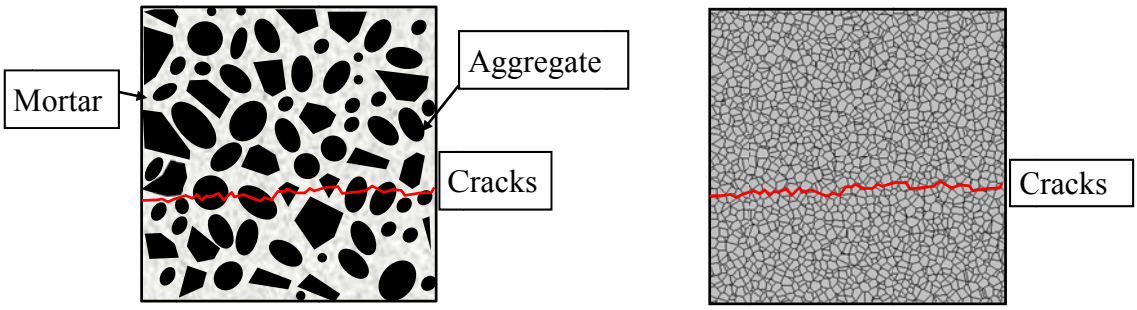

Fig.2.4 Representation of real cracks behavior of high strength concrete into mesh size

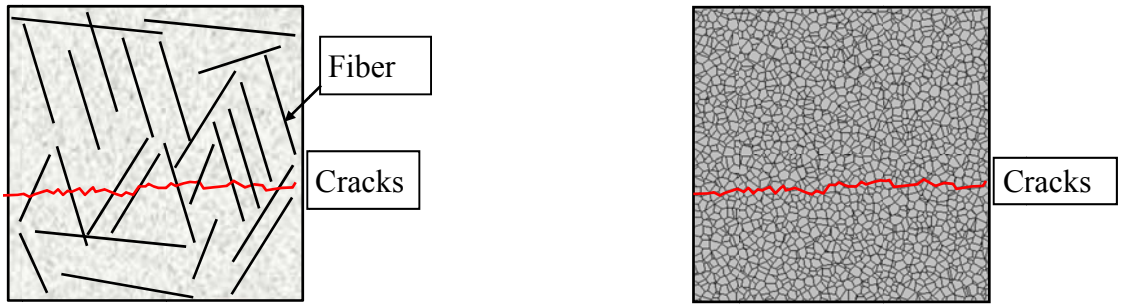

Fig.2.5 Representation of real cracks behavior of fiber reinforced mortar into mesh size

2.4 MESH CONSTRUCTION

As the propagation of cracks in reinforced concrete is one of the most important factors in investigating the behavior of reinforced concrete members, the mesh arrangement of the model in RBSM is important. In order to prevent cracks propagated in a non-arbitrary direction, a random geometry, called Voronoi Diagram, is used for the element meshing. The concrete element size is modeled approximately 10^3 to 20^3 mm^3 that is similar to the aggregate size as described above, while the size of the steel element is set according to the geometric complexity of the reinforcement bar arrangement. The geometry of steel elements is modeled in an accurate manner, by modeling a 3D arrangement of reinforcement bar, to properly account for the interlock between the reinforcement bar and concrete.

In the past, our research group has conducted 3D RBSM to study the behavior of reinforced concrete members. However, the simulations were limited in the small size of reinforced concrete members with simple reinforcement arrangement. Meanwhile, to simulate a beam column joint with multidirectional reinforcement arrangement, larger size of model is needed and the behavior is significantly affected by the reinforcement arrangement which cannot be simplified, so that the simulation was needed to be updated. Simulation has been developed so that 3D RBSM can model the same model

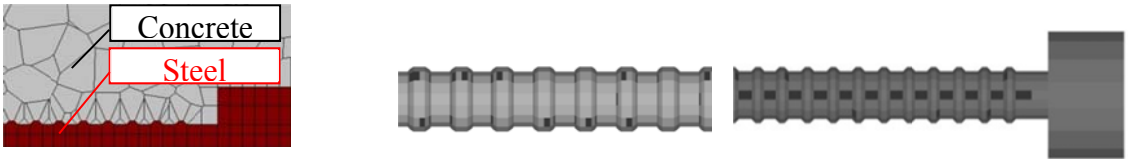

Fig.2.6 Mesh arrangement of concrete and reinforcement bars **(a)** Cross section; **(b)** Model of 3D rebar; **(c)** Model of 3D mechanical anchorage

and the same reinforcement arrangement as the real condition by simplifying the algorithm of the element meshing of a reinforcement bar in the simulation. Mesh arrangement of concrete and steel at meso-scale in this study is shown in **Fig.2.6**. Meanwhile, **Fig.2.7** shows various shapes of reinforcement bars that have been developed. For the 3D Voronoi meshing, the software QHULL is used.

To model a 3D reinforced concrete member, two types of elements are used, i.e. concrete elements and steel elements. The properties of the springs are determined so that the elements, when combined together, enable to predict the behaviour of the model as accurate as that of the experimental result. In this study, the simulation system, developed by Nagai *et al.* (2005), is used.

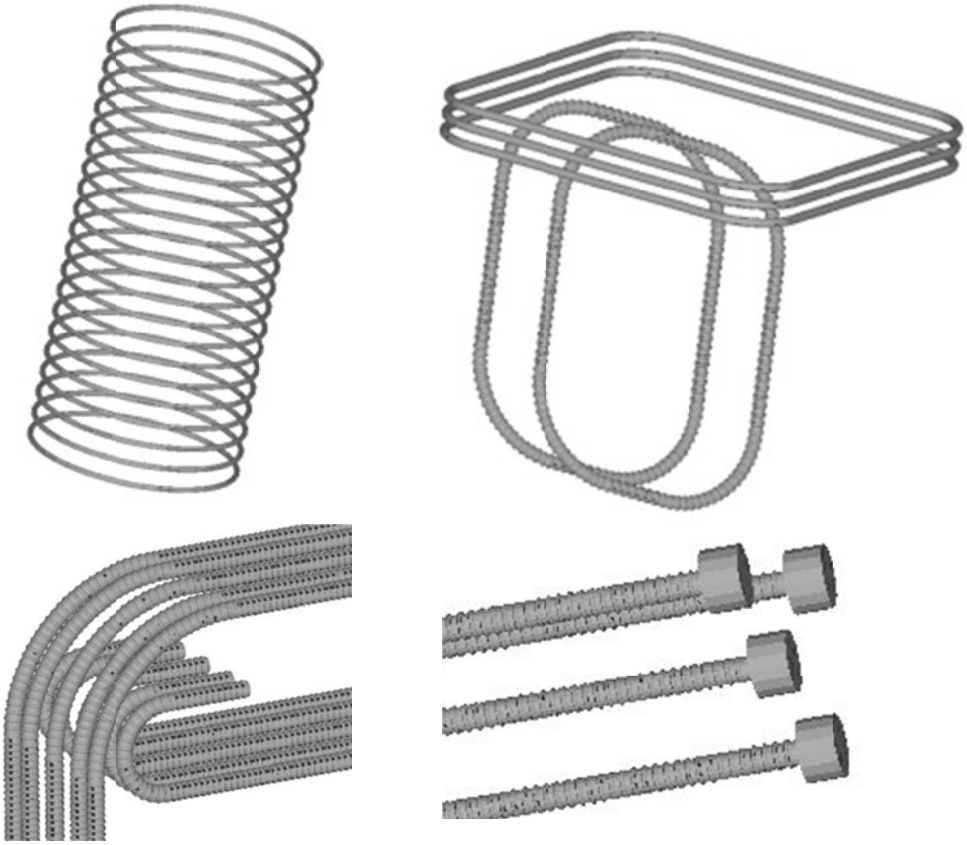

Fig.2.7 3D model of various shapes of reinforcement bars **(a)** Spiral; **(b)** Deformed and plain bars of stirrup; **(c)** Conventional 90 or 180 degree hooked bars; **(d)** Mechanical anchorages

2.5 CONCLUSIONS

1. In this chapter, the concept of selecting mesh size in RBSM is proposed so that rational cracks propagation can be reflected in simulation models that represents the real cracking pattern in concrete. Since the target of this study is normal concrete, 10x10x10 – 20x20x20 mm^3 of mesh size of simulation models is selected to represent the actual cracking propagation in a normal concrete that cracks propagate between 2 aggregates.
2. Simulation has been developed so that 3D RBSM can model the same model and the same reinforcement arrangement as the real condition by simplifying the algorithm of the element meshing of a reinforcement bar.

REFERENCES

Kawai, T., "New Discrete Models and Their Application to Seismic Response Analysis of Structure," *Nuclear Engineering and Design*, 48, 207-229. 1978.

Nagai, K., Sato, Y., and Ueda, T., "Mesoscopic Simulation of Failure of Mortar and Concrete by 3D RBSM," *J. Adv. Conc. Technol.* 3(3):385-402. 2005.

http://www.qhull.org/

Chapter THREE

CONSTITUTIVE MODEL

3.1. CONCRETE MODEL

In this study, a constitutive model for the concrete at the meso scale is developed because the constitutive model in the macro scale cannot be applied to meso scale analysis.

In the analysis, because of the original characteristics of RBSM, the values of the material properties at the meso level given to the elements are different from the material properties of the object analyzed at the macroscopic level. The material properties for the elements were determined in such way as to give the correct macroscopic properties. In discrete analysis, the shape and fineness of elements affect analysis results (Nagai *et al.* 2005).

Since crack direction may affect the crack pattern, the size of each concrete element is approximately 10x10x10 – 20x20x20 mm^3, similar to the maximum aggregate size. The assumption was made to represent the fracture behavior in normal concrete that cracks occur between 2 aggregates because the mortar is weaker than aggregate and it can be assumed that aggregates as rigid bodies in which deformation of aggregates at the meso scale level is very small particularly in normal concrete, subjected to loads.

In the elastic analyses, the relationship between the macroscopic and mesoscopic Poisson's ratios and the effect of the mesoscopic Poisson's ratio on the macroscopic elastic modulus have been confirmed by Nagai *et al*. (2005). The same concepts were adopted, represented in **Eqns. 3.1** and **3.2**

$$\vartheta_{elem} = -24.8\vartheta^4 + 31.9\vartheta^3 - 16.4\vartheta^2 + 4.28\vartheta \quad (3.1)$$

$$E_{elem} = \left(-33.7{\vartheta_{elem}}^4 + 17.0{\vartheta_{elem}}^3 - 4.13{\vartheta_{elem}}^2 + 0.327\vartheta_{elem} + 1\right)E \quad (3.2)$$

where E and ν are the macroscopic elastic modulus and Poisson's ratio of component of the analysis object, respectively.

The material characteristics of each component are presented by means of modeling springs. In normal spring, compressive and tensile stresses (σ) are developed. Shear springs develop shear stress (τ). The elastic modulus of normal spring (k_{nsp} and k_{ssp}) was presented in the previous chapter. For calculation of shear stress on 3D analysis, a resultant value of strains generated in two shear springs in adopted as a shear strain in the constitutive model presented in this chapter. The strains and stresses are calculated as follows.

$$\varepsilon = \frac{\delta_n}{h_1 + h_2}$$
$$\gamma = \frac{\delta_s}{h_1 + h_2} \qquad (3.3)$$
$$\sigma = k_{nsp}\varepsilon$$
$$\tau = k_{ssp}\gamma$$

where ε and γ are the strain of normal and shear springs, respectively. δ_n and δ_s are the normal and shear relative displacement of elements of those springs, respectively.

In this study, the constitutive model of concrete element has been developed based on the some simulations in the material scale level that will be presented at the next chapter. The constitutive models for the normal and shear springs of the concrete elements are shown in **Fig. 3.1.**

The constitutive models of a normal spring and a shear spring of concrete element, used in this study, are shown in Figure 3. Basically, the concept of the concrete model is same as the original simulation developed by Nagai *et al.* (2005) where the compressive failure is not allowed at the meso-scale. In tension zone, crack, between 2 rigid bodies, occurs when the tensile stress of the normal spring exceeds the tensile strength of the concrete (f_t). After exceeding the tensile strength (f_t), the tensile stress of a normal spring is assumed to decrease bi-linearly, depending on the crack width, to zero at the maximum crack width (w_{max}), which is assumed 0.3 mm (see **Fig. 3.1.a**). Meanwhile, an elasto-plastic behavior is assumed for the shear spring of concrete element (see **Fig. 3.1.b**) with the τ_{max} is calculated based on **Eq. 3.4**.

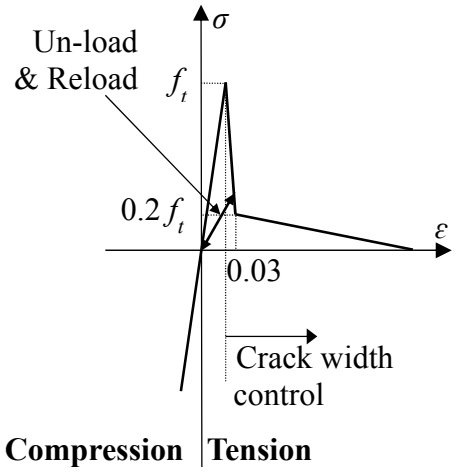

(a) Normal spring

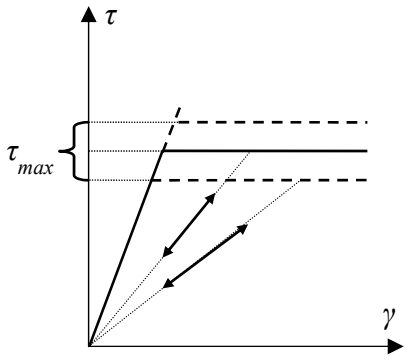

(b) Shear spring

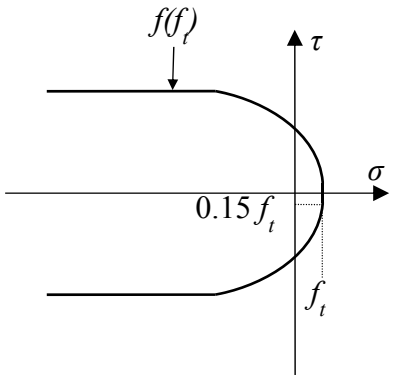

(c) Failure criterion

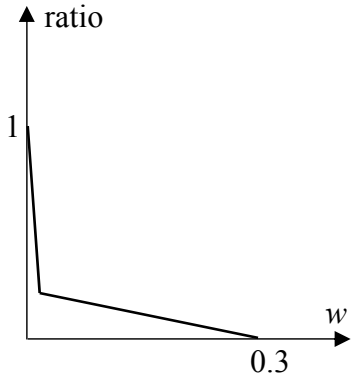

(d) Shear reduction factore

Fig. 3.1 Constitutive models of concrete elements

$$\tau_{max} = \pm\left(1.6{f_{telem}}^2(-\sigma + f_{telem})^{0.4} + 0.15f_{telem}\right) if\ (\sigma \geq 3f_{telem})$$
$$\tau_{max} = \pm\left(1.6{f_{telem}}^2(-3f_{telem} + f_{telem})^{0.4} + 0.15f_{telem}\right) if\ (\sigma < 3f_{telem}) \qquad (3.4)$$

Furthermore, when fracture occurs in the normal spring, the calculated shear stress is reduced according to the reduction of the normal stress. As the result, shear spring cannot carry the stress when the crack width of the normal spring reaches w_{max} (see **Fig. 3.1.d**).

In next chapter, a parametric study is also done to examine the effect of parameters in constitutive models through simulations both in material scale and in structural scale. For constitutive models of concrete, a parametric study will be done not only for the constitutive model of normal springs but also for the constitutive model of shear spring.

3.2. STEEL MODEL

The geometry of steel elements is modeled in an accurate manner to properly account for the interlocking between the reinforcement and concrete. In this study, the strain hardening region is introduced so that the normal springs of steel elements are assumed to behave as the same as the actual steel (**Fig. 3.2**). Meanwhile, the shear springs are assumed to be perfectly elastic.

The constitutive model of the normal spring used in this simulation is represented by the following equations (adopted from *Shima et al.* 1987).

$$\begin{aligned} \sigma &= E_s \varepsilon && if\ (\varepsilon < \varepsilon_y) \\ \sigma &= f_y && if\ (\varepsilon_y < \varepsilon < \varepsilon_{sh}) \\ \sigma &= f_y + \left(1 - e^{\frac{\varepsilon_{sh}-\varepsilon}{k}}\right)\left(1.01 f_u - f_y\right) && if\ (\varepsilon > \varepsilon_{sh}) \end{aligned} \tag{3.5}$$

where

k : $0.032(400/f_y)^{1/3}$

σ : stress (MPa)

ε : strain

f_y : yield strength (MPa)

f_u : tensile strength (MPa)

ε_{sh} : initial strain of hardening, assumed 1.5%

As the comparison, the effect of modeling strain hardening region will be investigated through the simulation of tension stiffening and simulation of structural scale, i.e. simulation of beam column joint with mechanical anchorage (**Fig. 3.3**).

3.3. CONCRETE-STEEL INTERFACE

At concrete-steel interface, the constitutive model of a normal spring and a shear spring is considered to be the same as that of the concrete element. To consider the interface as a weak region, the tensile strength of the interface elements is assumed to be half of that of concrete elements in this study. **Fig.3.4** shows constitutive model of the interface elements.

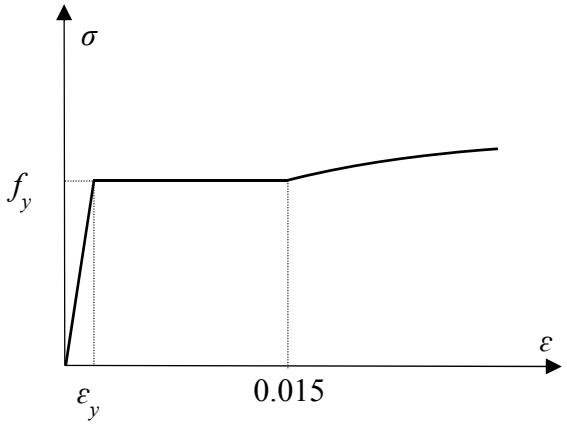

Fig. 3.2 Constitutive models of normal springs of steel elements (with strain hardening region)

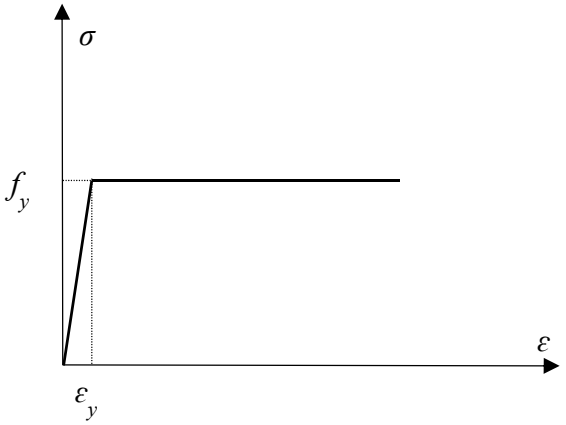

Fig. 3.3 Constitutive models of normals spring of steel elements (without strain hardening region)

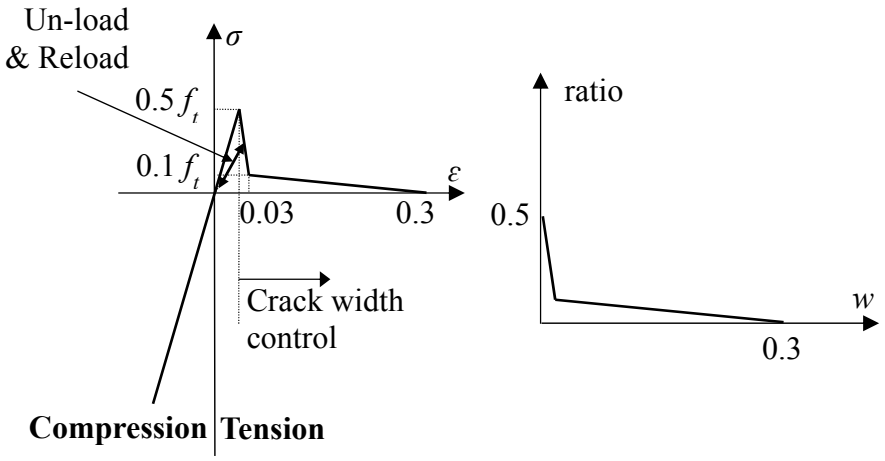

(a) Normal spring **(b)** Shear reduction factor

Fig. 3.4 Constitutive models of concrete-steel interface

3.4. CONCLUSIONS

Constitutive models have been improved based on the some simulations in the material scale of concrete, and bond between concrete and steel.

REFERENCES

Shima, H., Chou, L. L., and Okamura, H., "Micro and macro models for bond in reinforced concrete," *Journal of the Faculty of Engineering*, *39*(2), 133-194.

Nagai, K., Sato, Y., and Ueda, T., "Mesoscopic Simulation of Failure of Mortar and Concrete by 3D RBSM," *J. Adv. Conc. Technol.* 3(3), 385-402., 2005.

Chapter FOUR

SIMULATION OF CONCRETE AT MATERIAL SCALE

4.1 INTRODUCTION

In this chapter, three-dimensional simulations of concrete are conducted. The purpose of this study is for the prediction of the behavior of concrete, especially in uniaxial compression, uniaxial tension, and biaxial compression. The modified Newton-Raphson method is used as the convergence algorithm nonlinear analysis. Convergence criterion and the maximum iteration number are set to 10^{-5} and 400 in this study. Displacement of loading boundary is controlled in the analysis.

4.2 OVERVIEW OF EXPERIMENT STUDIES OF BIAXIAL STRENGTH OF CONCRETE BY KUPFER ET AL (1969)

As the initial step, it is necessary to check the reliability of 3D RBSM in simulating biaxial stress condition since the target of this study is the simulation of beam column joint where biaxial stress condition exists in this region which develops because of the combination of concrete compressive stresses and reinforcement bars tensile stresses. The reliability of 3D RBSM will be checked through the comparison with the experimental results done by Kupfer *et al.* (1969). Kupfer *et al.* (1969) conducted experimental studies of the biaxial strength of concrete by introducing a new testing apparatus by using "brush bearing plate". These plates consist of a series of closely spaced small steel bars with 3 x 5 mm of cross section and from 100 to 140 mm of length variation which are flexible enough so that concrete can deform without any restraint due to friction between the plates and concrete that can increase the apparent strength of the test piece.

The dimension of the concrete specimens in these experimental studies was 20x20x5 cm and the target of uniaxial compressive strength of concrete 190, 315, and 590 kg/cm^2. The maximum aggregate size was 15 mm. As described above, the length of the small steel bars in the brush bearing plate were varied. To test concrete with higher compressive strength, shorter steel bars were used to prevent buckling of the steel bars.

To verify the applicability this new apparatus, 20x20x5 cm of concrete specimens were

tested under uniaxial compression condition with and without brush bearing plates. Furthermore, the compressive strength of the concrete with brush bearing plates should be equal to that of without bearing plates in order to prove that the boundary condition had no additional restraint to the specimens.

In the experiment, the ratio of σ_1/σ_2 was maintained constant throughout the test. The experimental results show that the compressive strength of concrete increased approximately 16 percent under biaxial compressive stress. Meanwhile, the tensile strength of concrete under biaxial tensile stress was equal to that of uniaxial tensile stress. Furthermore, the results did not change significantly with different compressive strength of concrete.

4.3 DETAIL OF NUMERICAL MODELS

4.4.1 *Numerical Models*

In total of eight numerical models with different tensile strength of springs were simulated under uniaxial compressive loading and biaxial compressive loading. Four numerical models were simulated under uniaxial compressive loading and other four numerical models were simulated under biaxial compressive loading. By setting the tensile strength of springs in meso-scale, the uniaxial compressive strength and uniaxial tensile strength of concrete in macro-scale were obtained. The relationship between the compressive strength and the tensile strength which was obtained at the same tensile strength of springs will be compared with that of JSCE (2007) equation.

$$f_t = 0.23 {f_c}^{2/3} \tag{4.1}$$

Meanwhile, the biaxial compressive strength of simulation results will be compared with that of experimental results done by Kupfer *et al.* (1969).

4.4.2 *Geometry of Numerical Models*

Figs. 4.1 and 4.2 show the geometry of the simulation models for uniaxial test and biaxial test, respectively. The dimension of simulation model for uniaxial test is 150x150x300mm, and the dimension of simulation model for biaxial test is 400x400x100 which is twice than that of experimental specimens done by Kupfer *et al.*

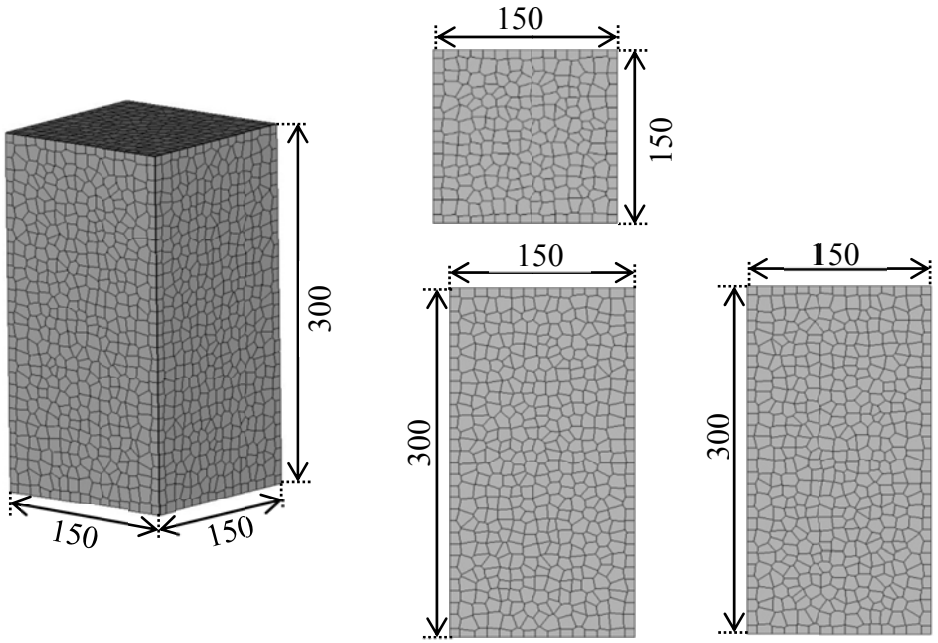

Fig.4.1 Geometry of numerical model of uniaxial test (Units: mm)

(1969). The tensile strengths of springs are set in 0.5 MPa increments from 2 MPa to 3.5MPa which represents the range of strength of normal concrete. Numbers of elements of uniaxial models and biaxial models are 6750 elements and 16000 elements, respectively.

4.4.3 *Boundary condition*

Figs. 4.3 and 4.4 show the boundary condition of simulation models for uniaxial test and biaxial test, respectively. In case of uniaxial test, fixed condition in all directions is assumed at the bottom of the models. Monotonic displacement-loading is applied at the top of the models. Displacement is increased by 0.002 mm at each loading step. 600 steps of loading displacement-loading are applied in the simulation of uniaxial compression test. Meanwhile, 200 steps of loading displacement-loading are applied in the simulation of uniaxial tension test.

In case of biaxial test, steel plates were modeled located at the four sides of the numerical models which are the same as experimental specimens. The stiffness of the steel plates was assumed rigid enough, so that the deformation of the steel plates will be prevented. In order to model frictionless between the steel plates and the models, forces are transferred only through normal springs between the steel plates and the models. To check the applicability of this boundary condition, the same concept as experimental

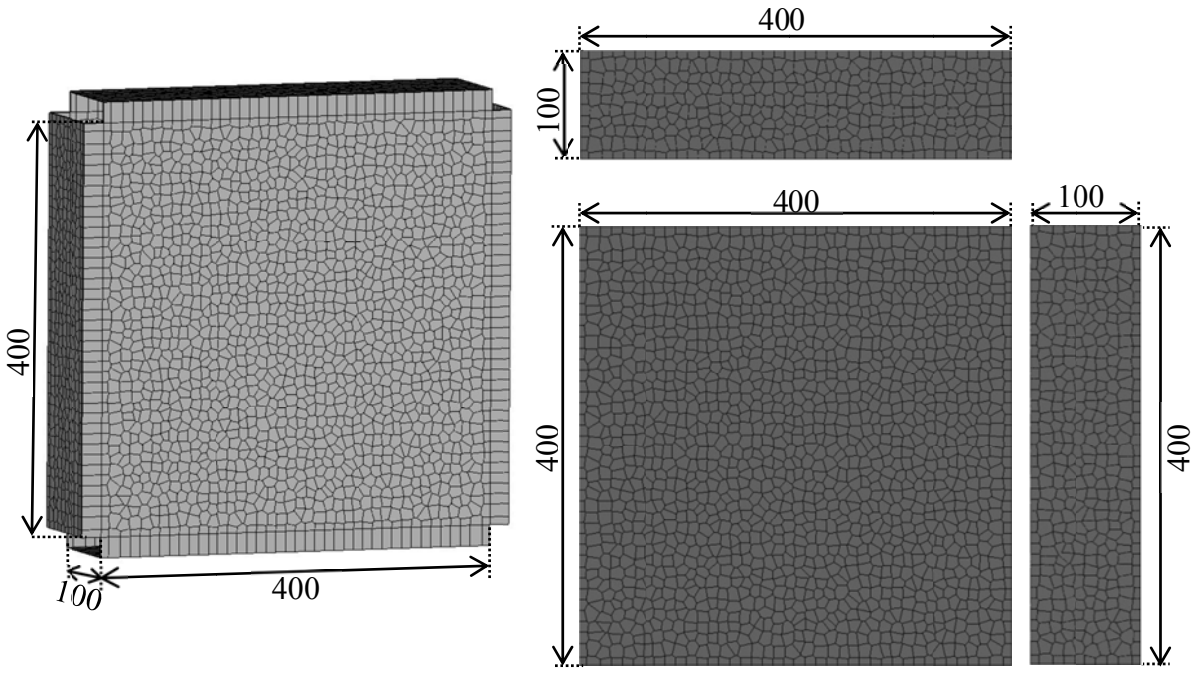

Fig.4.2 Geometry of numerical model of biaxial test (Units: mm)

tests is adopted that the uniaxial compressive strength of concrete with steel plates should be equal to that of without steel plates. Fixed in all directions is assume at the bottom side of models. Monotonic displacement-loading is applied to the left side, top side, and top side. The ratio of σ_1/σ_2 was maintained constant throughout the simulation which is the same as the experimental tests. 600 steps of loading displacement-loading are applied.

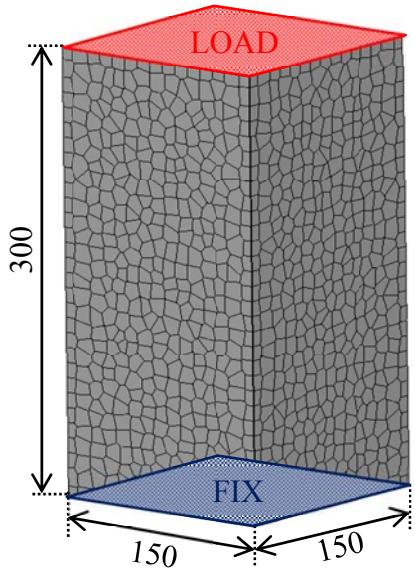

Fig.4.3 Boundary condition of numerical model of uniaxial test (Units: mm)

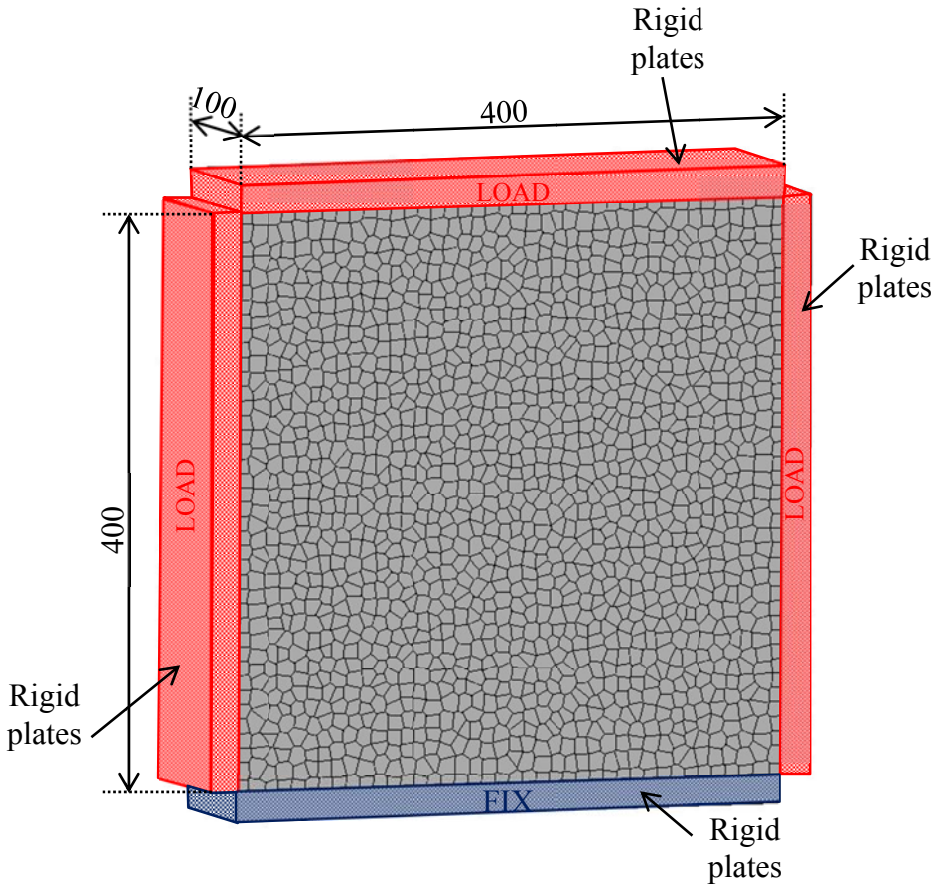

Fig.4.4 Boundary condition of numerical model of biaxial test (Units: mm)

As described before, in order to check whether the boundary condition may affect the simulation results, uniaxial compressive loading test is conducted for this numerical model with and without the steel plates. The simulation was conducted by setting 2 MPa of tensile strength of springs. **Fig. 4.5** shows the stress-strain relationship of simulation results. The stress-strain relationship of simulation result with bearing plates does not differ significantly with that of without bearing plate. It can be concluded that frictionless condition can be obtained by setting no shear stress between the steel plates and concrete.

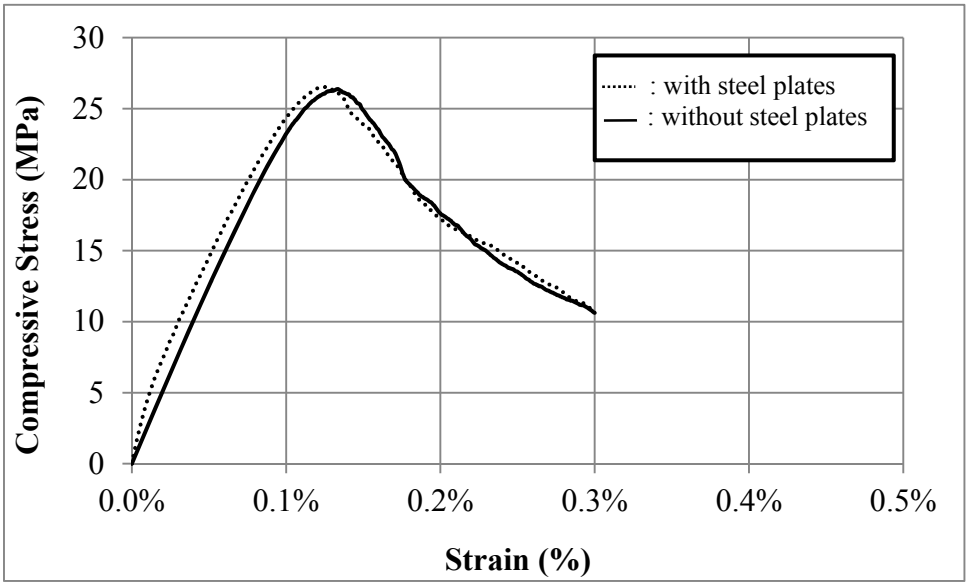

Fig.4.5 Uniaxial compressive strength with and without steel plates

4.4 RESULT AND DISCUSSION

4.4.1 *Uniaxial Compression and Tension Test*

Figs. 4.6 and **4.7** show the stress-strain relationships of uniaxial compression and tension test of numerical models, respectively, by setting different tensile strength of springs, i.e. 2 MPa, 2.5MPa, 3 MPa, and 3.5 MPa.

The stress of stress-strain relationships was determined based on the load which was applied on the top surface of models divided by the area of the top surface of the numerical models. The strain of stress-strain relationships was calculated based on the displacement which was applied on the top surface of models divided by the initial length of the numerical models. The maximum stresses of numerical models were predicted at a strain between 0.12% until 0.3%.

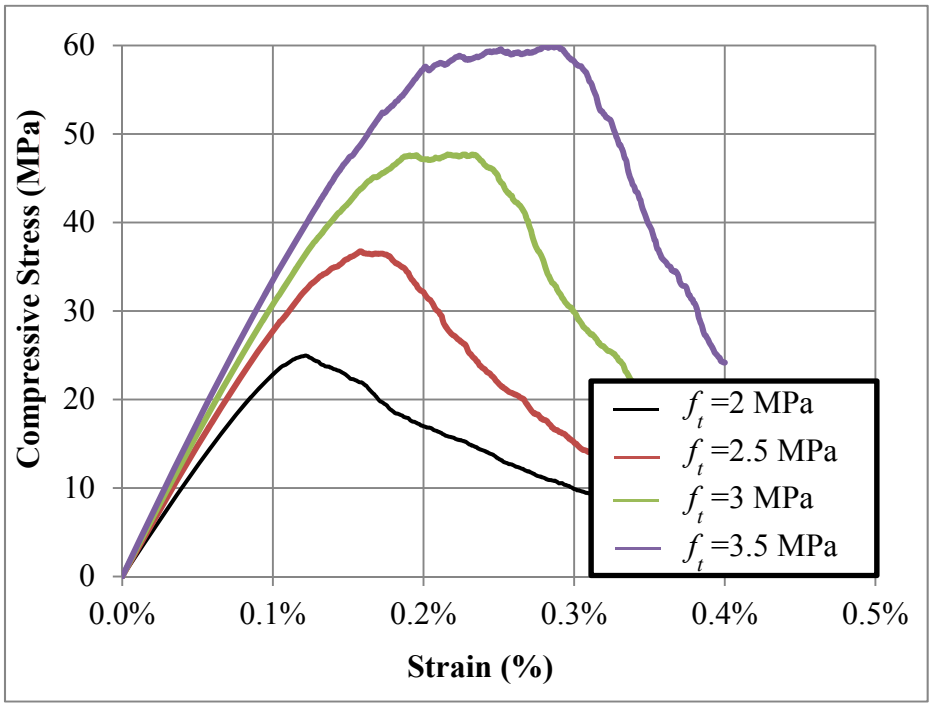

Fig.4.6 Simulation results of uniaxial compressive stress-strain relationship of concrete

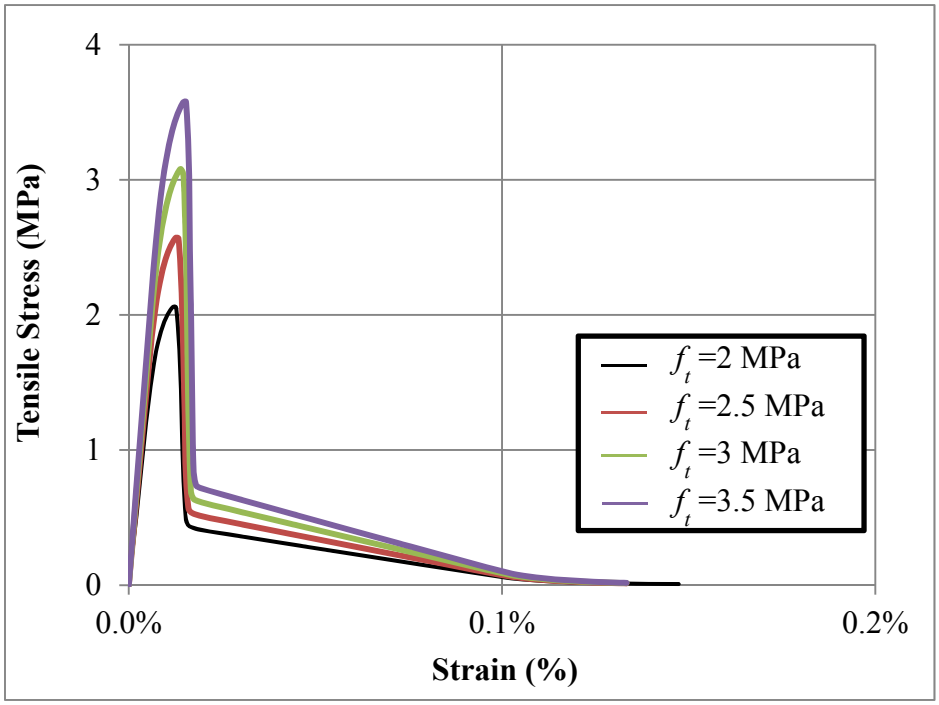

Fig.4.7 Simulation results of uniaxial tensile stress-strain relationship of concrete

Table.4.1 Uniaxial compressive and tensile strength of simulation predictions

f_t of springs (MPa)	Simulation Prediction		JSCE equation	
	Comp.strength (MPa)	Tensile strength (MPa)	Comp.strength (MPa)	Tensile strength (MPa)
2	24.96	2.06	25.6	2
2.5	36.90	2.57	35.8	2.5
3	47.68	3.08	47	3
3.5	60.01	3.58	59.25	3.5

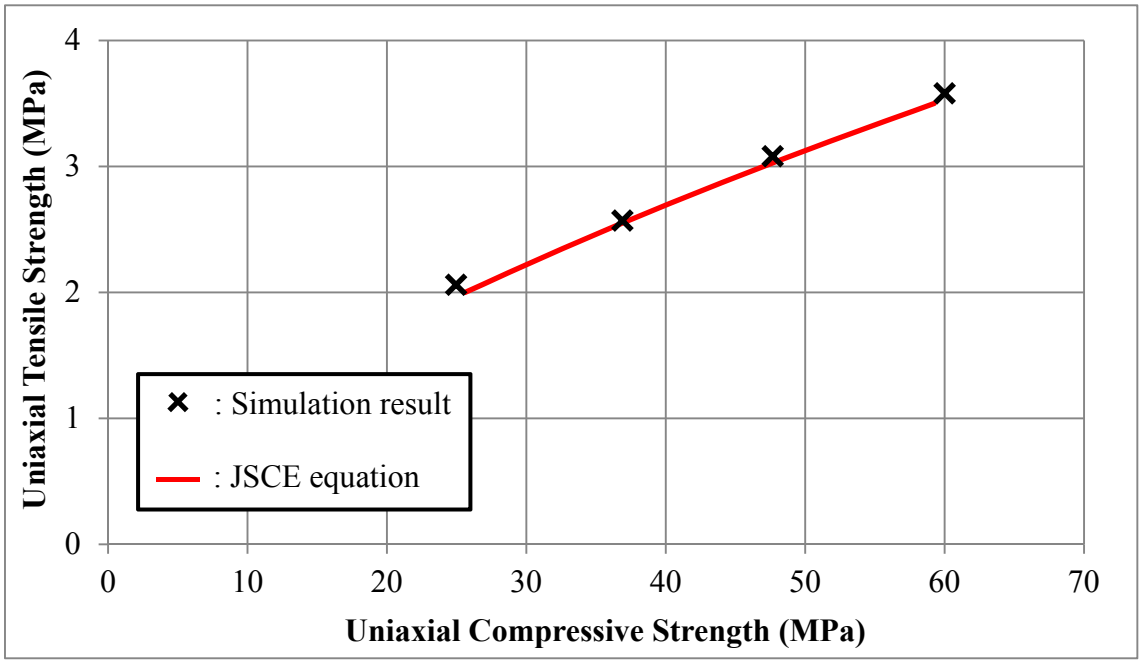

Fig.4.8 Relationship of compressive and tensile strength of concrete

Table.4.1 and Fig.4.8 show the relationship of the uniaxial compressive and tensile strength at the same tensile strength of springs, compared with that of JSCE equation. The simulation results are in a good agreement with the relationship of uniaxial compressive strength and uniaxial tensile strength proposed by JSCE equation. Furthermore, **Figs.4.9** and **4.10** show the surface cracks of numerical models after failure in case of uniaxial compressive loading and uniaxial tensile loading, respectively.

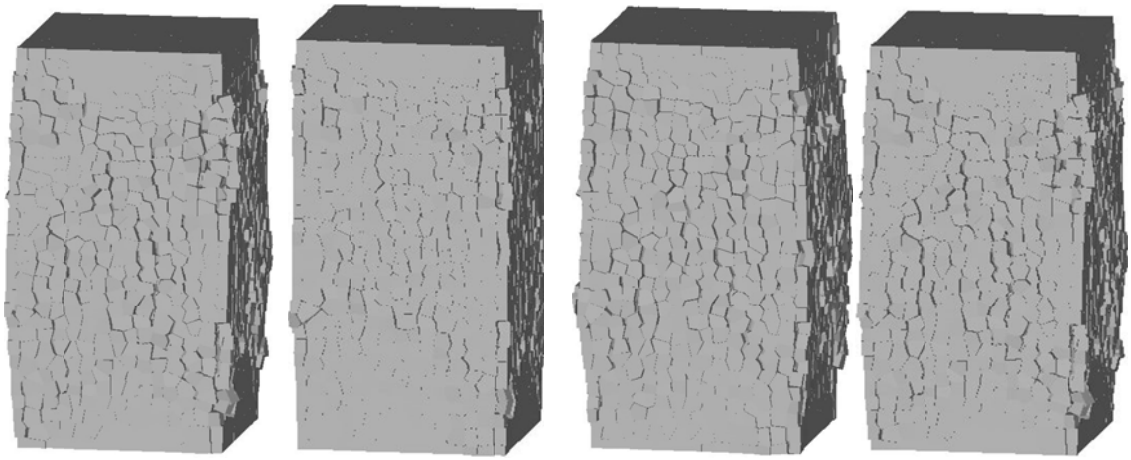

(a) f_t =2 MPa **(b)** f_t =2.5 MPa **(c)** f_t =3 MPa **(d)** f_t =3.5 MPa

Fig.4.9 Surface cracks after failure in case of uniaxial compressive loading (Def.×5)

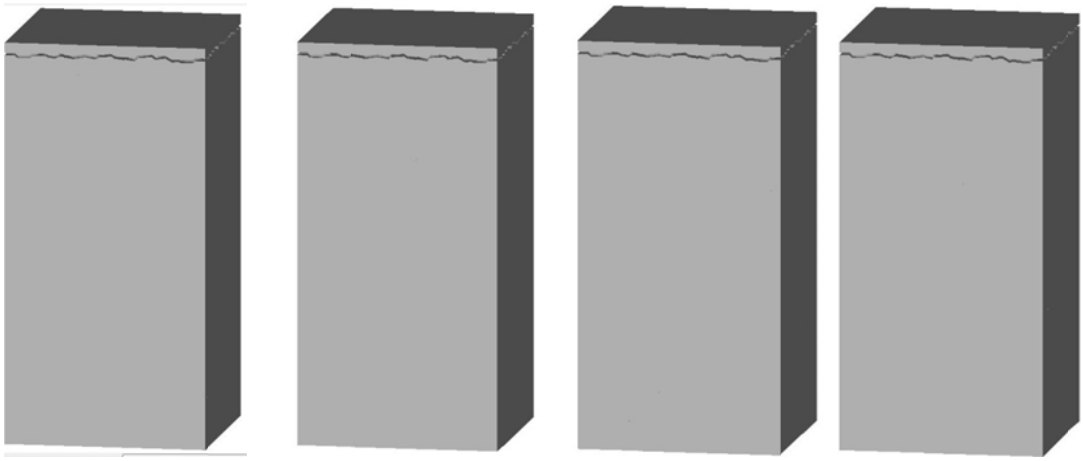

(a) f_t =2 MPa **(b)** f_t =2.5 MPa **(c)** f_t =3 MPa **(d)** f_t =3.5 MPa

Fig.4.10 Surface cracks after failure in case of uniaxial tensile loading (Def.×5)

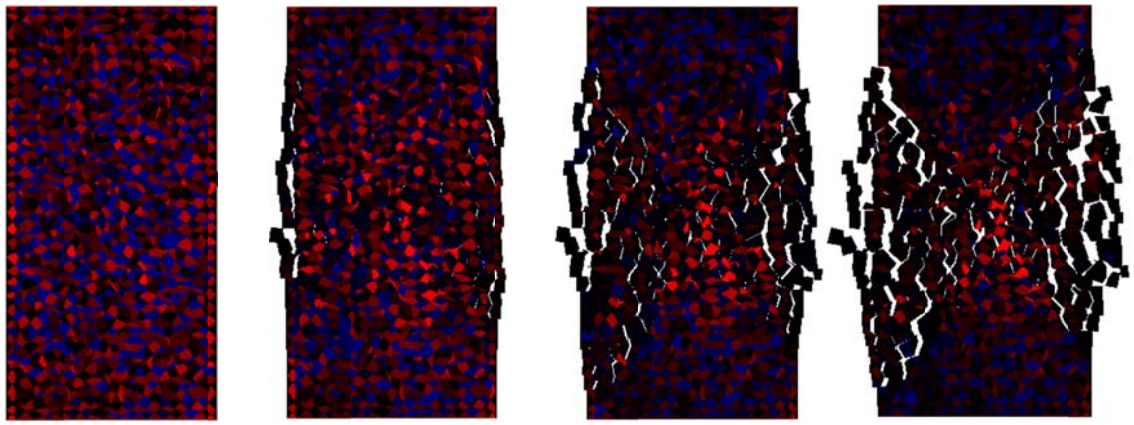

ε = 0.1% ε = 0.2% ε = 0.3% ε = 0.4%

(a) f_t = 2 MPa

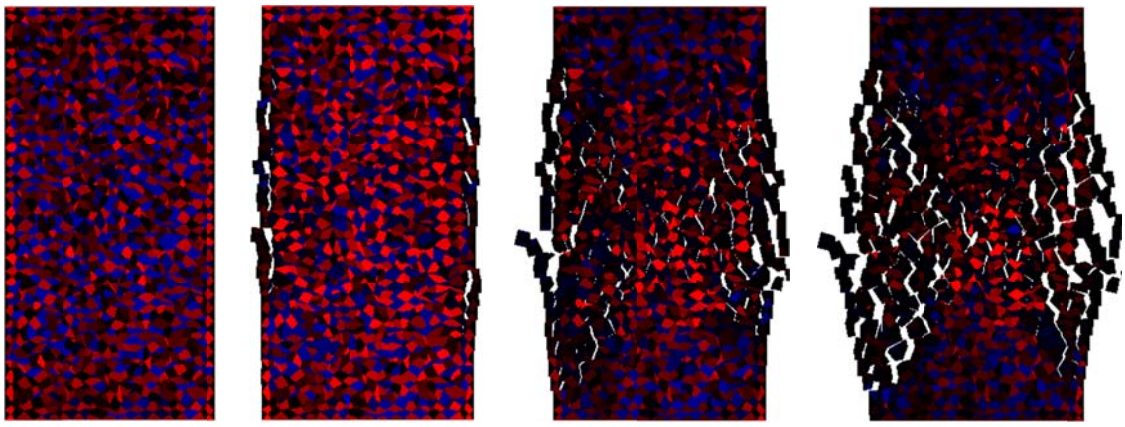

ε = 0.1% ε = 0.2% ε = 0.3% ε = 0.4%

(b) f_t = 2.5 MPa

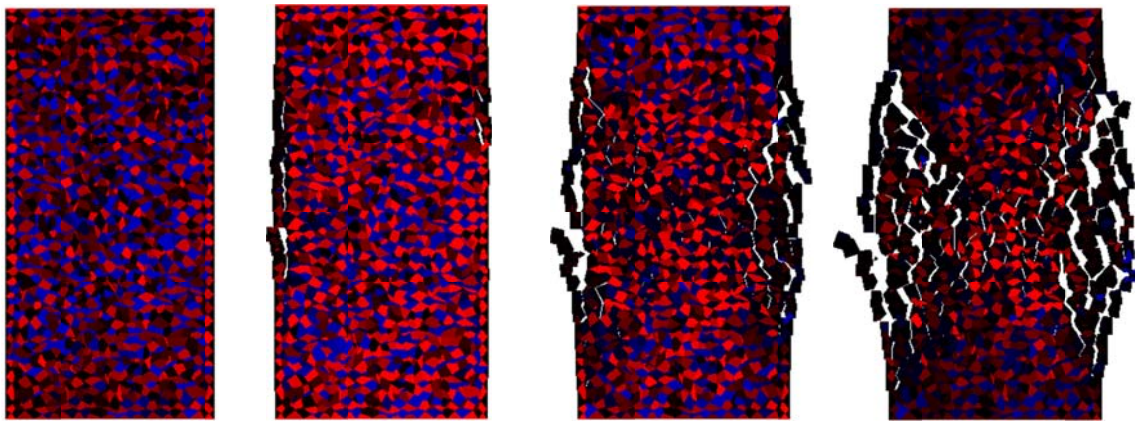

ε = 0.1% ε = 0.2% ε = 0.3% ε = 0.4%

(c) f_t = 3 MPa

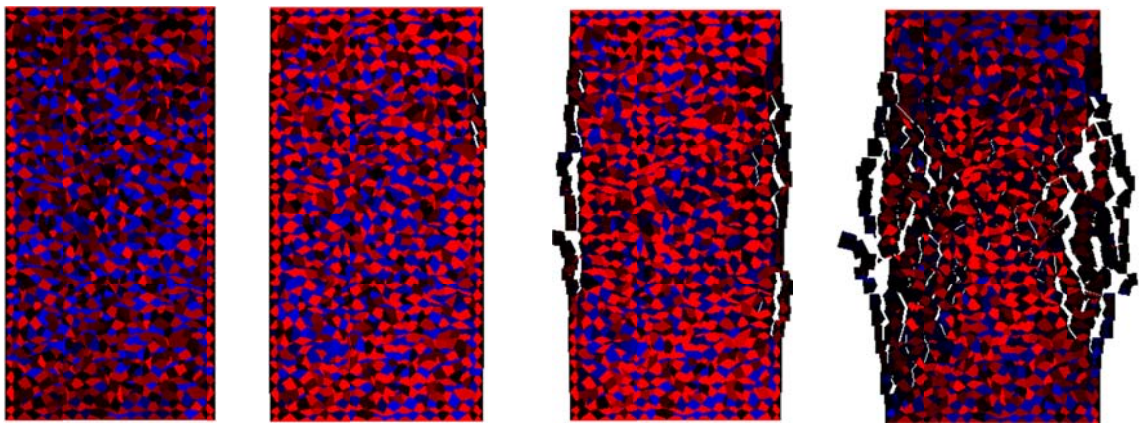

ε = 0.1% ε = 0.2% ε = 0.3% ε = 0.4%

4MPa 50MPa

Tension Comp.

(d) f_t = 3.5 MPa

Fig.4.11 Internal stress and internal cracking in case of uniaxial compressive loading (Deformation × 10)

Fig.4.11 shows the internal stress and internal cracking of numerical models subjected to uniaxial compressive loading. When the load is relatively small, no cracks occur in the numerical models. As the load increases, the slopes of the stress-strain relationships changes as the result of the formation of microcracks in the numerical models. Furthermore, splitting cracks which are parallel to the loading direction are predicted. After failure, diagonal shear cracks were predicted in the numerical models as the result of the interaction of the normal stress and the shear stress in the models.

4.4.2 *Biaxial Compression Test*

Figs. 4.12, 4.13, 4.14, and 4.15 show the stress-strain relationships of biaxial compression tests of numerical models when the tensile strength of springs is 2 MPa, 2.5MPa, 3 MPa, and 3.5 MPa, respectively. The stress of stress-strain relationships was determined based on the load which was applied on the top surface of models divided by the area of the top surface of the numerical models. In this study, the stress applied on the top surface of models is equal to the stress applied on the left side or the right side of the models. The strain of stress-strain relationships was calculated based on the displacement which was applied on the top surface of models divided by the initial length of the numerical models. **Table 4.2** shows the biaxial compressive strength of concrete, predicted by the simulation results.

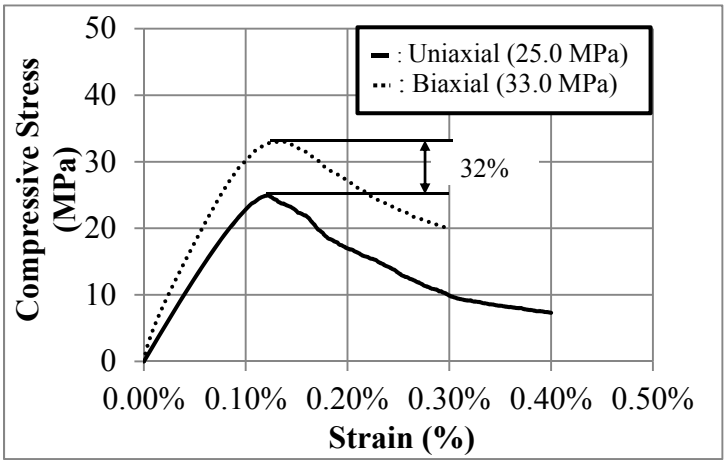

Fig.4.12 Biaxial compressive strength of concrete (tensile strength of spring 2 MPa)

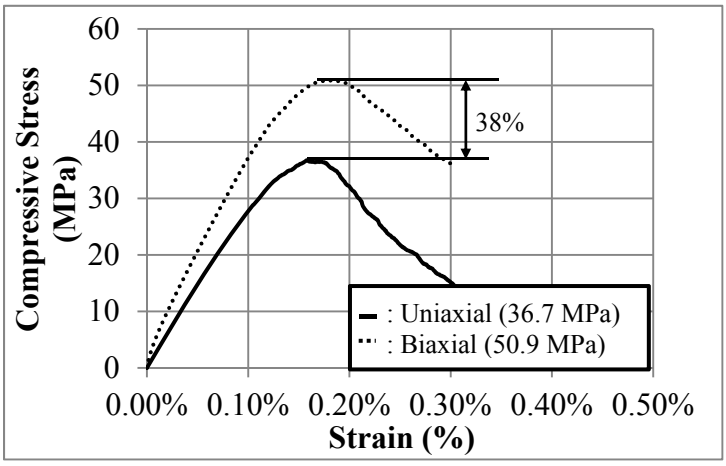

Fig.4.13 Biaxial compressive strength of concrete (tensile strength of spring 2.5 MPa)

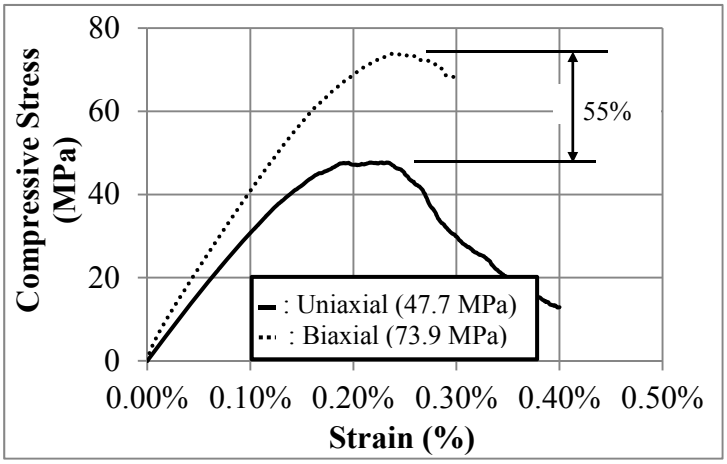

Fig.4.14 Biaxial compressive strength of concrete (tensile strength of spring 3 MPa)

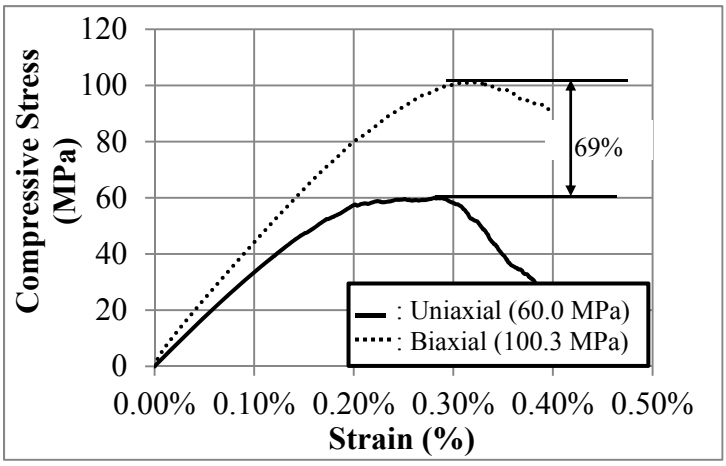

Fig.4.15 Biaxial compressive strength of concrete (tensile strength of spring 3.5 MPa)

Table.4.2 Biaxial compressive strength of simulation results

f_t of springs (MPa)	Uniaxial Compressive Strength (MPa)	Biaxial Compressive Strength (MPa)	Ratio (Biaxial/Uniaxial)
2	24.96	33.03	1.32
2.5	36.90	50.87	1.38
3	47.68	73.85	1.55
3.5	60.01	101.23	1.69

Based on the simulation results, the strength of concrete subjected to equal biaxial compressive stresses increases approximately by 32%-69% depending on the compressive strength of concrete. Higher compressive strength of concrete shows higher strength increase. Meanwhile, in the experimental results conducted by Kuper *et al.* (1969), the compressive strength subjected to equal biaxial stress increases by 16% which is not depended on the compressive strength of concrete. In case of smaller compressive strength of concrete, i.e. 2 MPa and 2.5 MPa, simulation results are almost the same as the experimental results. However in case of higher compressive strength of concrete, i.e. 3 MPa and 3.5 MPa, simulation results overestimate compared with experimental results.

Figs.4.16 and **4.17** show internal cracks and surface cracks of numerical models after failure. The simulation results predict that major cracks parallel to the loading condition occur. This behavior is in a good agreement with experiments done by Kupfer *et al.* (1969).

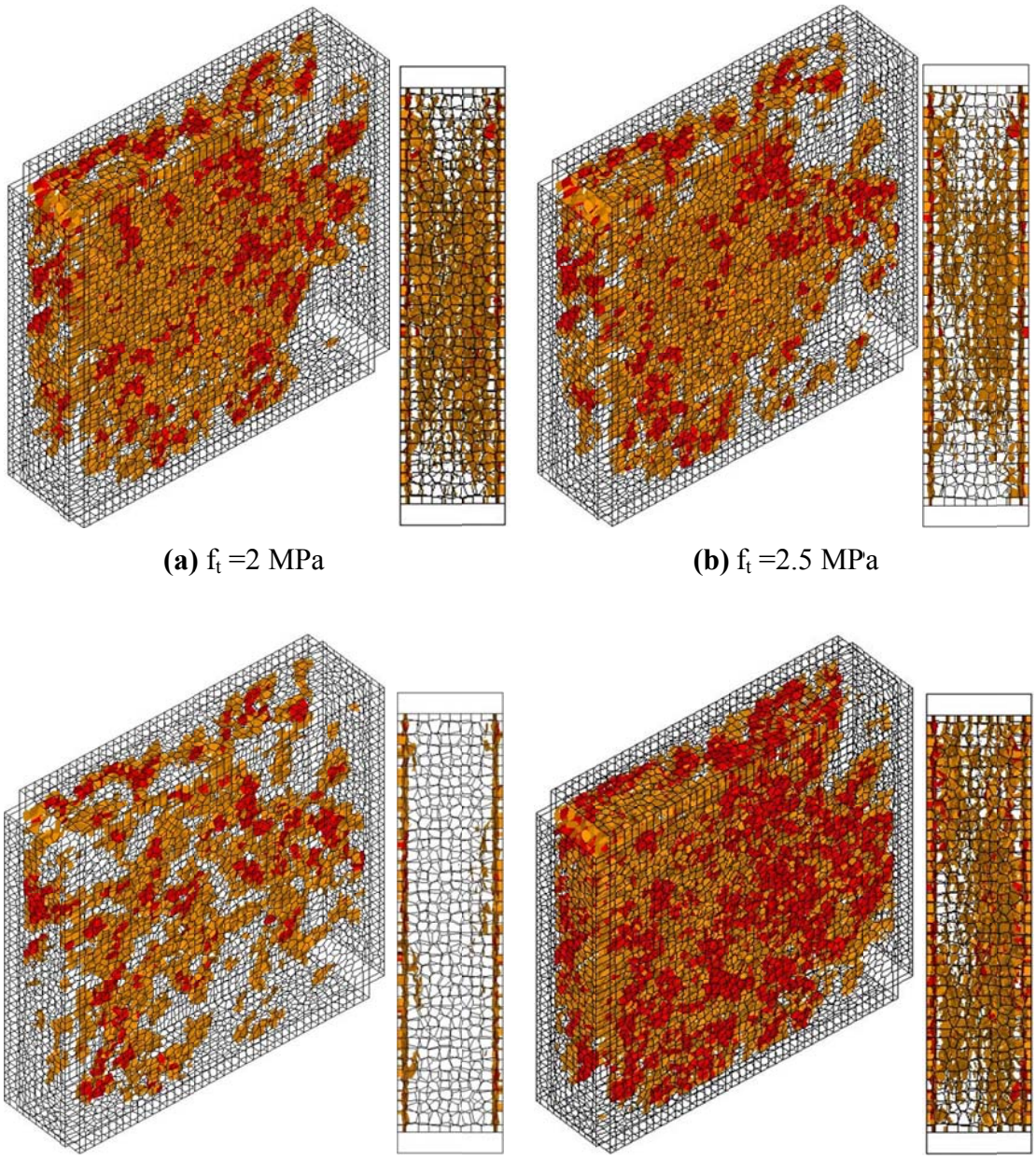

(a) f_t =2 MPa **(b)** f_t =2.5 MPa

(c) f_t =3 MPa **(b)** f_t =3.5 MPa

Fig.4.16 Internal cracks after failure in case of biaxial compressive loading

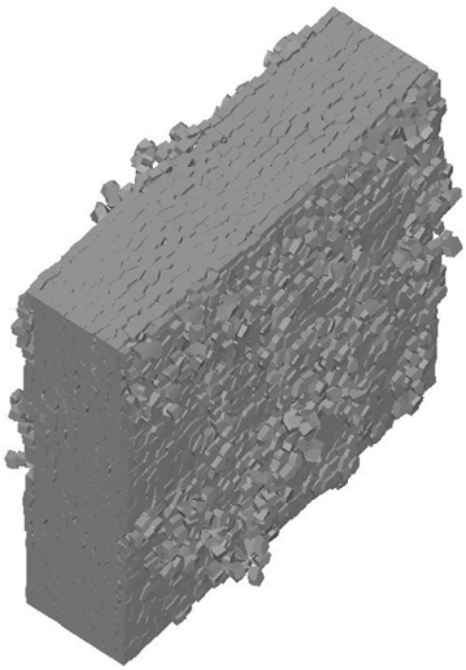

(a) f_t =2 MPa

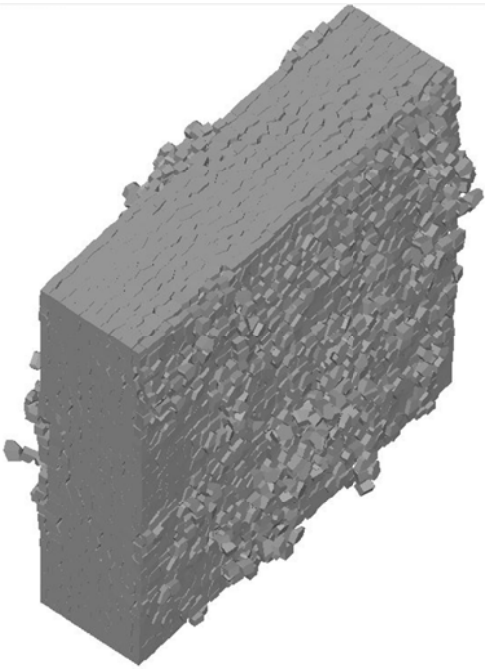

(b) f_t =2.5 MPa

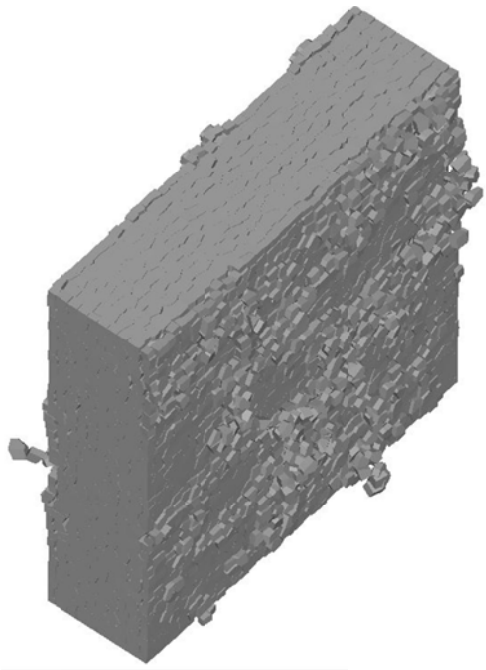

(c) f_t =3 MPa

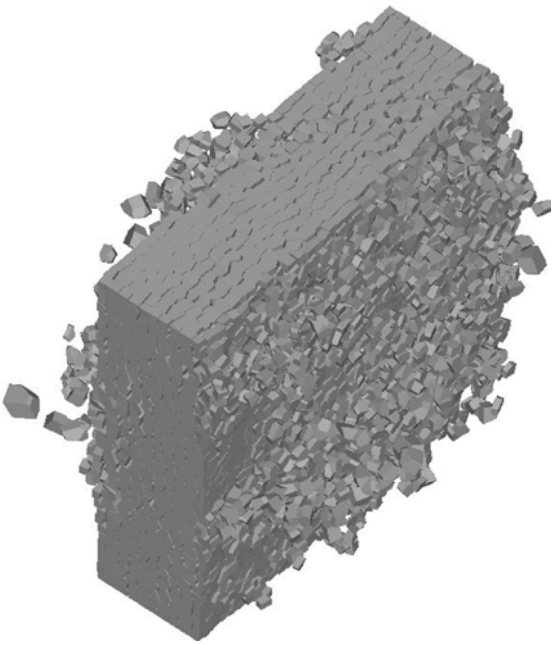

(d) f_t =3.5 MPa

Fig.4.17 Surface cracks after failure in case of biaxial compressive loading (Def.×10)

4.5 POISSON'S RATIO

Fig. 4.19 shows the lateral deformation and the Poisson's ration of numerical models subjected to uniaxial compressive loading when the tensile strength of springs is 2 MPa,

2.5MPa, 3 MPa, and 3.5 MPa, respectively. **Fig. 4.20** shows the lateral deformation and the Poisson's ration of numerical models subjected to uniaxial tensile loading when the tensile strength of springs is 2 MPa, 2.5MPa, 3 MPa, and 3.5 MPa, respectively. Lateral strains are calculated by the relative deformation between elements A and B in **Fig. 4.18** and Poisson's ratio is calculated by dividing the lateral strain by the axial strain of concrete.

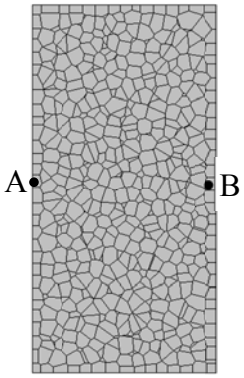

Fig.4.18 Middle cross section of numerical models

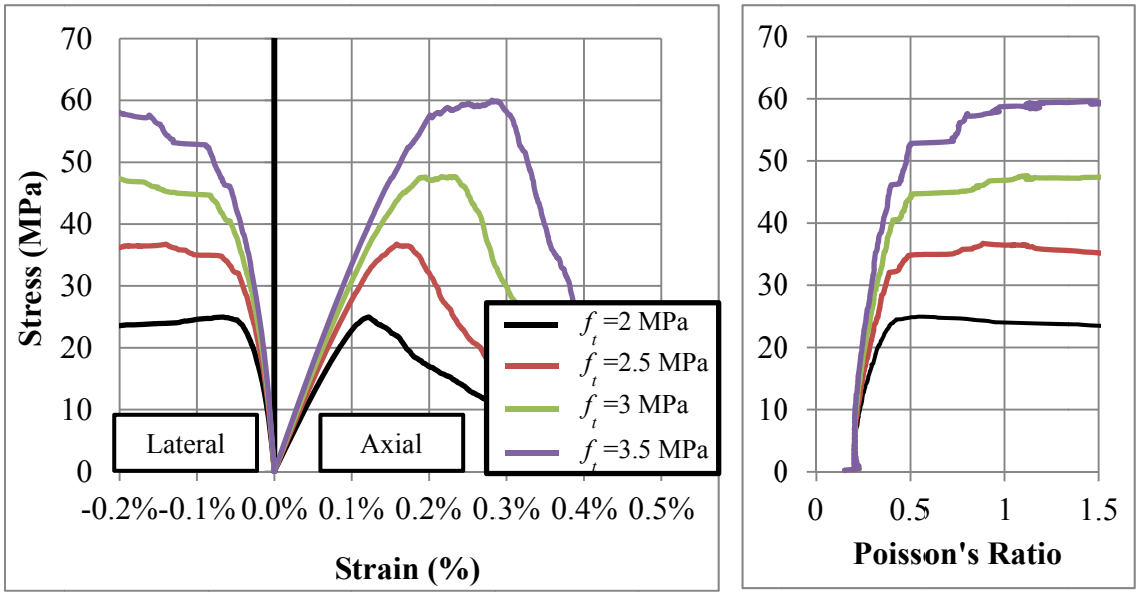

(a) Stress-strain curves **(b)** Poisson's Ratio

Fig.4.19 Lateral deformation and Poisson's ratio under uniaxial compression

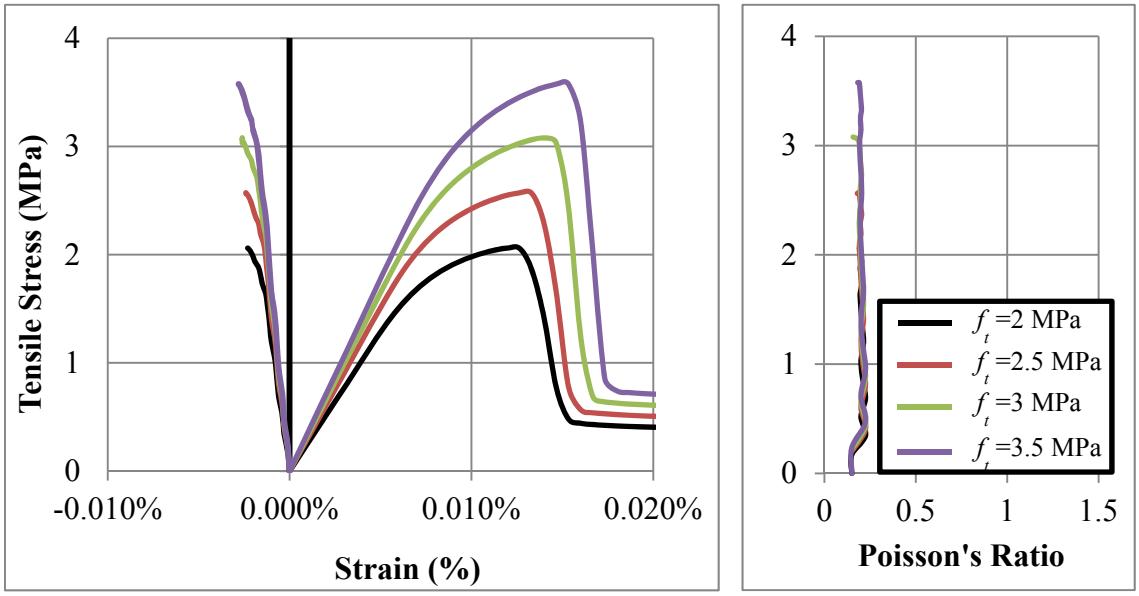

(a) Stress-strain curves **(b)** Poisson's Ratio

Fig.4.20 Lateral deformation and Poisson's ratio under uniaxial tension

When the load is relatively small, the simulation results predict the value of Poisson's ratio is predicted in the range of 0.15-0.25 subjected to uniaxial compressive loading. As the load increases, around 80%-90% of its capacity, because of the beginning of the formation the splitting cracks that are parallel to the loading direction, the Poisson's ratio increases. When the numerical models are loaded with uniaxial tensile loading, the simulation results predict that the Poisson's ratios are almost constant until the loads reach the maximum load.

4.6 EFFECT OF MESH ARRANGEMENT

The mesh arrangement may affect the simulation results because in this study the voronoi points were introduced randomly. In order to check whether the mesh arrangement may affect the simulation results, 5 numerical models with different arrangement will be investigated through the comparison of stress-strain relationship, internal stress, and surface cracks. Numerical models will be loaded by uniaxial compressive loading and uniaxial tension loading. **Fig.4.21** shows the cross section of numerical models with different mesh arrangements. Simulations are conducted only for 2.5 MPa of tensile strength of springs.

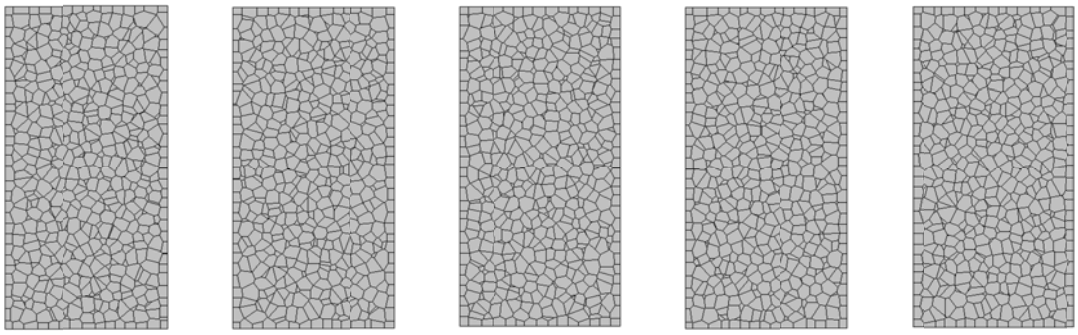

(a) Model 1 **(b)** Model 2 **(c)** Model 3 **(d)** Model 4 **(e)** Model 5

Fig.4.21 Numerical models with different mesh arrangements

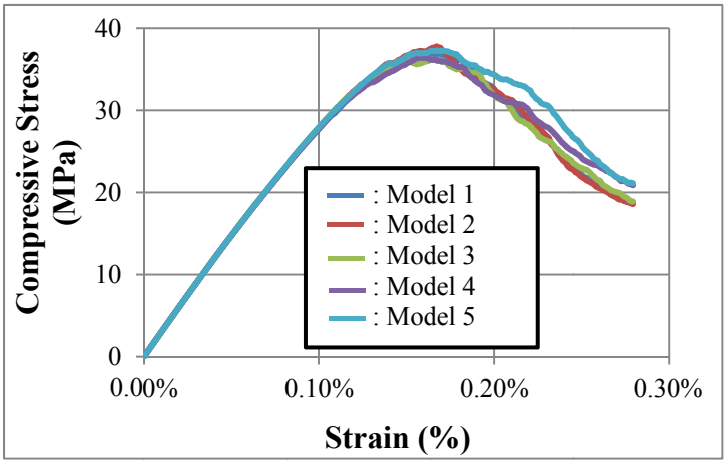

Fig.4.22 Stress-strain relationship of uniaxial compressive loading with different mesh arrangements

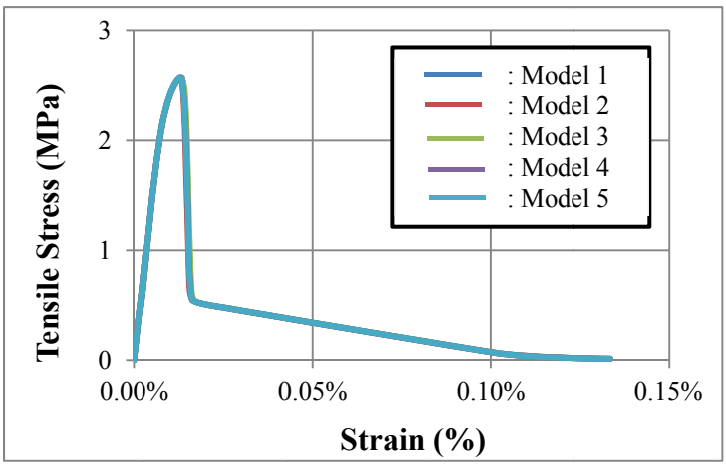

Fig.4.23 Stress-strain relationship of uniaxial tensile loading with different mesh arrangements

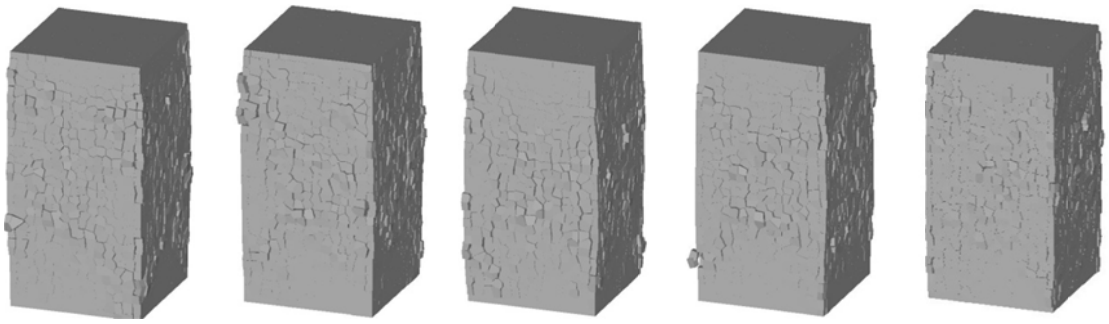

(a) Model 1 **(b)** Model 2 **(c)** Model 3 **(d)** Model 4 **(e)** Model 5

Fig.4.24 Surface cracks after failure in case of uniaxial compressive loading with different mesh arrangement (Def.×5)

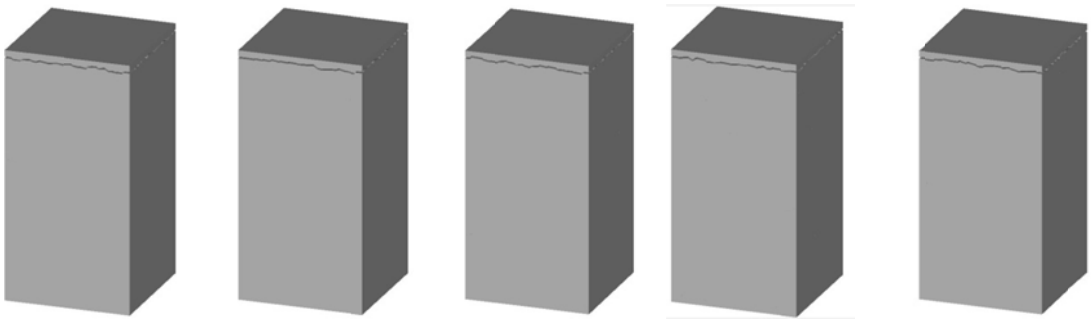

(a) Model 1 **(b)** Model 2 **(c)** Model 3 **(d)** Model 4 **(e)** Model 5

Fig.4.25 Surface cracks after failure in case of uniaxial tensile loading with different mesh arrangement (Def.×5)

Figs. 4.22 and 4.23 show the stress-strain relationships of numerical models with different mesh arrangement subjected to uniaxial compressive and tensile loading, respectively. Based on the stress-strain relationships either in case of uniaxial compressive loading or uniaxial tensile loading, there is no significant difference of macroscopic response. Small difference is predicted at approximately 80% of the ultimate load. **Figs. 4.24 and 4.25** show the surface cracks of numerical models with different mesh arrangement subjected to uniaxial compressive and tensile loading, respectively. Diagonal shear cracks that usually occur are predicted in all numerical models subjected to uniaxial compressive loading. Local cracking patterns are slightly different due to different mesh arrangement.

4.7 EFFECT OF FAILURE CRITERION OF CONCRETE

Before proposing constitutive models of concrete elements, some parametric studies were conducted to examine the effect of parameters on the concrete behavior subjected

to uniaxial compressive loading, uniaxial tensile loading, and biaxial loading. In this chapter, a parametric study is conducted for the constitutive model of the failure criterion of concrete. The effect of this constitutive model will be investigated. **Fig. 4.26** shows different failure criteria of concrete that becomes a parametric study in this chapter. The study will be done for all cases of tensile strength of springs, i.e. 2MPa, 2.5 MPa 3MPa, 3.5 MPa. Nagai *et al.* (2005) signifies constitutive model that proposed by Nagai *et al.* (2005) (**Eq.4.2**). The proposed constitutive model will be signified by Proposal (**Eq.4.3**). Trial signifies the proposed constitutive model without capping in compression (**Eq.4.4**).

$$\tau_{max} = \pm\left(0.3{f_{telem}}^{2.5}(-\sigma + f_{telem})^{0.4} + 0.15f_{telem}\right) \tag{4.2}$$

$$\tau_{max} = \pm\left(1.6{f_{telem}}^{2}(-\sigma + f_{telem})^{0.4} + 0.15f_{telem}\right) if\ (\sigma \geq 3f_{telem})$$
$$\tau_{max} = \pm\left(1.6{f_{telem}}^{2}(-3f_{telem} + f_{telem})^{0.4} + 0.15f_{telem}\right) if\ (\sigma < 3f_{telem}) \tag{4.3}$$

$$\tau_{max} = \pm\left(1.6{f_{telem}}^{2}(-\sigma + f_{telem})^{0.4} + 0.15f_{telem}\right) \tag{4.4}$$

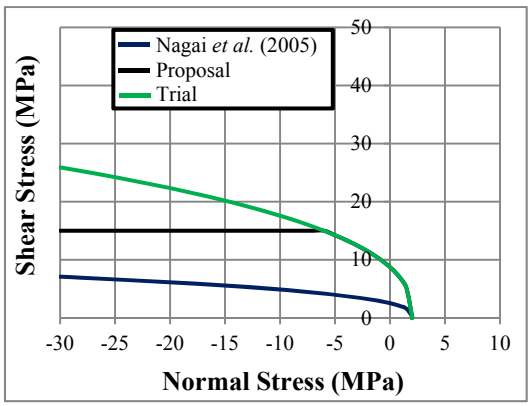

(a) f_t =2 MPa

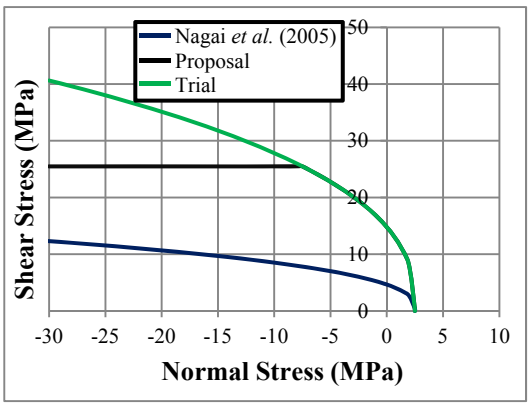

(b) f_t =2.5 MPa

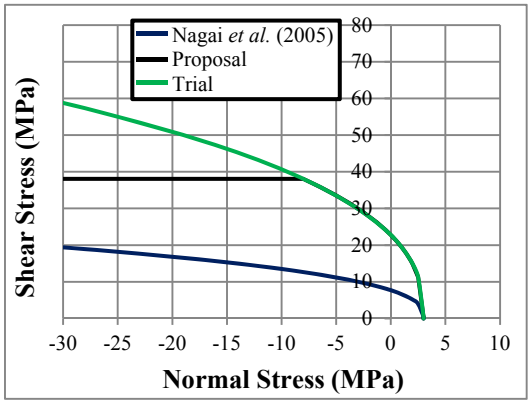

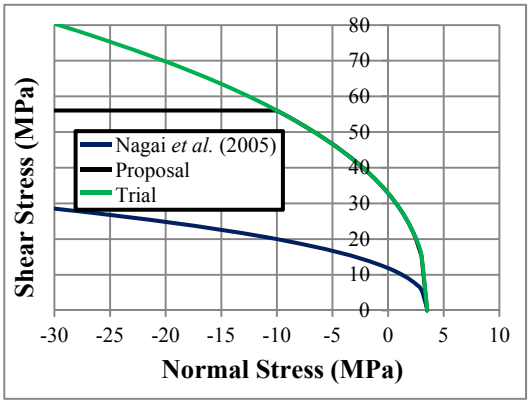

(c) f_t =3 MPa **(d)** f_t =3.5 MPa

Fig.4.26 Different failure criteria of concrete

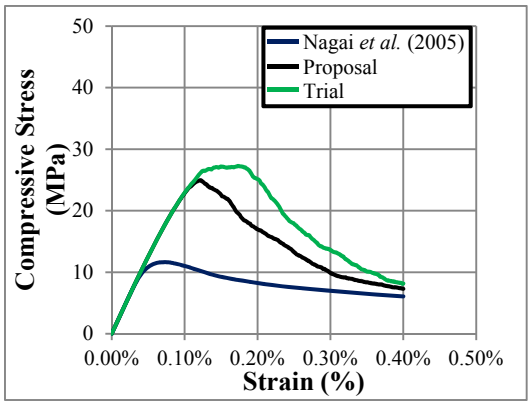

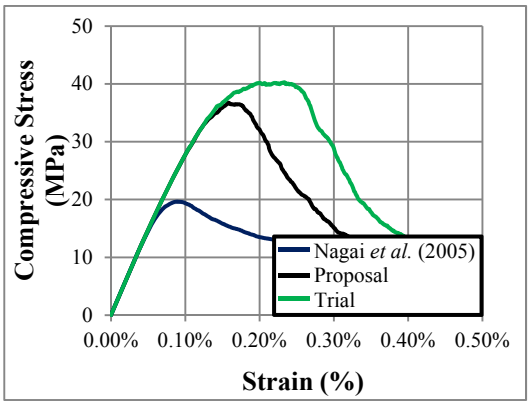

(a) f_t =2 MPa **(b)** f_t =2.5 MPa

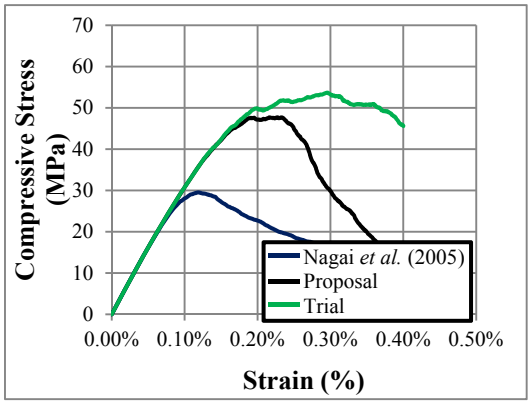

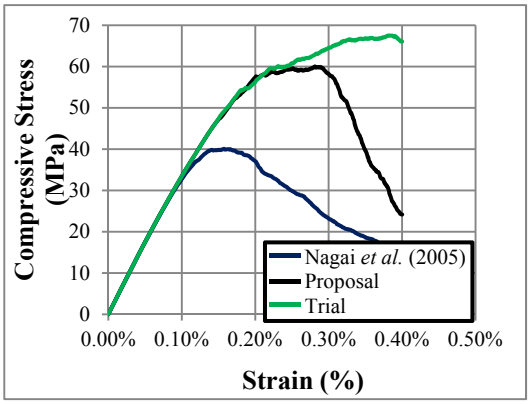

(c) f_t =3 MPa **(d)** f_t =3.5 MPa

Fig.4.27 Uniaxial compressive stress-strain relationships of concrete with different failure criteria

Table 4.3 Uniaxial compressive strength of concrete with different failure criteria

Tensile strength of springs (MPa)	Nagai *et al.* (2005)	Proposal	Trial
2	11.64	24.96	27.27
2.5	19.63	36.90	40.26
3	29.52	47.68	53.68
3.5	40.04	60.01	67.51

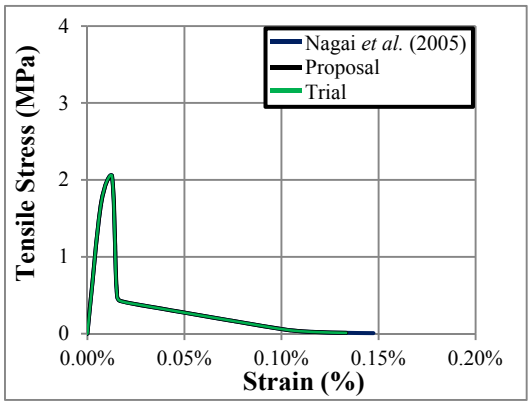

(a) f_t =2 MPa

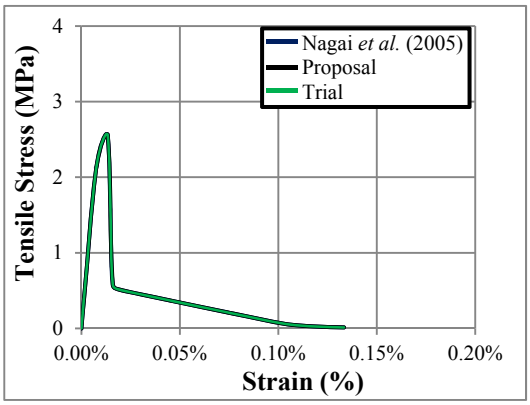

(b) f_t =2.5 MPa

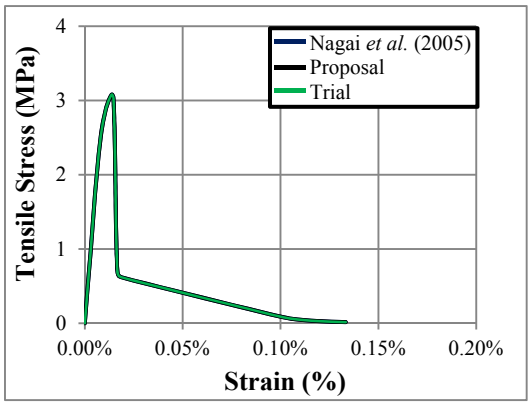

(c) f_t =3 MPa

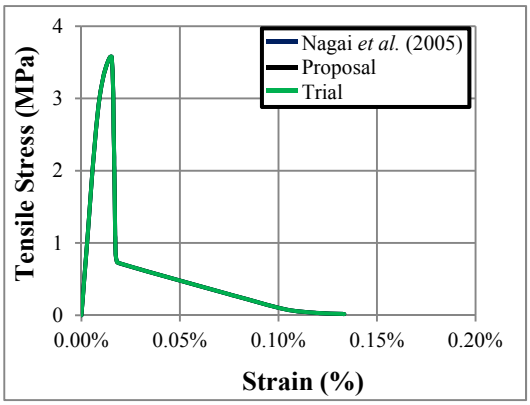

(d) f_t =3.5 MPa

Fig.4.28 Uniaxial tensile stress-strain relationships of concrete with different failure criteria

Figs. 4.27 and 4.28 show the stress-strain relationships of simulation results when the numerical models are loaded with uniaxial compressive and tensile load, respectively with different failure criteria. **Table 4.3** shows the uniaxial compressive strength of concrete with different failure criteria. Based on the uniaxial tensile stress-strain relationships of simulation results, the failure criterion of concrete does not affect the

behavior of uniaxial tensile stress-strain of concrete in macroscopic level. On the other hand, the failure criterion of concrete affects significantly the behavior of uniaxial compressive stress-strain of concrete in macroscopic response. By increasing the failure criterion of concrete, it is well understood that uniaxial compressive stress of concrete will increase because the failure of concrete will be delayed and simulation results predict the same tendency. However, simulation results predict that the uniaxial compressive strength of failure criterion without capping in compression increases only by 10% compared with that of with capping in compression.

Figs. 4.29, 4.30, and 4.31 show the stress-strain relationships of simulation results when the numerical models are loaded with biaxial compressive load with different failure criteria, i.e. failure criterion model-1, failure criterion model-2, and failure criterion model-3., respectively. By increasing the failure criterion of concrete, the biaxial compressive strength also increases which is the same phenomenon as the uniaxial compression because the failure of concrete will be delayed. Furthermore, by capping the failure criterion in compression zone causes earlier failure of concrete which results the biaxial compressive strength is lower compared with in case of failure criterion without capping in compression zone. The simulation predicts that strengths of concrete under biaxial compression vary from 30 percent to 42 percent larger than that of the uniaxial compression strength in case of failure criterion model-1. In case of failure criterion model-2, the strengths of concrete under biaxial compression vary from 32 percent to 69 percent larger than that of the uniaxial compression strength and in case of failure criterion model-3, the strengths of concrete under biaxial compression vary from 62 percent to more than 84 percent larger than that of the uniaxial compression strength.

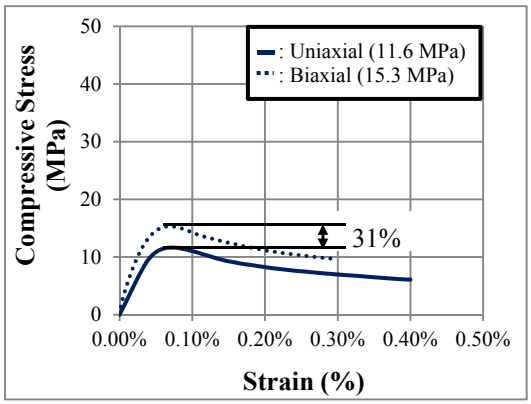

(a) f_t =2 MPa

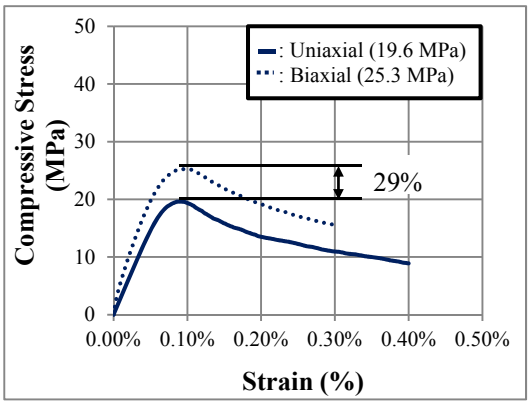

(b) f_t =2.5 MPa

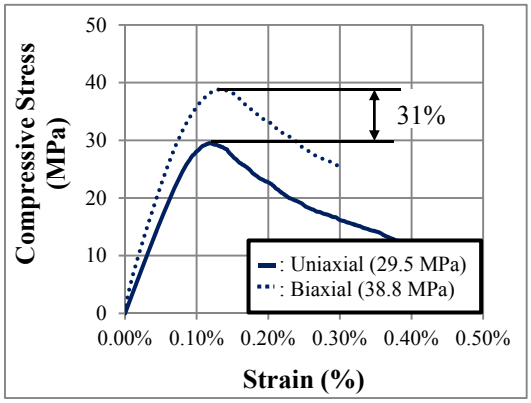

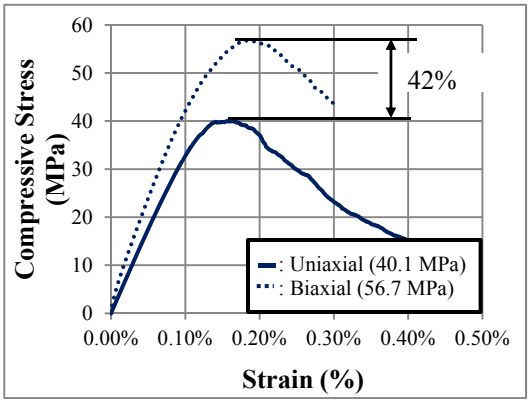

(c) f_t =3 MPa **(d)** f_t =3.5 MPa

Fig.4.29 Stress-strain relationship of uniaxial and biaxial compression of failure criterion model-1

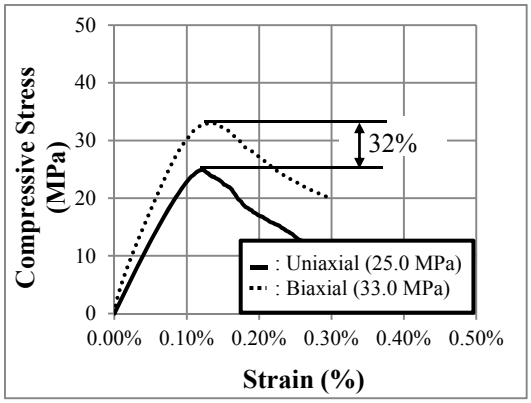

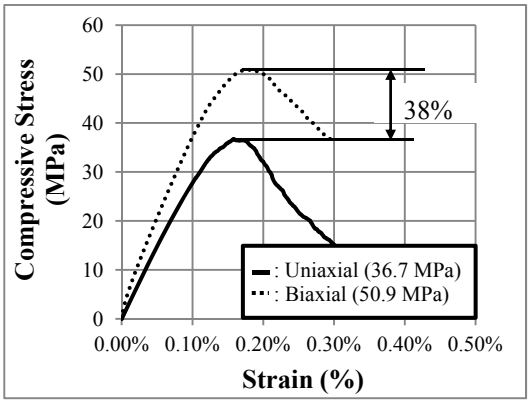

(a) f_t =2 MPa **(b)** f_t =2.5 MPa

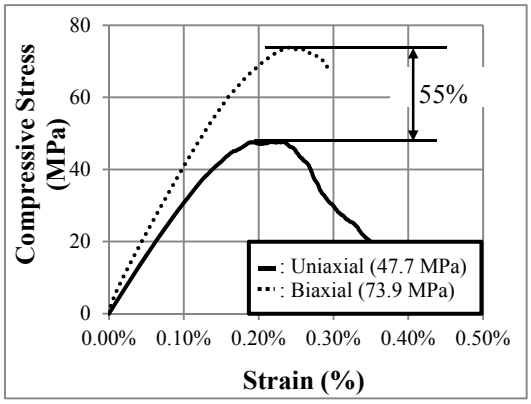

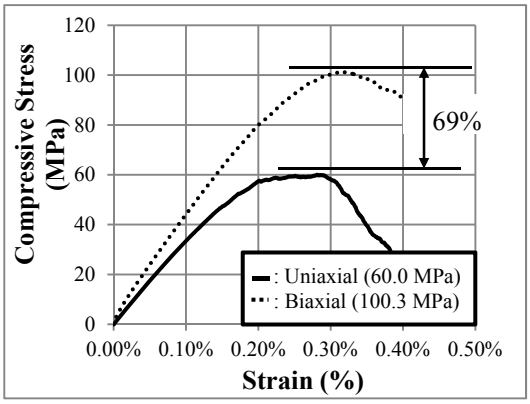

(c) f_t =3 MPa **(d)** f_t =3.5 MPa

Fig.4.30 Stress-strain relationship of uniaxial and biaxial compression of failure criterion model-2

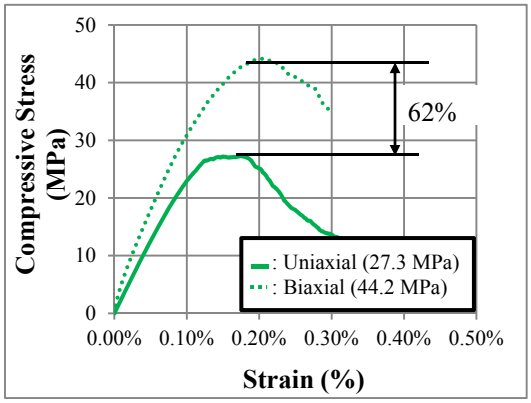

(a) f_t =2 MPa

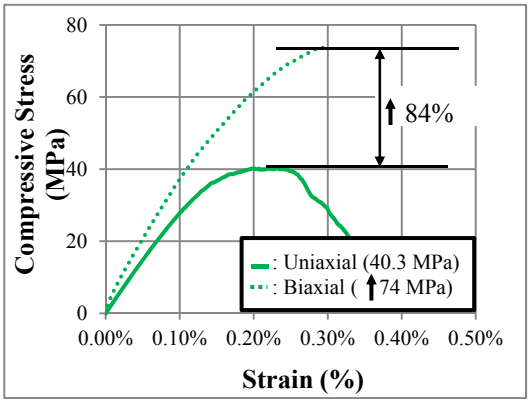

(b) f_t =2.5 MPa

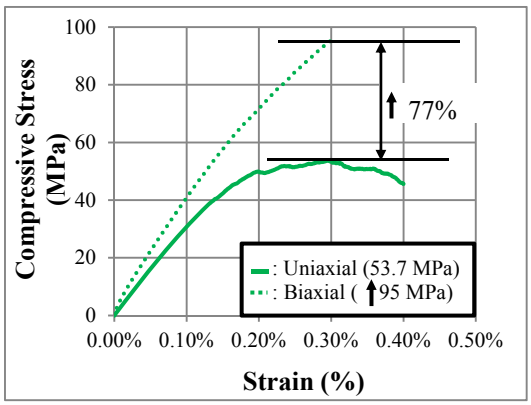

(c) f_t =3 MPa

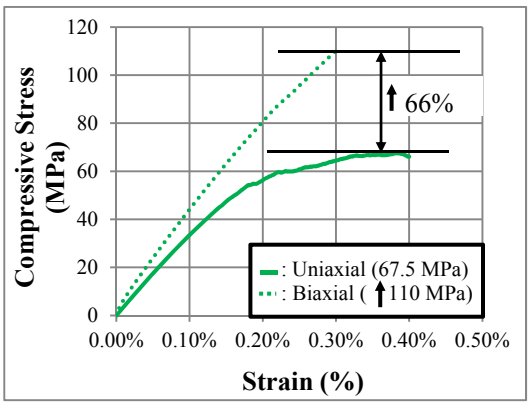

(d) f_t =3.5 MPa

Fig.4.31 Stress-strain relationship of uniaxial and biaxial compression of failure criterion model-3

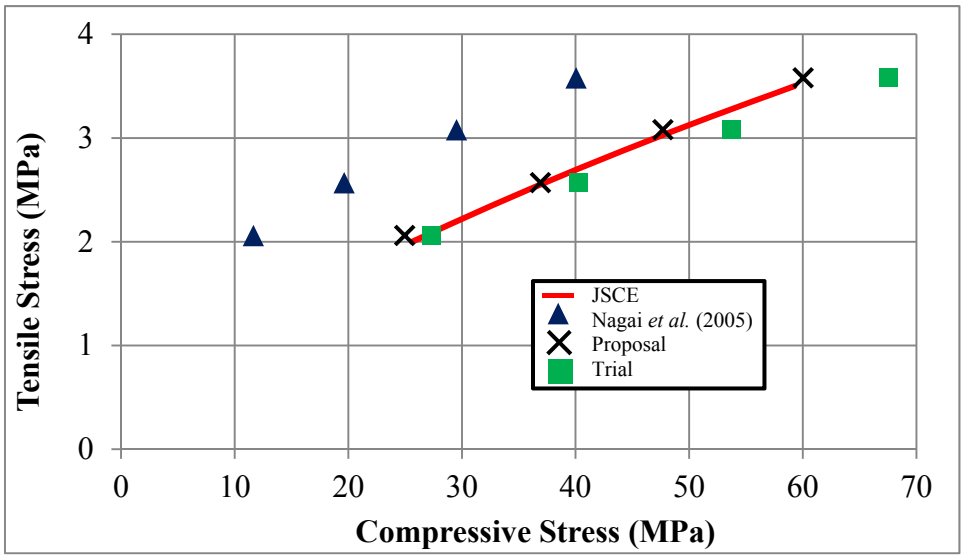

Fig.4.32 Relationship of compressive and tensile strength of concrete with different failure criterion of concrete

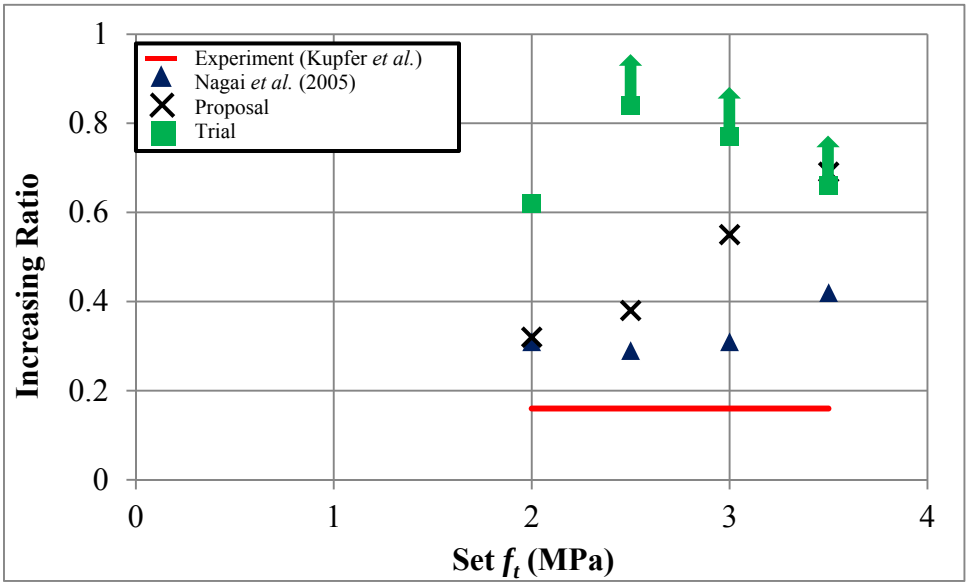

Fig.4.33 Increasing ratio of biaxial compressive strength compared with uniaxial compressive strength with different failure criterion

Fig.4.32 shows the relationship of compressive and tensile strength of concrete with different failure criterion of concrete. Based on this relationship, proposal model and trial model show a good agreement with JSCE equation. Furthermore, Nagai *et al.* (2005) model shows an underestimate result. Meanwhile **Fig.4.33** shows the increasing ratio of biaxial compressive strength compared with uniaxial compressive strength with different failure criterion. Based on this increasing ratio, Nagai *et al.* (2005) model shows the closest result with the experimental result and the proposal model is higher than Nagai *et al.* (2005) model. The Trial model shows the highest increasing ratio of biaxial compressive strength. Thus, based on these reasons, in this study the proposal model is selected because Nagai *et al.* (2005) model shows an underestimate result in case of uniaxial compressive strength and trial model shows the highest increasing ratio of biaxial compressive strength.

4.8 EFFECT OF TENSION SOFTENING OF CONCRETE

In this chapter, a parametric study is also conducted for the constitutive model of the tension softening of concrete of normal springs. Two types of constitutive models of tension softening concrete, i.e. linear softening of concrete and bi-linear softening of concrete, will be investigated through the simulation of uniaxial compression and uniaxial tension. The simulation is conducted only in case of 2.5 MPa of tensile strength of springs. **Fig. 4.34** shows the constitutive model of linear and bi-linear softening of

concrete.

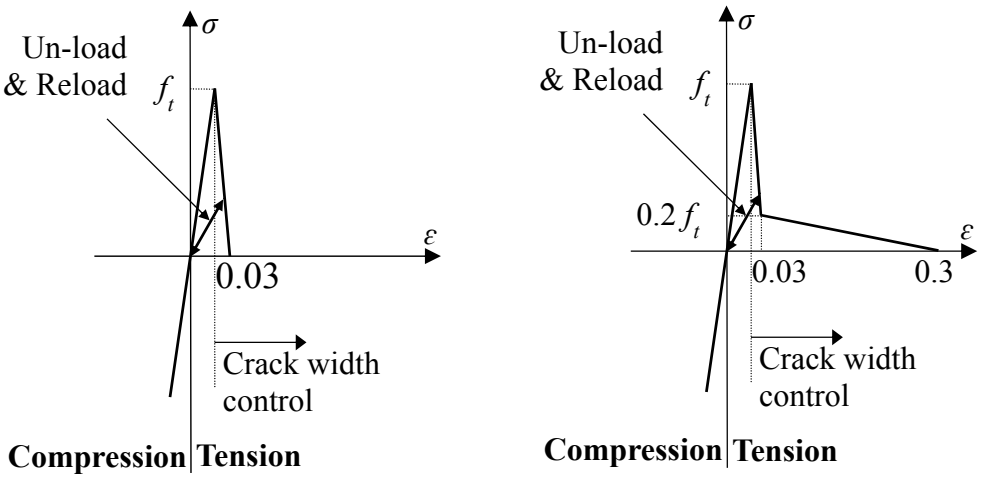

(a) Linear model (Hayashi *et al*. 2013) **(b)** Bi-linear model

Fig.4.34 Constitutive model of normal spring of concrete

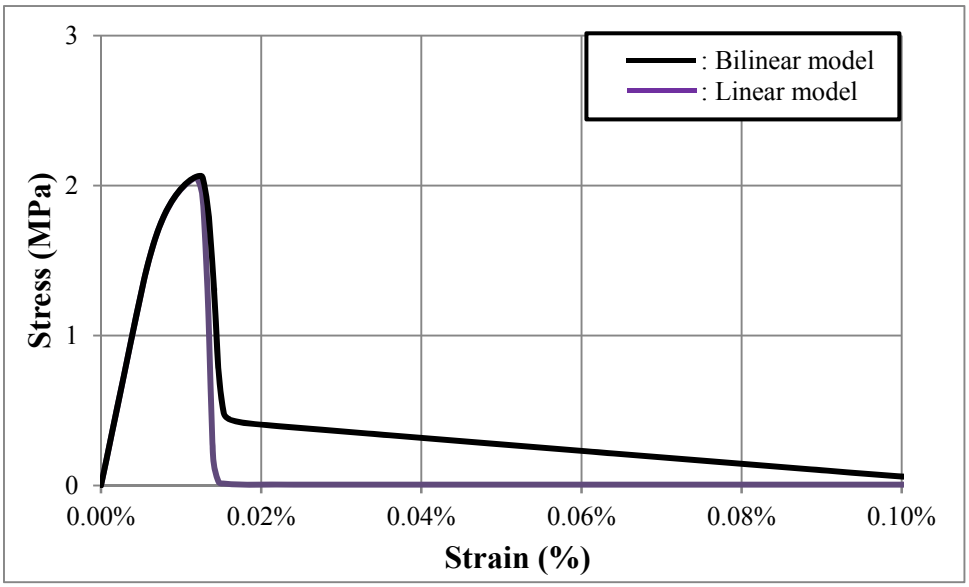

Fig.4.35 Stress-strain relationship of uniaxial compression with different tension softening of concrete

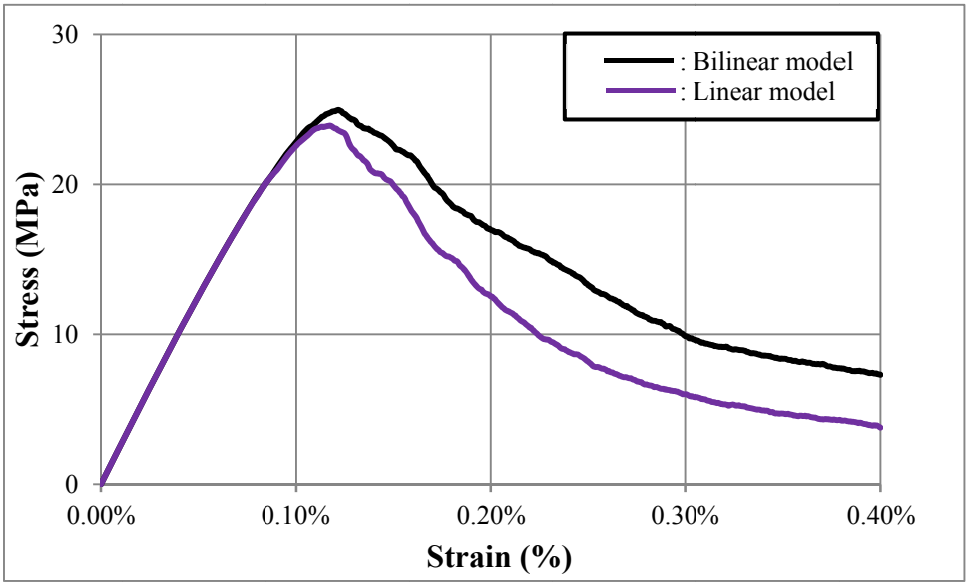

Fig.4.36 Stress-strain relationship of uniaxial tension loading with different tension softening of concrete

Figs. 4.35 and 4.36 show stress-strain relationships of uniaxial compression and tension with different tension softening of concrete. Both stress-strain relationships show that the constitutive model of tension softening of concrete of normal springs affects the softening of concrete after exceeding the maximum load of uniaxial compressive and tensile load. In addition, the constitutive model of tension softening of normal springs of concrete doesn't change the strength of uniaxial compression and tension.

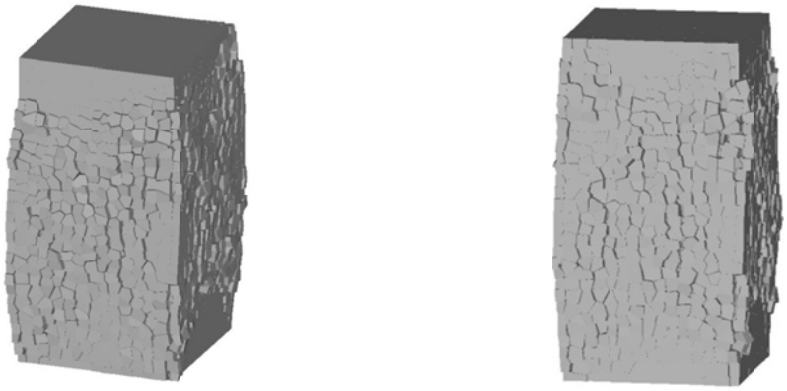

(a) Linear model (Hayashi *et al*. 2013) **(b)** Bi-linear model

Fig.4.37 Surface cracks after failure of uniaxial compression with different tension softening of concrete

(a) Linear model (Hayashi *et al*. 2013) **(b)** Bi-linear model

Fig.4.38 Surface cracks after failure of uniaxial tension with different tension softening of concrete

CONCLUSIONS

1. The constitutive models of concrete elements were proposed based on the simulation in material scales, i.e. uniaxial compression and tension, and biaxial compression
2. By using the proposed constitutive models, the simulation results of uniaxial compression and tension show a good agreement with the JSCE equation. However, simulation results overestimate the concrete strength under biaxial compressive loading.
3. Under uniaxial compressive loading, when the displacement is relatively small, no cracks occur in the numerical models. As the results, the stress increases linearly and Poisson's ratio keeps constant. As the load increases, around 80-90% of its capacity, splitting cracks which are parallel to the loading direction occur that changes the slope of the stress-strain relationships and Poisson's ratio increases. Ultimately, diagonal cracks occur in the numerical models after failure. Meanwhile, under uniaxial tensile loading, simulation results show that the stress increases linearly and Poisson's ratio keeps constant until its capacity.
4. Based on the study of mesh arrangement of numerical models, the simulation results don't change significantly. The same behaviors are predicted in all numerical models with different mesh arrangement. Some differences of local cracking may occur which are caused by the different mesh arrangement.
5. Based on the parametric study of failure criterion of concrete, failure criterion of concrete affects significantly to the behavior of uniaxial compression. Meanwhile,

the behavior of uniaxial tension doesn't change with different failure criterion of concrete.

6. Based on the parametric study of the tension softening of concrete, the tension softening concrete of normal springs affect significantly the behavior of the uniaxial tension and the softening of the uniaxial compression . On the other hand, the behavior of uniaxial compression does not change until the maximum load.

REFERENCES

JSCE., "Standard specification for concrete structures, Materials and contruction," Tokyo: JSCE, 2002.

Hayashi, D., and Nagai, K., "Investigating the anchorage performance of RC by using three-dimensional discrete analysis," Engineering Computations, 30(6), pp.815-824. 2013.

Kupfer, H., Hilsdorf, K.H., and Rusch, H., "Behavior of concrete under biaxial stress," ACI Journal, 66(8), 656-666.1969.

Chapter Five

SIMULATION OF TENSION STIFFENING

5.1 INTRODUCTION

The deformation behavior of reinforced concrete members is affected by many factors. One of the important factors, affecting the deformation of reinforce concrete, is the constitutive laws of bond between concrete and steel reinforcement, due to the stretching of the anchored bars in the connections of reinforced concrete members and the tension stiffening effect in the reinforced concrete members. Popov (1984) described that very large contribution made to the tip deflection by the fixed-end rotation of the beam caused by the fixed-end rotation of the beam caused by a pullout of the bars from the anchorage zone. In the other hand, the tension stiffening effect influences the stiffness of the reinforced concrete members as the stiffness of the members is decreased by the propagation of cracks. Since the bond behavior of deformed bars is more complicated than that of plain bars, the tension stiffening effect in reinforced concrete, reinforced with a deformed bar, will be mainly discussed.

The behavior of the tension stiffening effect in the reinforced concrete members can be defined by the capability of the concrete to develop tensile stress away from the crack section by the presence of bond between concrete and the reinforcement bar. When a reinforced concrete member is loaded by an axial tensile force, the tensile stress, working both in the concrete and in the reinforcement bar, will vary along the member and the stresses are different each other, depending on their modulus elasticity. Furthermore, the equilibrium at any section of the reinforced concrete member can be expressed generally by **Eq. 5.1**.

$$P = A_g\sigma_c + A_s\sigma_s \tag{5.1}$$

As the tensile force increases, the first crack occurs when the tensile stress, working in the concrete, exceeds the tensile capacity of the concrete and the force will be fully resisted by the reinforcement bar at the cracked section. Furthermore, the force is gradually transferred to the concrete at each side of the crack by the presence of bond between concrete and reinforcement bar. As the result, new cracks will occur at a certain distance from the previous crack when the tensile force increases. Furthermore,

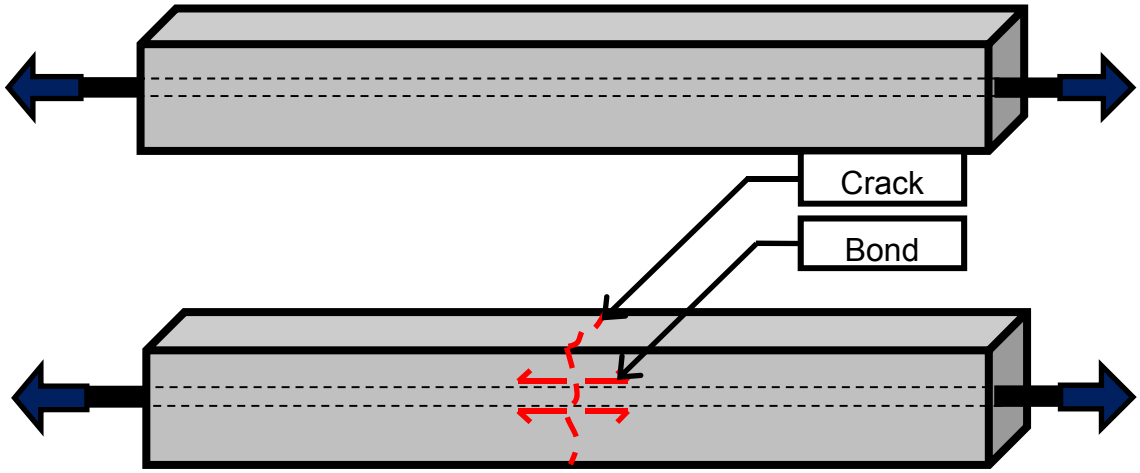

Fig.5.1 Tension stiffening

although at the crack section the tensile force is fully resisted by the reinforcement bar, concrete between cracks is still able to develop tensile stress by the occurrence of the bond between concrete and reinforcement bar. Eventually, it can be concluded that the propagation of cracks and the bond behavior between concrete and the reinforcement bar play important roles in the behavior of the tension stiffening effect in the reinforced concrete members (**Fig. 5.1**).

In order to study the tension stiffening effect in the reinforced concrete members, there are two alternatives i.e. experimental works in laboratories and computational numerical simulations. Through experimental works, the bond behavior and the tension stiffening effect in the reinforced concrete have been well established. Goto *et al.* (1971) successfully studied the propagation of cracks, i.e. internal cracks, primary cracks, secondary cracks, and longitudinal cracks formed around the deformed bar, when a reinforced concrete member is loaded by an axial tensile force. In the other hand, Shima *et al.* (1987) successfully modeled the bond behavior in a massive concrete by a unique bond-slip-strain relationship and the tension stiffening effect in the reinforced concrete by the concept of average stress-strain relationships of concrete and the reinforcement bar.

Hayashi *et al.* (2012) has modeled the anchorage of reinforcement in reinforced concrete beam-column joints by using a 3-dimensional RBSM, but the analysis was limited in the uniaxial tests and without yielding of the bar. In the other hand, Ikuta *et al.* (2012) has modeled the anchorage of reinforcement in L beam-column joints However, the accuracy of RBSM in modeling the bond behavior between concrete and the steel

reinforcement has not been clarified yet, so that further studies are needed. In this study, by modeling the tension stiffening effect in the reinforced concrete by a 3-dimensional RBSM is one way to study the bond behavior between concrete and the steel reinforcement. Eventually, the purpose of this study is to simulate the tension stiffening effect in the reinforced concrete by 3-dimensional discrete model.

5.2 OVERVIEW OF EXPERIMENTAL STUDIES BY SHIMA ET AL

Shima *et al.* (1987) has successfully modeled the tension stiffening effect in the reinforced concrete by the concept of average stress-strain relationships of concrete and the reinforcement bar. The method to determine the average stress-strain relationships of concrete and the reinforcement bar is as follows. As strains were measured along the reinforcement bar, average strain can be calculated by dividing the integration of strain distribution along the reinforcement bar by the length of the specimen. At each measured point, stress can be calculated by the strain-stress relationship of a bare bar. The same concept with the average strain was applied. The average stress can be calculated by dividing the integration of stress distribution along the reinforcement bar by the length of specimen. The load carried by a reinforcement bar is calculated by multiplying the average stress by its cross section. Finally, total load resisted by concrete can be calculated by subtracting total load by total load resisted by the reinforcement bar and the average stress of concrete can be calculated by dividing the total load resisted by concrete by concrete sectional area.

Based on this model, it was found that when a bar at crack section yields, the steel stresses outside the crack section should be lower than the yield strength. As the result, the average stress-strain of steel should have lower yielding point than the yielding point of bare bar.

In this study, the simulation was conducted for two experimental specimens conducted by Shima *et al.* (1987), low yield strength of reinforcement bar and normal yield strength of reinforcement bar. The dimension of the experimental specimen is shown in **Fig.5.2**.

A steel bar is arranged in the center of concrete prism for the tension test. A deformed bar having diameter of 19 mm was used. In order to measure strain, strain gages were places at an interval of 10 ribs at two opposite sides of the reinforcement bar. The length of specimen was determined as long as possible depending on the experimental

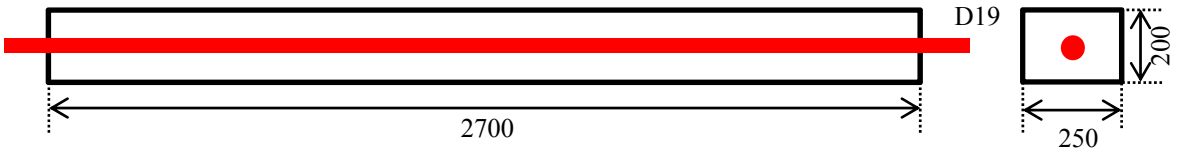

Fig.5.2 Experimental specimen

limitations since higher accuracy will be obtained in case of longer specimen.

5.3 DETAIL OF NUMERICAL MODELS

5.3.1 *Numerical Models*

Simulations were conducted for experiments conducted by *Shima et al.* (1987). The purpose of the experiments was to obtain the average stress strain relationship in the post yield of a bar in concrete since at that time the stiffness of reinforcement bars in reinforced concrete was assumed as same as that of bare bar. Furthermore, this assumption was inapplicable for the post-yield range of reinforcement bars.

In the experiments, the specimens with different concrete strength, reinforcement ratio, yield strength of reinforcement bars, and curing condition were tested under uniaxial tensile loading. In this study, the effect of the yield strength of reinforcement bars is the main focus.

Numerical models are listed in **Table 5.1**. Two numerical models, with different yield strength of reinforcement bars, were modeled.

Table 5.1 Detail of numerical models

Case	Parameter	Material Properties of Concrete			Re-bar		Number of Elements
		Compression f'_c (MPa)	Tension f_t (MPa)	Elasticity E_s (MPa)	Yield f_y (MPa)	Elasticity E_s (MPa)	
1	Yield strength	25	1.5	25500	350	190000	93422
2	Yield strength	25	1	25500	610	190000	93422

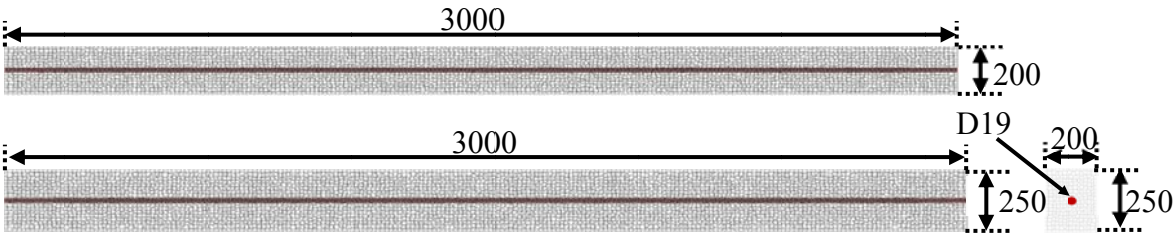

Fig.5.3 Geometry of numerical models (Units: mm)

5.3.2 *Geometry of Numerical Models*

Fig.5.3 shows the geometry of the numerical models. The same dimensions, as the experimental specimens, were modeled. The reinforcement arrangement of numerical models was modeled as the same as that of experimental specimens. A deformed bar of 19 mm was used as the main reinforcement located at the center of concrete prism. The material properties of numerical models are the same as those of experimental specimens

5.3.3 *Boundary Condition*

Fig.5.4 shows the boundary condition of numerical models. A 150 mm of un-bonded length was modeled at both sides of the numerical models to eliminate the confinement near the loaded end and the fixed end. Monotonic displacement-loading is applied to the steel element at the loaded end face. Displacement is increased by 0.0015 mm at each loading step. 1000-2000 steps of displacement-loading are applied in the simulated. Meanwhile, fixed in all direction was assumed at the steel element at the fixed end.

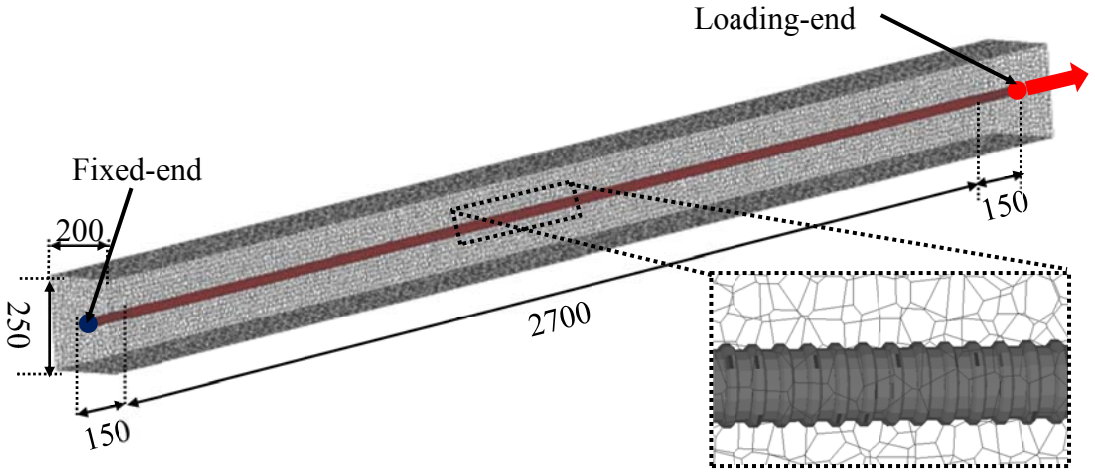

Fig.5.4 Boundary condition

5.4 DISCUSSION AND RESULTS

5.4.1 *Load-displacement Relationships*

The results of tension stiffening can be presented in macroscopic response, i.e. load-average strain relationship, and in microscopic response, i.e. average stress-strain of reinforcement and average stress-strain of concrete. The simulation results are compared with the experimental results, conducted by Shima *et al.* (1987). **Fig.5.5** shows the simulation results compared with the experimental results in case of normal yield strength and low yield strength.

Based on the load-average strain relationship, the tensile stiffness of a reinforced concrete element is higher than that of a bare bar both normal yield strength case and low yield strength case. Therefore, the tension stiffening effect of reinforced concrete can be simulated well by using RBSM, as the result of the presence of bond between reinforcement bar and concrete. Furthermore, since the yield strength of numerical model 1 is lower than that of numerical model 2, simulation predicts that the capacity of numerical model 1 is lower than that of numerical model 2 which is the same tendency as the experimental results.

Based on the average stress-strain of reinforcement bar, it was predicted that the yielding point of the average stress-strain relationship of reinforcement is lower than that of the bare bar in both cases. It is well known that when a reinforcement bar at crack section yields, the stress of reinforcement bar between 2 cracks should be less than that of the bare-bar. Furthermore, it is predicted that the yielding point of the average stress-strain relationship of reinforcement in normal yield strength case is higher than that of in low yield strength case. Simulation predicts that the yielding point begins at the average strain around 0.07 % and 0.28% in case of low and normal yield strength, respectively. The same tendency was observed in the experiment. However, the yielding point of the average stress-strain relationship of reinforcement in low yield strength case of simulation results is predicted higher than that of experimental results.

Simulations results also predict that there is no yield plateau in the average stress-strain of reinforcement which is usually found in the stress-strain relationship of a reinforcement bar.

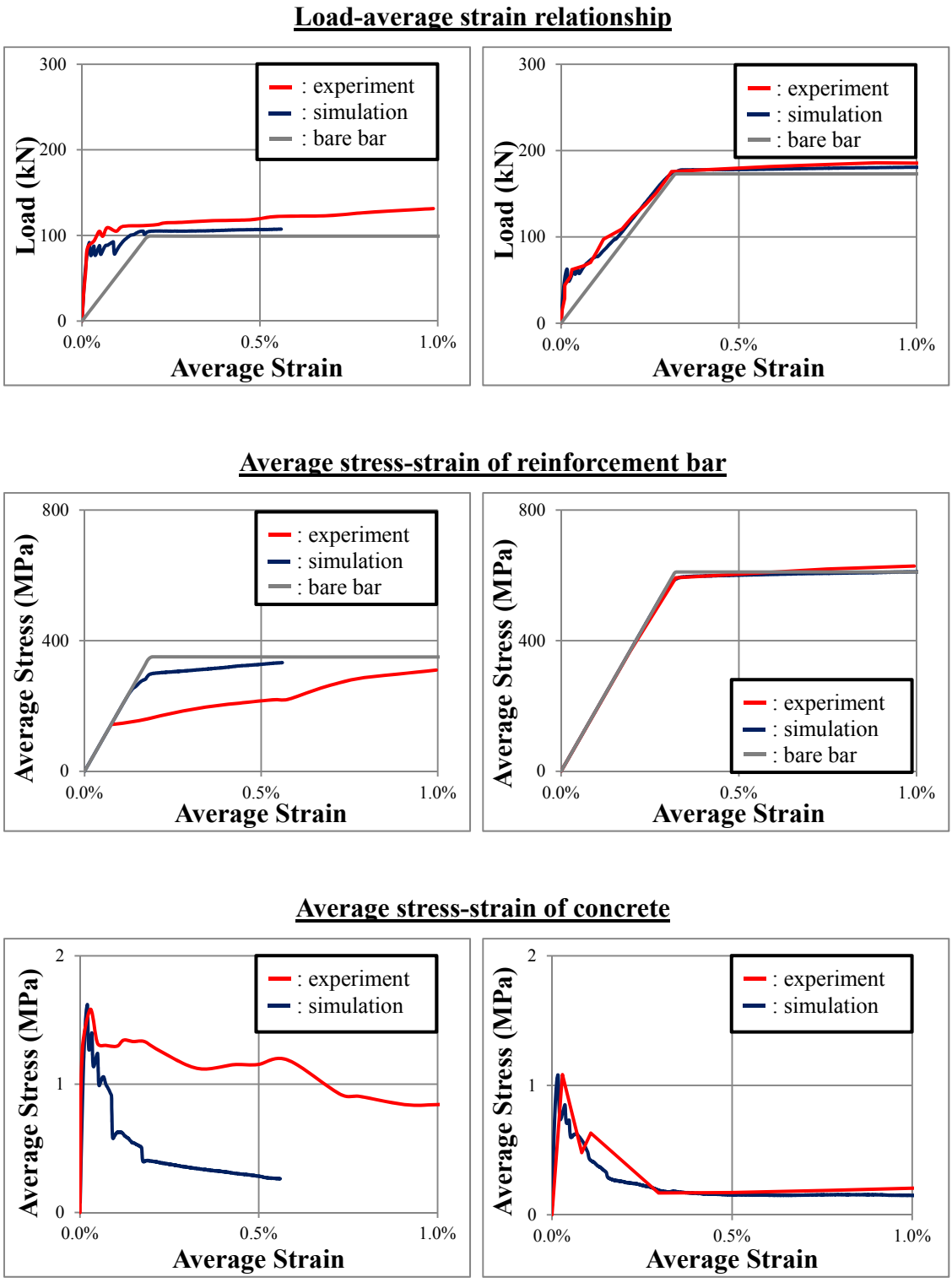

(a) f_y = 350MPa **(b)** f_y = 610MPa

Fig.5.5 Load-average strain and average stress-average strain relationships with different yield strength of reinforcement bar

Moreover, it is revealed from the average stress-strain relationship of concrete that the concrete still can resist the tensile load in the post cracking range. Eventually, the load-average strain, the average stress-strain relationship of reinforcement bar and the average stress-strain relationship of concrete of simulation results are roughly the same as those of experimental results.

5.4.2 *Strain profile, internal cracks, and surface cracks*

Fig.5.6 shows the internal cracks and strain profiles of the simulation results compared with the strain profile obtained from the experimental results in case of normal yield strength. Meanwhile, **Fig.5.7** shows the internal cracks and strain profiles of the simulation results compared with the strain profile obtained from the experimental results in case of normal yield strength.

When the load is relatively small, at the average strain of 0.015%, both cases show that small amount of cracks occurs in the numerical models. Furthermore, at the location of the formation of cracks, the strain of the reinforcement bar is higher than other locations. It indicates that at the location of cracks, the force is fully resisted by the reinforcement bar and simulation can simulate this behavior. As the load increases, at the average strain of 0.044%, new cracks are formed at the certain distances from the previous cracks in both cases because of the occurrence of bond between concrete and the reinforcement bar. It can be concluded that simulation can simulate the propagation of cracks gradually as the load increases because of bond between concrete and the reinforcement bar.

Simulation result predicts that yielding occurs at a certain location when the average strain is still lower than the yield strain of a bare bar. Furthermore, when a reinforcement bar yields at a certain location, stresses at other locations are lower than the yield stress. As the result, the average stress is lower than the yield stress of a bare bar.

In case of numerical model 1, the reinforcement bar yields earlier than numerical model 2 because of lower yield strength of reinforcement bar. Simulation results predict that the reinforcement bar yields at average strain 0.07% and 0.25% in numerical model 1 and 2, respectively.

Load-displacement relationship

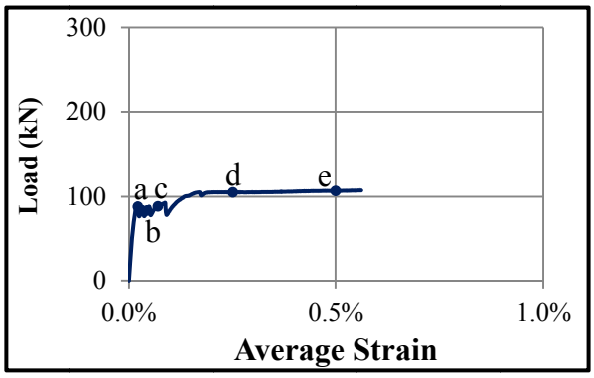

Crack Width:
- : 0.1 mm
- : 0.3 mm
- : 1 mm

Strain:
- : Yield strain
- : Strain hardening strain

a. Average strain 0.015%

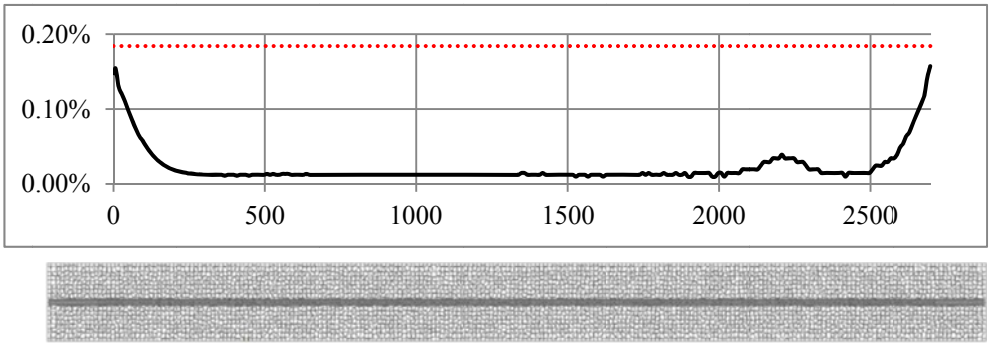

b. Average strain 0.044%

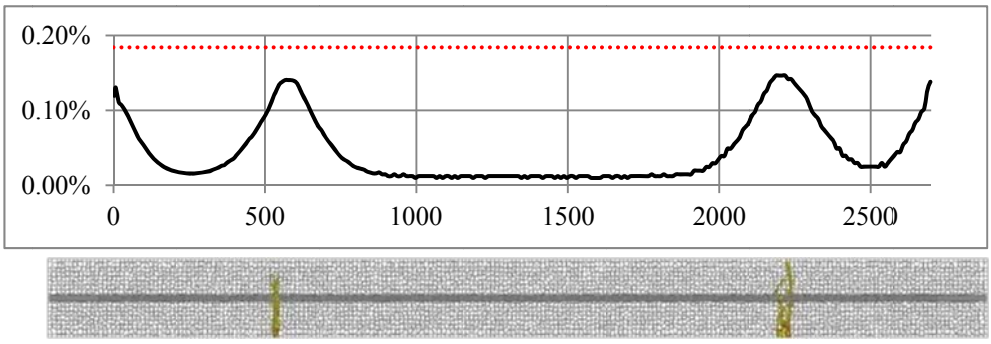

c. Average strain 0.070%

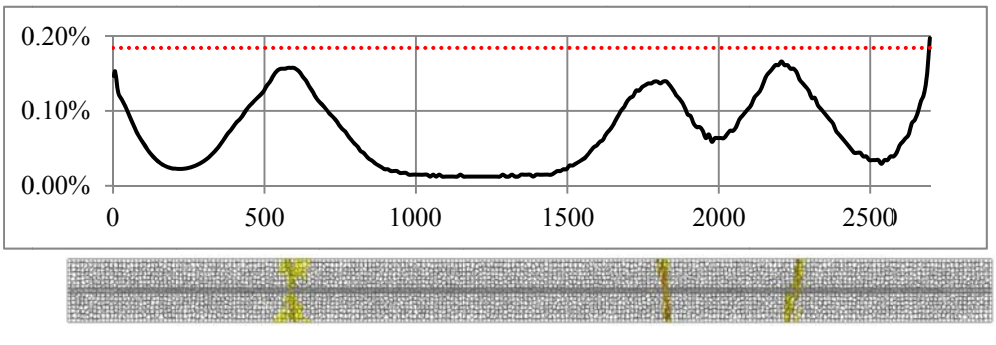

d. Average strain 0.25%

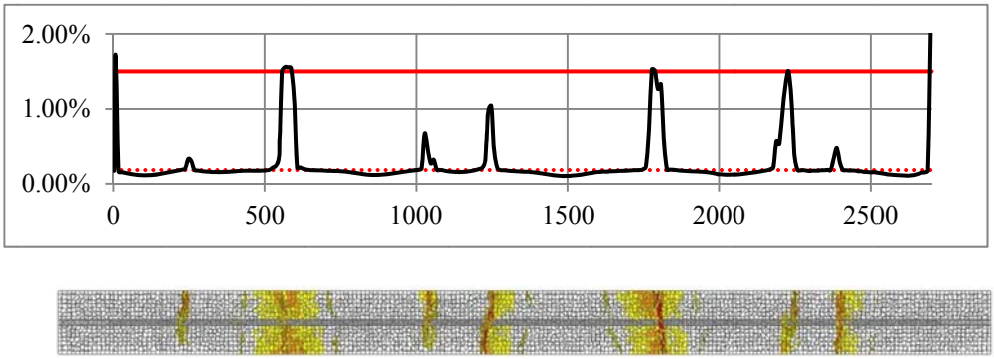

e. Average strain 0.50%

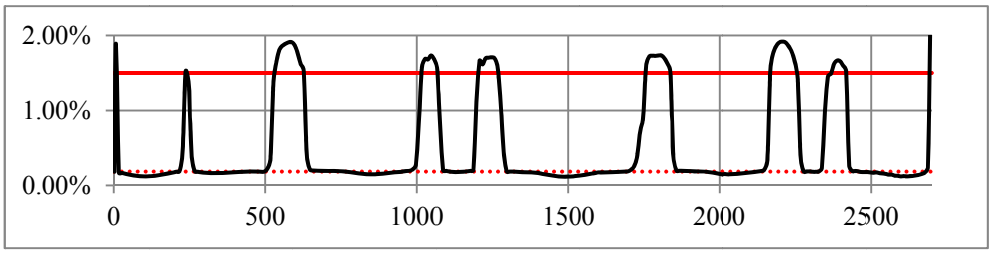

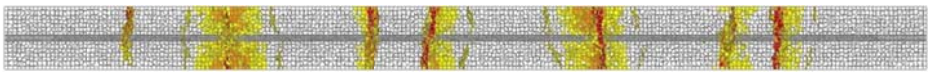

(Deformation ×10)

Strain profile of experiment:

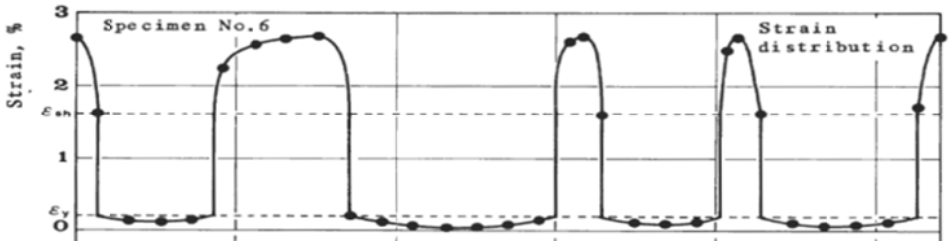

Fig.5.6 Strain profile and internal cracks in case of low yielding strength

Load-displacement relationship

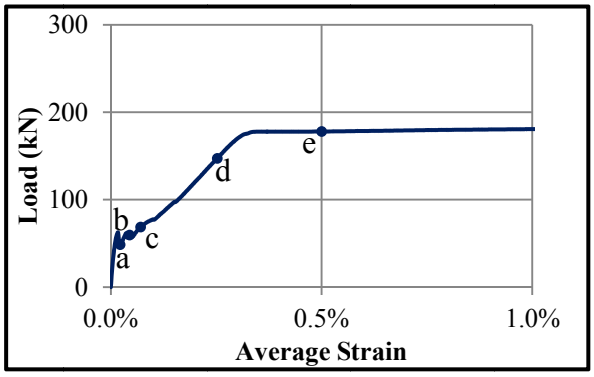

Crack Width:
- : 0.1 mm
- : 0.3 mm
- : 1 mm Strain:
- : Yield strain
- : Strain hardening strain

a. Average strain 0.015%

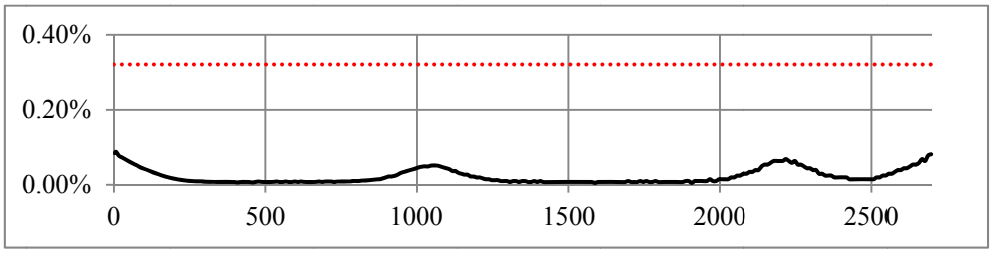

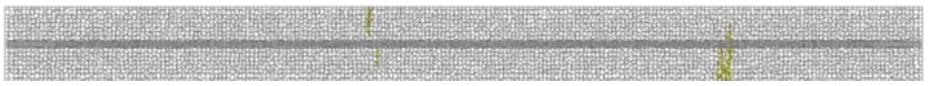

b. Average strain 0.044%

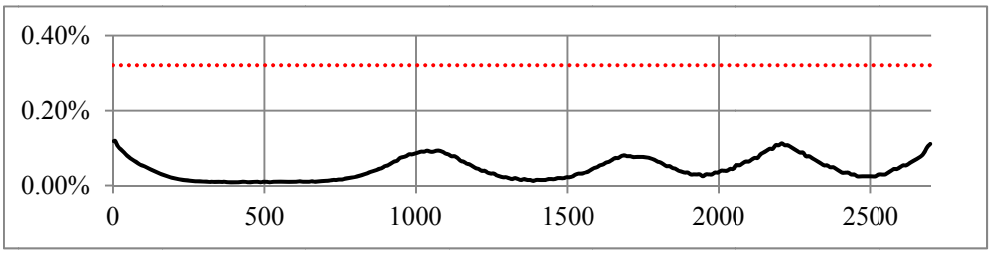

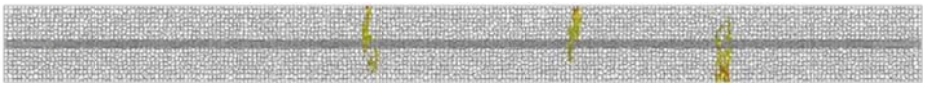

c. Average strain 0.28%

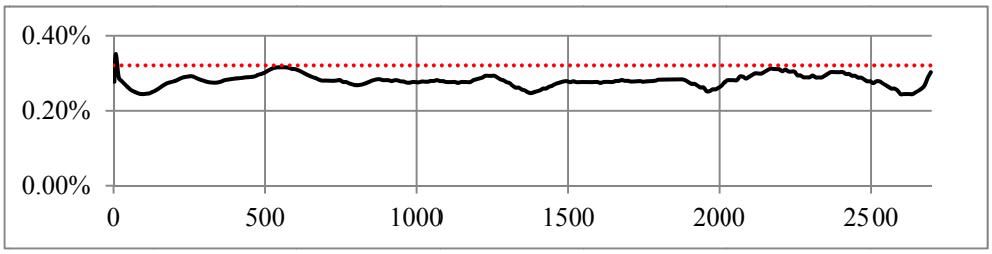

d. Average strain 0.39%

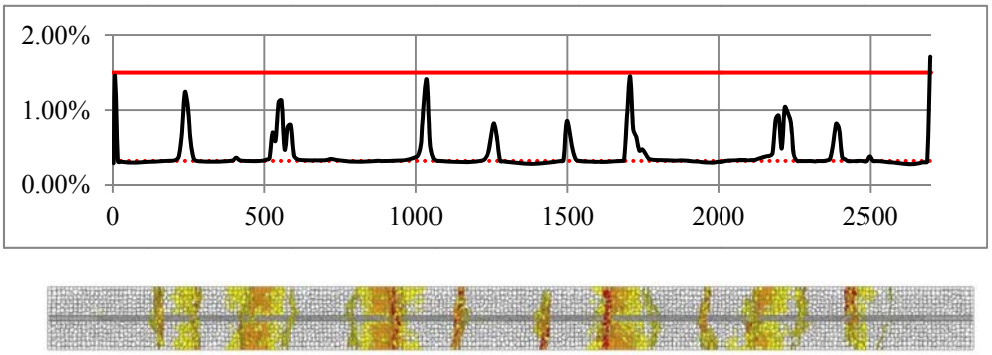

e. Average strain 0.50%

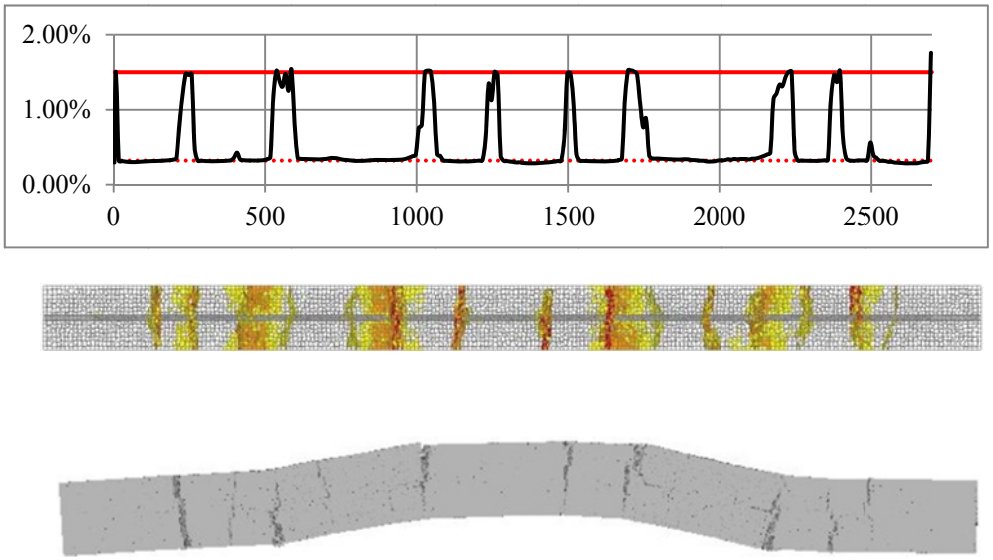

(Deformation ×10)

Strain profile of experiment:

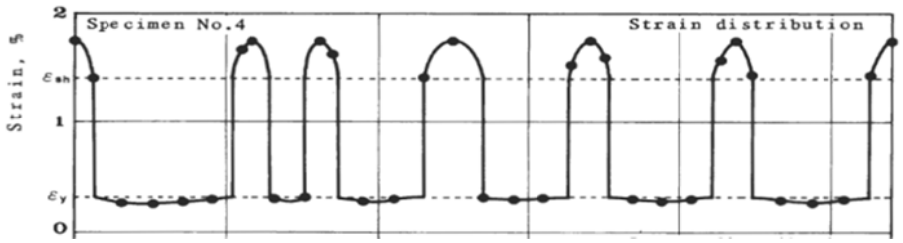

Fig.5.7 Strain profile and internal cracks in case of normal yielding strength

5.5 EFFECT OF TENSILE STRENGTH REDUCTION OF INTERFACE ELEMENTS

As described in the previous chapter, in order to consider the interface as a weak region, the tensile strength of the interface elements is assumed to be half of that of concrete elements. In this chapter, the assumption of this tensile strength reduction will be investigated through the parametric studies. Three types of tensile strength of interface elements will be simulated, i.e., no reduction of tensile strength (=f_t concrete), half of the tensile strength of concrete elements (=0.5×f_t concrete), very small value of tensile strength (= zero) (**Fig.5.8**). The yield strength of the reinforcement bar is 350 MPa. **Fig.5.9** shows the load-average strain, average stress-strain relationship of reinforcement bar, and average stress-strain relationship of concrete.

Based on the load-average strain relationships, simulation results predict that the stiffness in a reinforced concrete member slightly increases as the tensile strength of the interface elements increases before and after cracking. In addition, based on the average stress-strain relationship of concrete, the tensile strength and the stiffness of concrete slightly increase as the tensile strength of the interface elements is higher. As the result, it is well known that if the concrete strength is higher, the yielding point of the average stress-strain relationship of reinforcement bar is lower. It can be concluded that the tensile strength of the interface elements contributes to the concrete strength.

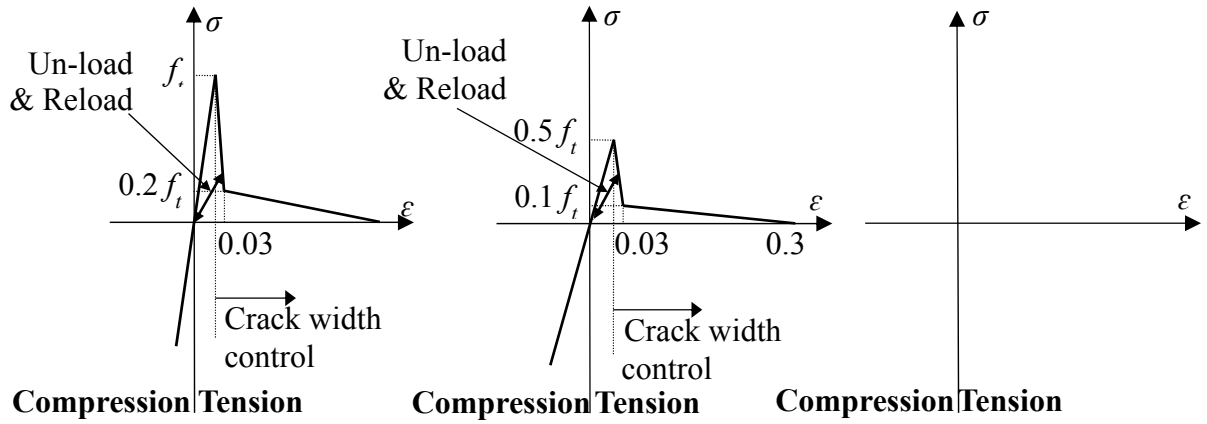

(a) f_t interface = f_t concrete **(b)** f_t interface = 0.5×f_t concrete **(c)** f_t interface = 0

Fig.5.8 Constitutive models of interface elements with different tensile strength

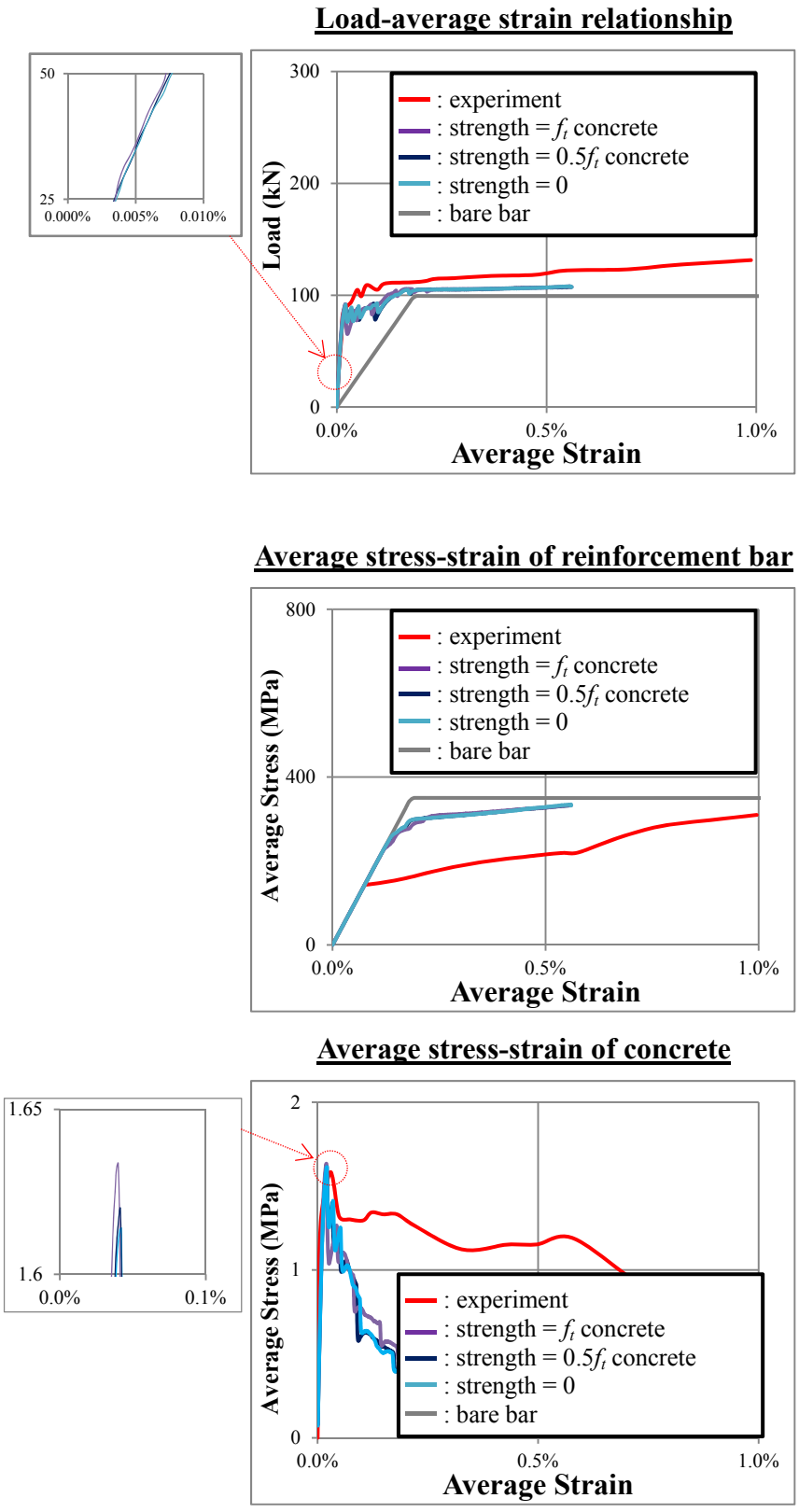

Fig.5.9 Load-average strain and average stress-average strain relationships with different tensile strength reduction of interface elements

Fig.5.10 shows the strain profiles with different tensile strength of interface elements. Since the tensile strength of interface elements slightly affects the load-average strain relationships, the strain profile along the reinforced concrete member does not change significantly.

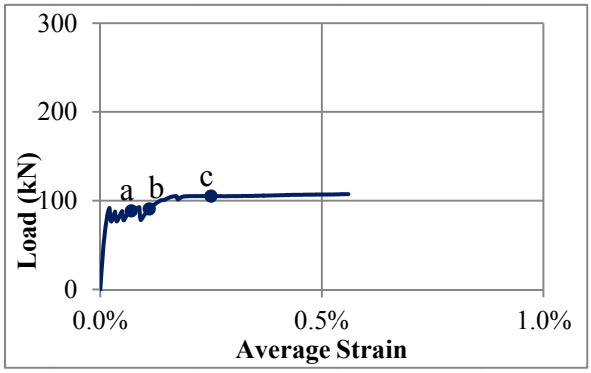

Crack Width:
- : 0.1 mm
- : 0.3 mm
- : 1 mm Strain:
- : Yield strain
- : Strain hardening strain

: strength = f_t concrete
: strength = 0.5f_t concrete
: strength = 0

a. Average strain 0.07%

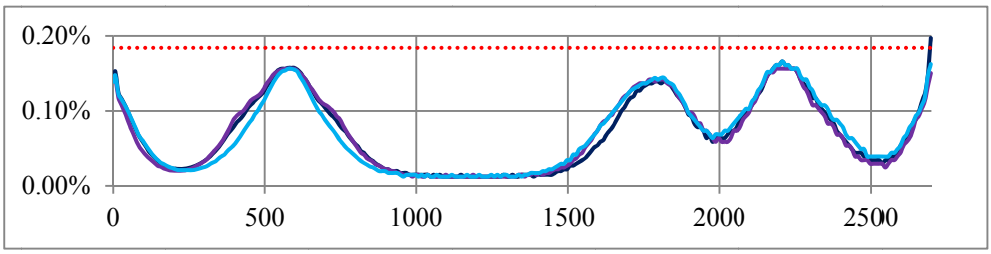

Interface = 0

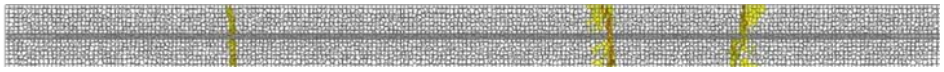

Interface = 0.5 f_t concrete

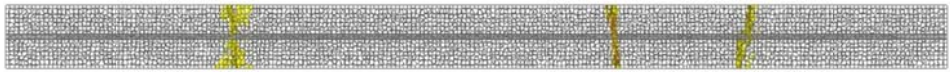

Interface = f_t concrete

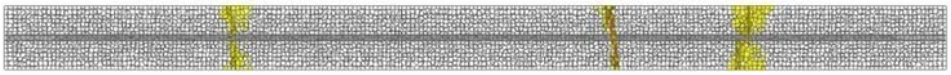

b. Average strain 0.11%

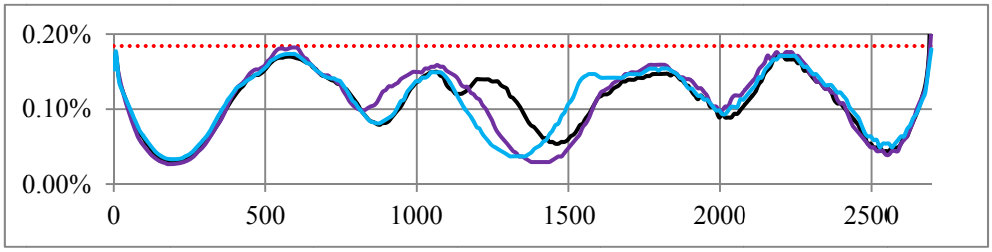

Interface = 0

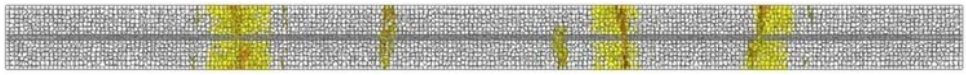

Interface = 0.5 f_t concrete

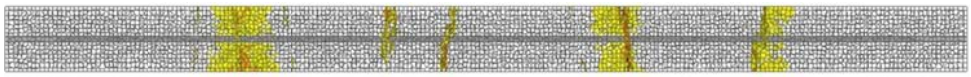

Interface = f_t concrete

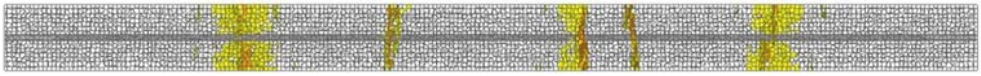

c. Average strain 0.25%

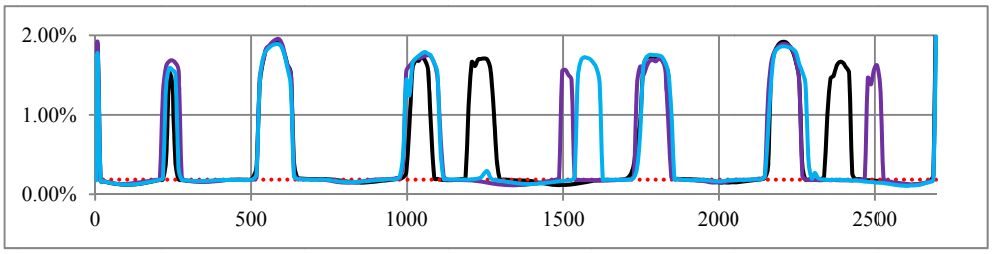

Interface = 0

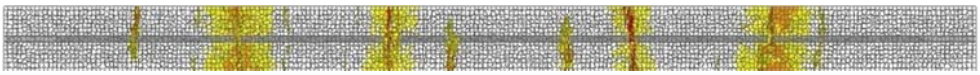

Interface = 0.5 f_t concrete

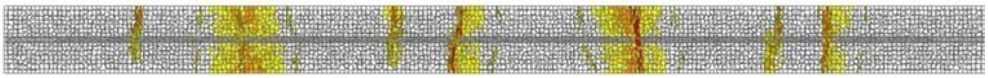

Interface = f_t concrete

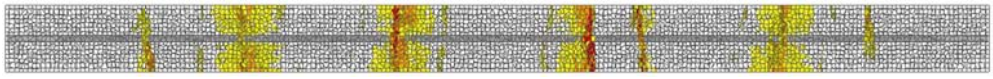

Fig.5.10 Strain profile and internal cracks in case of low yielding strength with different tensile strength of interface elements

5.6 EFFECT OF MODELING STRAIN HARDENING REGION OF STEEL ELEMENTS

In the previous study by Hayashi *et al.* (2012), strain hardening region of steel elements has not been introduced and a bilinear model was assumed. In this study, the strain hardening region is introduced (**Fig. 5.11**). The constitutive model of the normal spring used in this simulation is represented by the following equations (adopted from *Shima et al.* 1987).

$$\begin{aligned} \sigma &= E_s\varepsilon && if\ (\varepsilon < \varepsilon_y) \\ \sigma &= f_y && if\ (\varepsilon_y < \varepsilon < \varepsilon_{sh}) \\ \sigma &= f_y + \left(1 - e^{\frac{\varepsilon_{sh}-\varepsilon}{k}}\right)(1.01f_u - f_y) && if\ (\varepsilon > \varepsilon_{sh}) \end{aligned} \tag{5.2}$$

where

$k = 0.032(400/fy)^{1/3}$

σ : stress (MPa)

ε : strain

f_y : yield strength *(MPa)*

f_u : tensile strength (MPa)

ε_{sh} : initial strain of hardening, assumed 1.5%

The effect of modeling this strain hardening region will be investigated through the simulation of tension stiffening effect. **Fig.5.12** shows the load-average strain, average stress-strain relationship of reinforcement bar, and average stress-strain relationship of concrete with and without strain hardening region of steel elements.

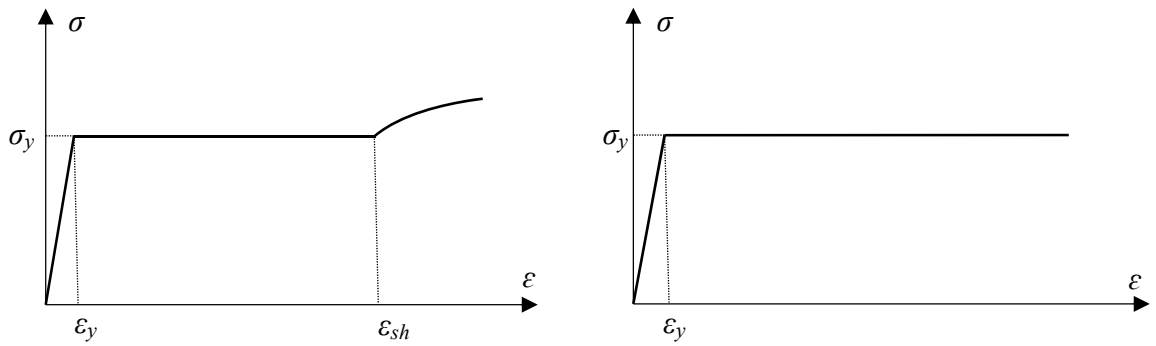

(a) With strain hardening **(b)** Without strain hardening

(Hayashi *et al.* 2012)

Fig.5.11 Constitutive models of steel elements

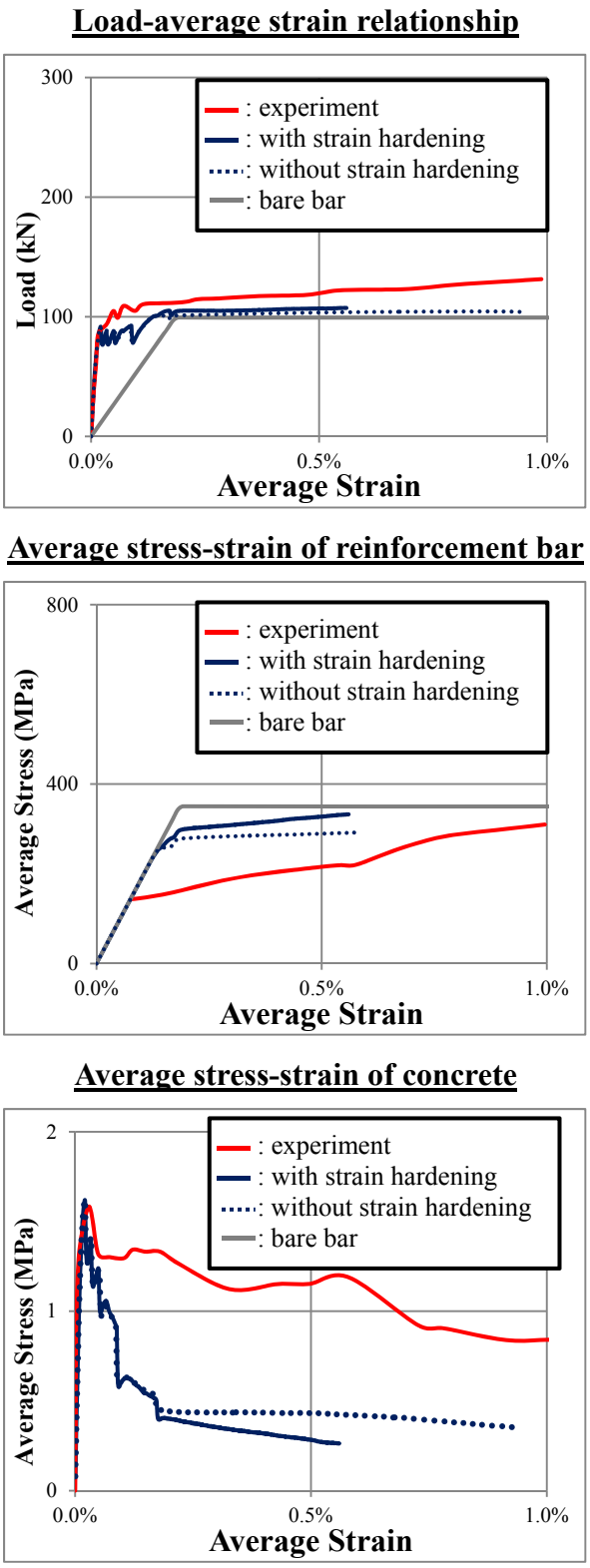

Fig.5.12 Load-average strain and average stress-average strain relationships with and without strain hardening region of steel elements.

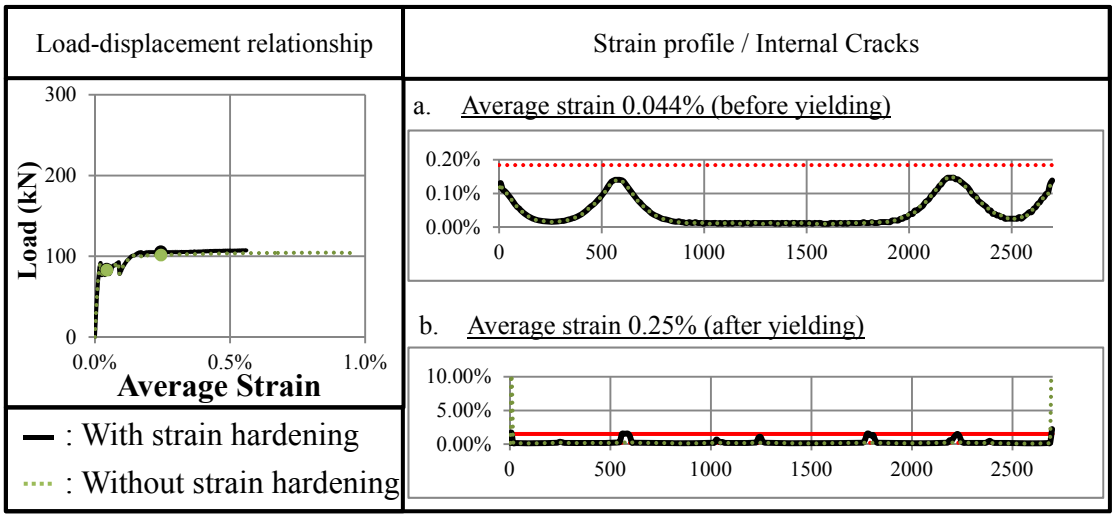

Fig.5.13 Strain profile with and without strain hardening region

Based on the load-average strain relationship and the average strain-stress relationship of the reinforcement bar, the difference occurs after the yielding point of the average stress-strain relationship of the reinforcement bar. The load carried by the reinforced concrete is lower in case of without strain hardening region. Furthermore, after the reinforcement bar yields at the crack section, yield plateau is found in the average stress-strain relationship of reinforcement bar if strain hardening region is not modeled.

In order to understand this difference, **Fig.5.13** shows the strain profile with and without modeling strain hardening region. Before yielding, at average strain of 0.044%, no difference of strain profile is predicted in both cases. As the load increases, at average stress of 0.25%, because of no strain hardening region, the strain jumps up dramatically after yield has occurred at both loading-end and fixed-end which indicates the failure of the reinforcement bar. In addition, strains are localized after yielding occurred. Meanwhile, since strain hardening region is modeled, the reinforcement bar can still carry more load.

CONCLUSIONS

1 In this chapter, the applicability of RBSM to simulate the bond behavior between concrete and reinforcement bar is investigated through the simulation of tension stiffening effect. When the displacement is relatively small, small amount of cracks occur in the numerical models. As the displacement increases, new cracks are formed at the certain distance from the previous cracks because of the bond between the concrete and the reinforcement bar. It can be concluded that RBSM

can simulate the bond behavior in a reinforced concrete member.

2 Simulation results also show that the yielding point of average stress-strain of reinforcement bar of low yield strength is lower than that of high yield strength. In case of low yield strength of reinforcement bar, the reinforcement bar yield just after the cracking started. The simulation results show in a good agreement with that of simulation result.

3 By the parametric study of the tensile strength of the interface element between concrete and the reinforcement bar, by increasing the tensile strength of the interface element between concrete and the reinforcement bar affects slightly the strength and stiffness of concrete in average stress-strain of concrete relationship. As the result the stiffness of load-average strain relationship and the yielding point of average stress-strain of reinforcement bar will be affected slightly.

4 The strain hardening region in the constitutive model of a reinforcement bar is introduced in this study that affects the average stress-strain relationship of a reinforcement bar. The absence of the strain hardening region causes the yield plateau in the average stress-strain of the reinforcement bar after the yielding point. Furthermore, strain localization will occur.

REFERENCES

Hayashi, D., Nagai, K., and Suryanto, B.: Investigating the Effects of Reinforcement Arrangement on the Anchorage of Reinforcement Using the Three-dimensional Discrete Analysis, Proceedings of the 4th Bond in Anchorage Conference, 2012, pp. 185-192.

Kawai, T.: New Discrete Models and Their Application to Seismic Response Analysis of Structure, Nuclear Engineering and Design, 48, 1978, 207-229.

Chapter Six

ANALYSIS AND RESIDUAL CAPACITY OF RESIDUAL RC CORBEL FAILED BY ANCHORAGE SPLITTING FAILURE

6.1 INTRODUCTION

Corbel is a short cantilever member that comes out from a column, a wall, or a bridge pier, to sustain a load, originating from a gantry girder or a precast concrete beam. A corbel is generally built monolithically with a column or a wall, and is characterized by a low shear span-to-depth ratio. To transfer a load from a beam to a corbel, a bearing pad is usually installed on the corbel. However, for the easiness of the construction, some bearing pads were installed in the wrong position, at the free end of corbels. The position of the bearing does not satisfy the requirement in the design code (JSCE 2007).

Based on the filed observation (Singapore, 2012), several corbels were found to be failed at a lower capacity than their expected capacity due to the faulty design of bearing pads positions. Bearing pads were found to be extended to the edge of the corbel. Meanwhile, based on the experimental results, conducted by Kriz and Raths (1965), several failure mechanisms can be classified into (see **Fig.6.1**):

1. Flexural tension failure
   This failure occurs when flexural reinforcement bars yield excessively. The tendency that the flexural cracks become very wide signifies this type of failure. In addition, concrete crushing occurs at the sloping end of the corbel.
2. Diagonal splitting failure
   This failure occurs along the diagonal compression strut after the occurrence of flexural cracks.
3. Sliding shear failure
   This failure is characterized by a series of short and step diagonal cracks. The corbel separates from the column face as these cracks interconnect.
4. Anchorage splitting failure
   This failure occurs when a load is applied to the edge of the corbel, at the position of the bending portion of the anchorage.
5. Bearing failure
   If the bearing plates are too small or too flexible, the concrete may crush underneath the bearing plates.

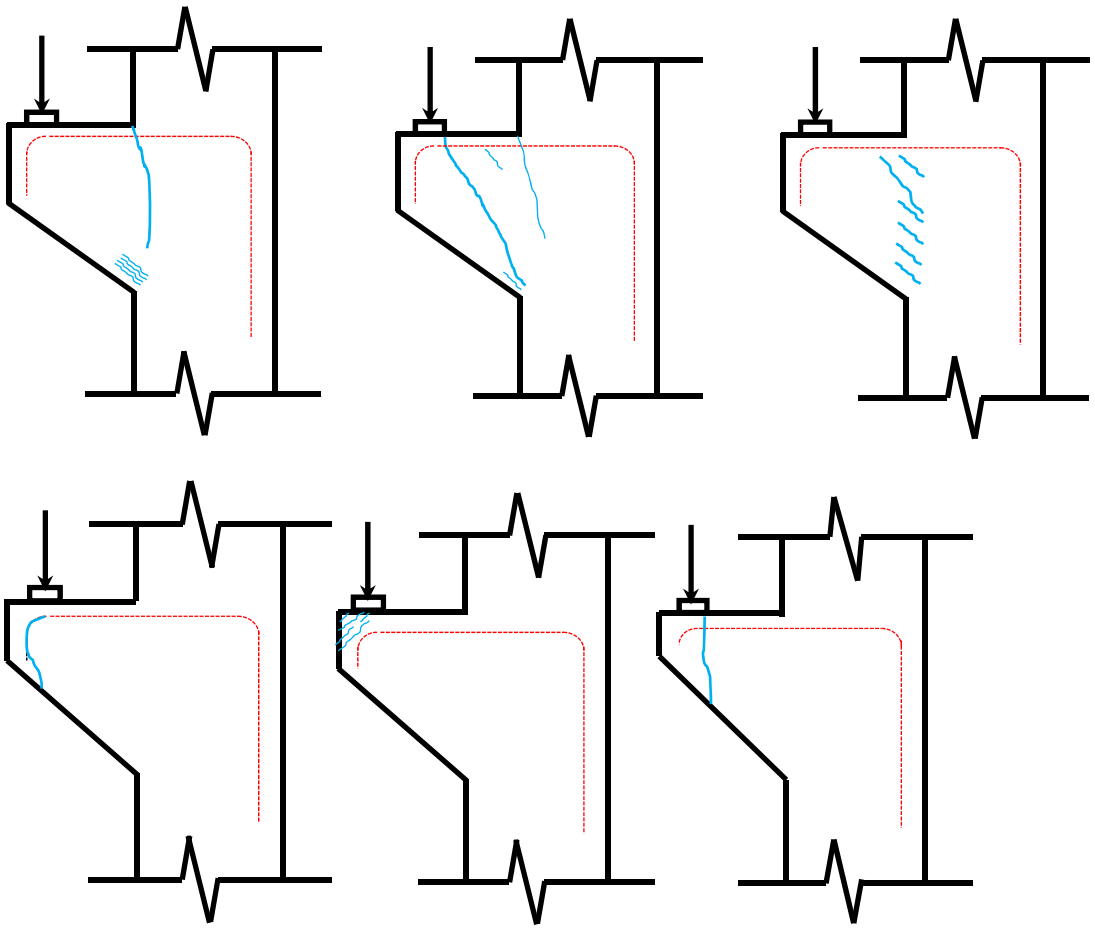

Fig. 6.1 Failure mechanisms in corbels (a) Flexural tension failure; (b) Diagonal splitting failure; (c) Sliding shear failure; (d) Anchorage splitting failure; (e) Crushing due to bearing; (f) Horizontal tension failure

6. Horizontal tension
   If the outer face of the corbel is too shallow and an adverse horizontal load is also introduced.

Based on this classification, such failure can be classified the anchorage splitting failure. Meanwhile, few cracks, either diagonal compression cracks or flexural cracks, occur in the corbel. Based on this behavior, if the location of bearing pad is moved to the straight portion of the flexural reinforcement of the corbel, there is still a possibility that the corbel is still able to resist the load, although a local failure occurs. Furthermore, the option to move the bearing pad to the straight portion of the flexural reinforcement might be a simple way for recovering the capacity of a corbel failed by the anchorage splitting failure. However, how much load that a corbel is still able to resist after a local

failure occurs, which is called residual capacity, has not been investigated.
In order to study the residual capacity of a reinforced concrete corbel failed by an anchorage splitting failure, there are 2 alternatives, i.e. experimental works and computational numerical simulations. Through experimental works, the real load-displacement relationship and surface cracks can be obtained easily. However, the internal cracks and the internal stress are difficult to be observed. Our research group has conducted a meso-scale analysis of reinforced concrete members by a 3-dimensional discrete element analysis, called RBSM. The study on a reinforced concrete member at the meso-scale, in which the local re-bar arrangement is considered by modeling the rib of re-bar, is useful for the precise evaluation of its behavior, since at this level, cracks occur as the result of the interlock mechanism between concrete and re-bar.

Eventually, the purpose of this study is to study the residual capacity of a reinforced concrete corbel failed by an anchorage splitting failure, both by experimental work and numerical simulation. Based on this finding, an efficient method to retrofit the damage corbel will be proposed based on the study of internal stress and internal cracks condition.

6.2 EXPERIMENTAL PROGRAMS

6.2.1. Experimental specimens

To study the residual capacity of a corbel failed by an anchorage splitting failure, 3 reinforced concrete corbels were loaded with different loading positions (see **Table 6.1**). The specimens were reinforced with reinforcement bars. The column segment was reinforced by four longitudinal deformed bars of 16 mm and six lateral ties of 10 mm. Deformed bars of 13 mm, that were used as the flexural reinforcements of the corbel, were bent through 90 degree at the edge of the corbels. Two deformed bars of 10 mm were used as the lateral ties of the corbel. The distance between the top surface of the concrete and the top surface of the outer stirrups, of all specimens was 20 mm. **Fig. 6.2** shows the dimension and the reinforcement bars arrangement of the experimental specimens.

For the recognition of the variable in each specimen, the following notations were used. EC signifies the specimen with bearing pads installed and loaded on the edge of the corbel. The purpose of corbel EC is to verify the occurrence of the anchorage splitting

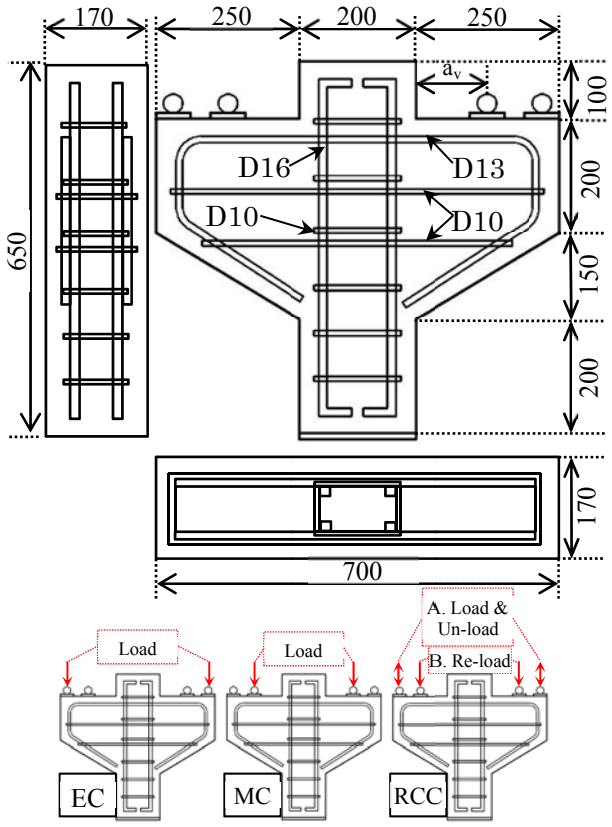

Fig. 6.2 Experimental specimens

cracks. MC signifies the specimen with bearing pads installed and loaded on the straight portion of the flexural reinforcement of the corbel. Corbel MC was intended as the control specimen. RCC signifies the specimen for investigating the residual capacity of a corbel. To study the residual capacity the corbel, corbel EC, after being failed by the anchorage splitting failure, was re-used as corbel RCC. Before the specimen was re-loaded on the straight portion of flexural reinforcement of the corbel, the specimen was un-loaded.

6.2.2. Material properties

(1) Concrete

A concrete compressive strength of 40 MPa was used for mix design, using maximum 20 mm of coarse aggregate size. Standard compressive cylinder tests and standard split cylinder tests were conducted to determine the values of the compressive strength and the splitting tensile strength of the concrete, respectively. The compressive strengths and the splitting tensile strengths of the concrete specimens are listed in **Table 6.1**.

Table 6.1 Detail of experimental specimens

			Reinforcement bars				Strength of Concrete	
			Column		Corbel			
	Parameter	Shear a_v(mm)	Longitudinal	Transverse	Longitudinal	Transverse	Comp. f'_c (MPa)	Tension f_t (MPa)
EC	Loading on Edge Pad	125	4-D16	6-D10	2-D13	2-D10	45.52	2.66
MC	Loading on Middle Pad	220	4-D16	6-D10	2-D13	2-D10	41.89	2.81
RCC	Residual Capacity	220	4-D16	6-D10	2-D13	2-D10	45.52	2.66

(2) Reinforcement Materials

Deformed bars of 16 mm, 13 mm, and 10 mm were used. The yield strengths of deformed bars of 16 mm and 13 mm are same in both diameters, i.e. 490MPa and the yield strength of deformed bars of 10 mm is 390 MPa.

6.2.3. Test setup and measurements

The corbels were loaded on the column segment in an upside-down position using a Universal Test Machine (UTM). Meanwhile, the corbels were seated on steel roller supports at different positions, depending on the position of the bearing pads. Thin layer of gypsum was used between the bearing plates and the specimen to ensure the stability during loading. Load was applied at a constant rate of 0.0084 mm per second. At each step of load, the total load was measured by using a load cell and relative displacements of bearing pads were measured by using Linear Voltage Differential Transducers (LVDTs). **Fig. 6.3** shows the detail of the test setup.

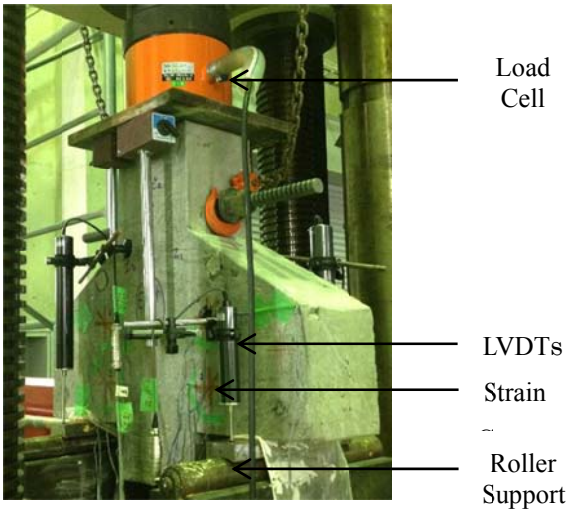

Fig. 6.3 Experimental setup

Table 6.2 Detail of numerical models

Case	Parameter	Shear a_v(mm)	Strength of Concrete: Compression f'_c (MPa)	Strength of Concrete: Tension f_t (MPa)	Number of elements	Maximum Load: EXP (kN)	Maximum Load: ANA (kN)
EC	Loading on Edge Pad	125	45.52	2.66	318494	428	328
MC	Loading on Middle Pad	220	41.89	2.81	318448	229	199
RCC	Residual Capacity	220	45.52	2.66	318747	409	301

6.3 DETAILS OF NUMERICAL MODELS

6.3.1 Numerical models

Table 6.2 shows the numerical models that were conducted in order to study the residual capacity of a corbel failed by an anchorage splitting failure. The same notations with experiment specimens were used. 3 numerical models, with different positions of bearing pads, were modeled.

6.3.2 Geometry of numerical models

The same dimensions, as experimental specimens, were modeled. However, for the simplification of the models and in order to reduce the computational time, only one side of the corbels was modeled and the stirrups in the column segment were not modeled. **Fig.6.4** shows the geometry of the numerical models.

6.3.3 Boundary conditions

Fig.6.5 shows the boundary conditions of numerical models. Fix condition in all direction is assumed at the top and the bottom of the column segment. Monotonically displacement-load controlled was applied on the bearing pad of the corbel. The displacement-load increases 0.016 mm for every step of load. 200 steps of displacement-load were applied in the simulation. The boundary condition in the column segment is different with the experimental test setup. However, it has been confirmed that this boundary condition does not affect the simulation results, i.e. load-displacement relationships and crack patterns.

In order to introduce the residual capacity analysis in the numerical simulation of Corbel RCC, 2 bearing pads were modeled in case of corbel RCC, i.e. an edge bearing

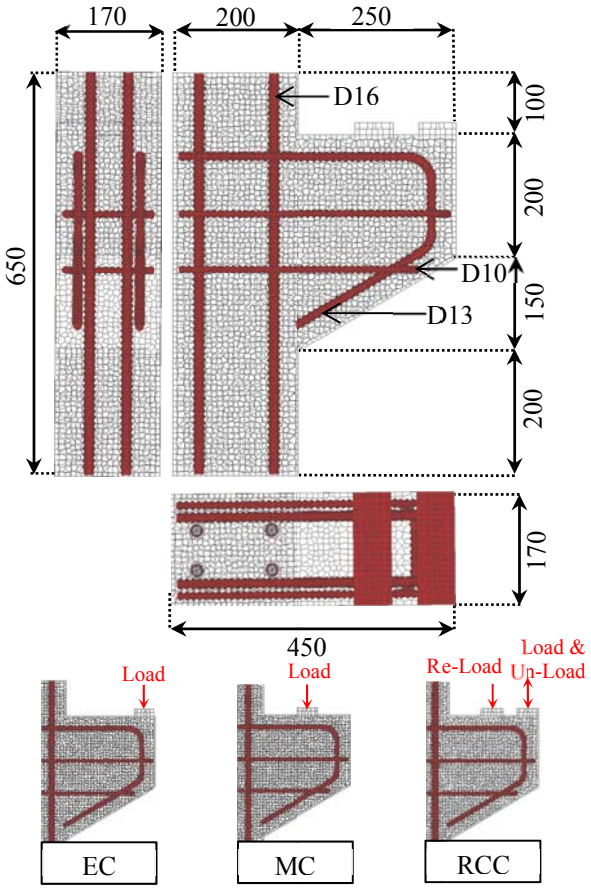

Fig. 6.4 Numerical models

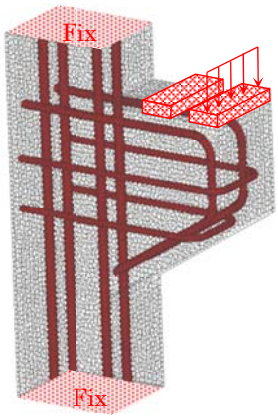

Fig. 6.5 Boundary condition

pad and a middle bearing pad. The same load pattern with experiment was applied. As the initial load, the load was applied on the edge bearing pad. After the load reached the maximum load, the load was un-loaded until the force was zero. After the un-loaded process was completed, the loading position was moved and applied on the middle bearing pad.

6.4 RESULTS AND DISCUSSION

6.4.1. Load-displacement relationships

Fig.6.6 and **Fig.6.7** show the load-displacement relationships of experimental specimens and numerical models, respectively. Table.2 shows the maximum loads of experimental specimens and numerical models. The load of load-displacement relationships of experimental specimens was calculated based on the total load which was measured by a load cell. The displacement of load-displacement relationships of experimental specimens was determined based on the average relative displacement,

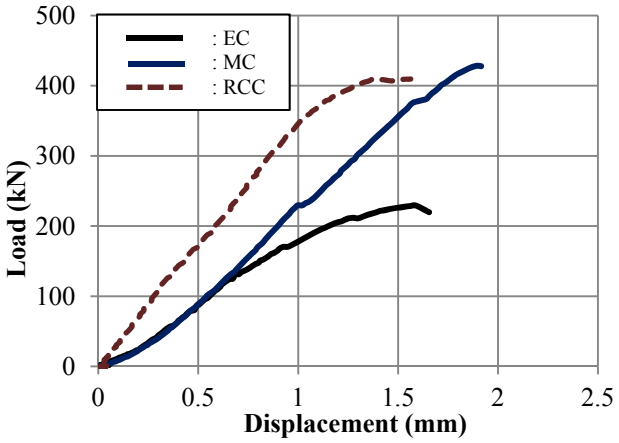

Fig. 6.6 Load-displacement relationships of experimental specimens

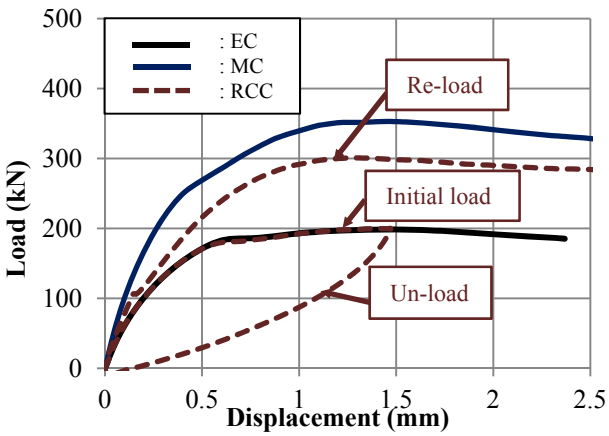

Fig. 6.7 Load-displacement relationships of numerical models

which was measured by a LVDT, located at the bearing pad of the corbel. It should be emphasized that the displacement that was measured by the LVDT is not the relative displacement between 2 points of measurement, i.e. the top surface and the bottom surface of the specimens. Furthermore, the rigid body movement of specimens is included into this measurement. Experimental results are shown until the peak load because the measurements were not stable in the post peak due to the brittle failure. Meanwhile, the load and the displacement of the load-displacement relationships of the numerical models were determined based on the load and the displacement which were applied on the bearing pad.

The maximum loads of the numerical models are roughly the same as those of experimental specimens, i.e. approximately 13-17% difference. In case of corbel EC, the simulation prediction is underestimate by 13%, and in case of corbel MC, the simulation prediction is underestimate by 17%. The initial stiffness of the experimental results is lower than that of simulation results. Crushing gypsum layer located at the bearing pad causes the rigid body movement of the specimens. Since the LVDT is located only at the bearing pad position, the rigid body movement of the specimen is included in the displacement measurement.

Both experimental and numerical results show that the maximum load of corbel EC is reduced by approximately 45 % of reduction ratio compared with that of corbel MC. It can be concluded that the position of the bearing pad is important. When the load is applied on the edge of the corbel, the load capacity of the corbel will be reduced significantly.

In case of corbel RCC, both experimental and numerical results show that the maximum load of corbel RCC is higher than that of corbel EC. The results show that the capacity of a corbel can be recovered when the loading position is moved to the straight portion of the flexural reinforcements of the corbel. Although the capacity of the corbel cannot be fully recovered, both experimental and numerical results show that the residual capacity of the corbel is still very large, i.e. 95% by experimental observation and 85% by numerical prediction. Initial damage may cause that the capacity of the corbel could not be fully recovered. Furthermore, the option to move the bearing pad to the straight portion of the flexural reinforcements can be a simple way for recovering the capacity of a corbel failed by an anchorage splitting failure. However, the site condition should be considered whether the position of the bearing pad can be moved.

6.4.2. Internal cracks of simulation results

Fig.6.8, **Fig.6.9**, and **Fig.6.10** show the internal cracks of corbel EC, corbel MC, and corbel RCC respectively. Yellow color, orange color, and red color indicate the crack face with crack width of 0.03 mm, 0.1 mm, and 0.3 mm, respectively. Generally, the crack propagations of the numerical models are roughly the same as those of the experimental specimens.

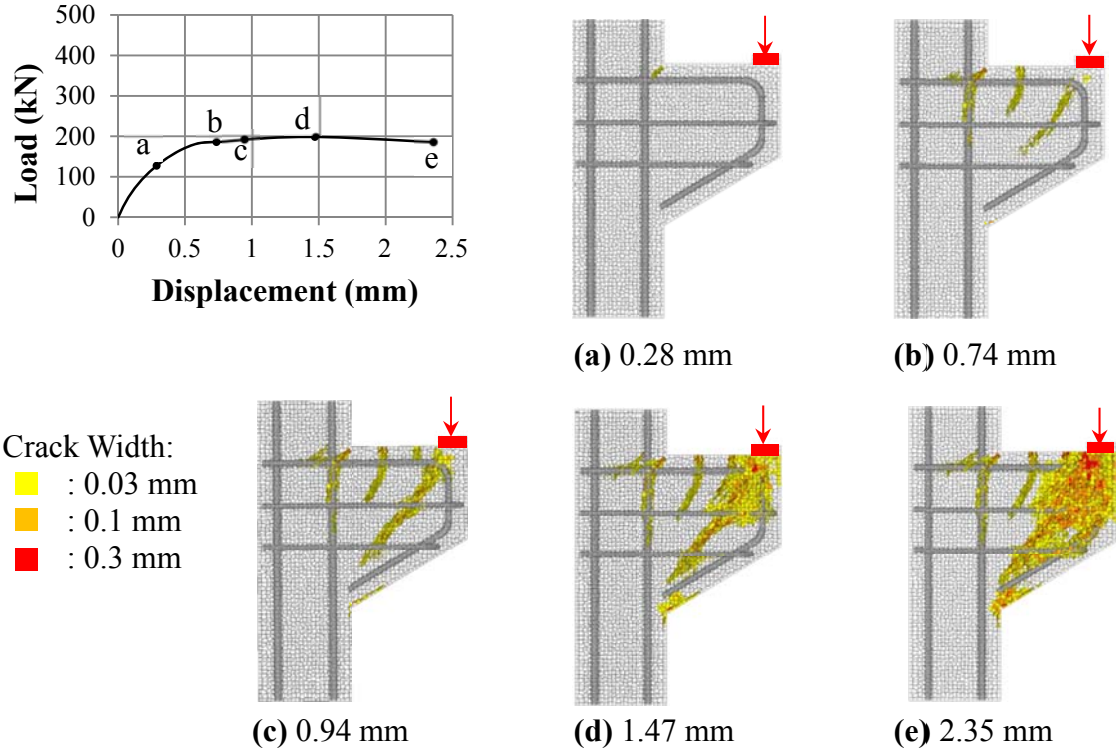

(a) 0.28 mm **(b)** 0.74 mm

(c) 0.94 mm **(d)** 1.47 mm **(e)** 2.35 mm

Fig.6.8 Internal cracks of numerical model of corbel EC

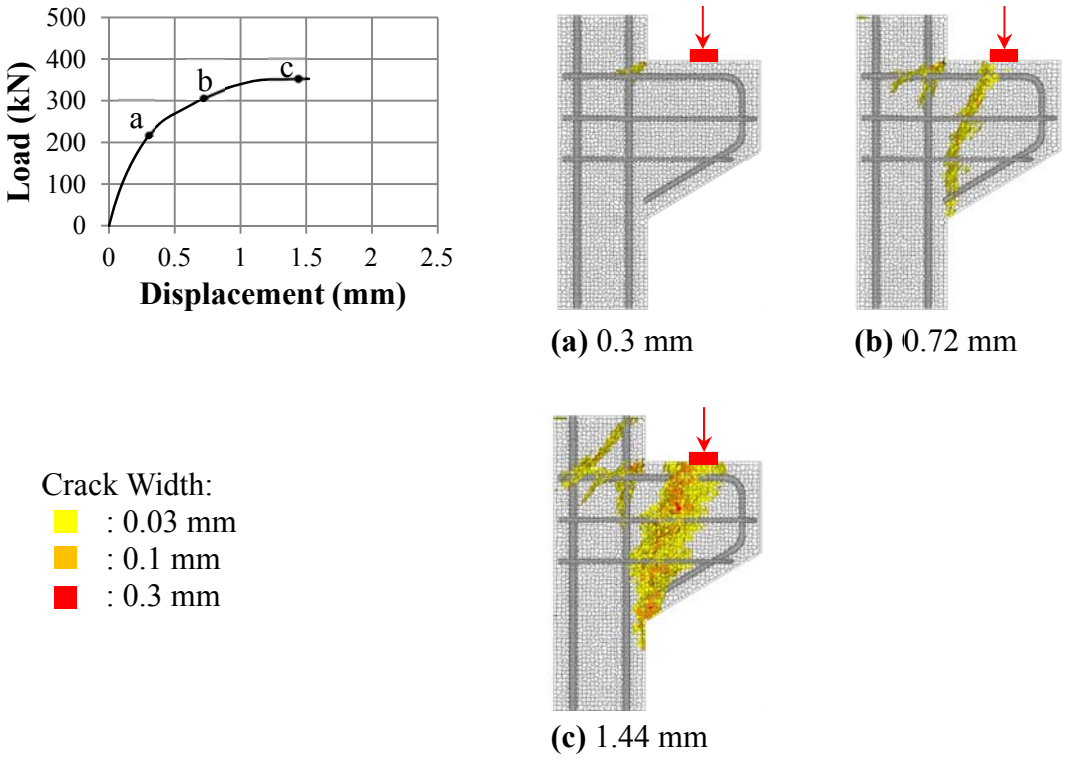

Fig.6.9 Internal cracks of numerical model of corbel MC

In case of corbel EC, when the load is relatively small, flexural cracks occur at the corbel-column interface (**Fig.6.8.a**). As the load increases, diagonal cracks occur, propagating from the position of the bearing pad to the sloping end of the corbel (**Fig.6.8.b**). In addition, simulation result can provide more detail information how the anchorage splitting cracks occur. In the early stage of the formation of the anchorage splitting cracks, cracks occur along the bending portion of the flexural reinforcements of the corbel (**Fig.6.8.c**). As the result, the stiffness of the load-displacement relationship is reduced dramatically. As the load increases, cracks propagate along the anchorage (**Fig.6.8.d** and **Fig.6.8.e**).

In case of corbel MC, when the load is relatively small, flexural cracks occur at the corbel-column interface (**Fig.6.9.a**). As the load increases, diagonal cracks, propagating from the position of the bearing pad to the sloping end of the corbel (**Fig.6.9.b**). When the load reaches the maximum load, no other type of cracks occurs in the corbel, beside the flexural cracks and diagonal cracks (**Fig.6.9.c**). Based on the simulation results, cracks occur in the column segment as the result of the simplification of the models, i.e. no stirrup of column was modeled.

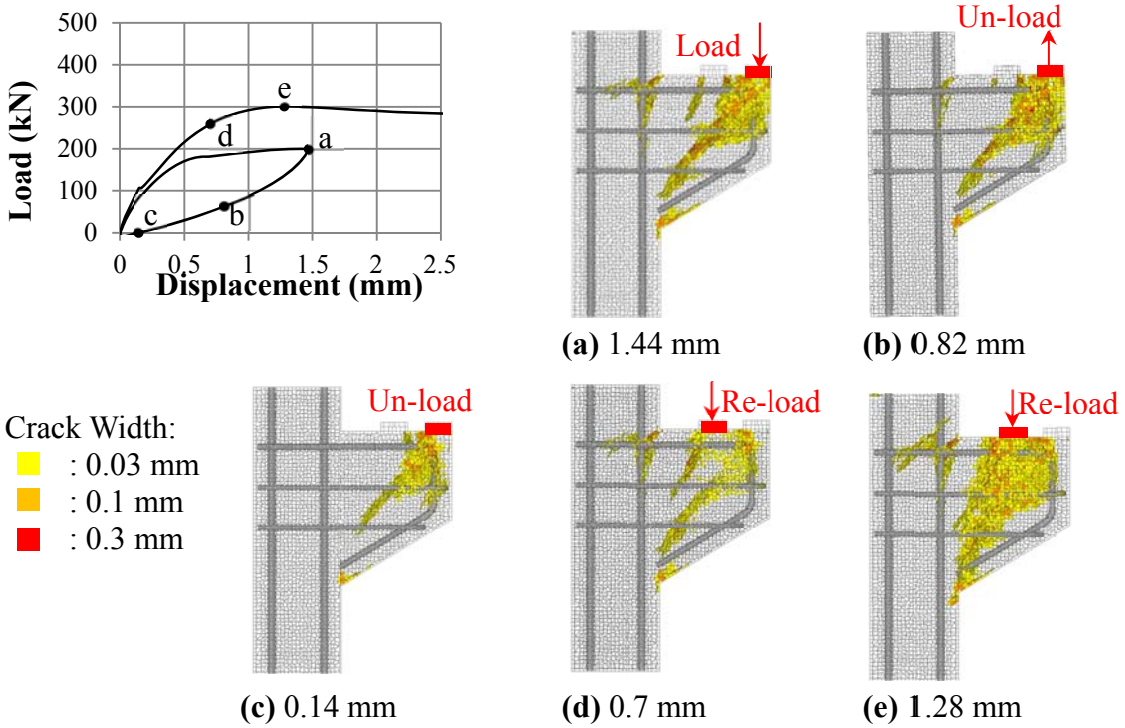

Fig.6.10 Internal cracks of numerical model of corbel RCC

In case of corbel RCC, when the load of the corbel is un-loaded, the process of the closing of cracks can be simulated well (**Fig.6.10.a**, **Fig.6.10.b**, and **Fig.6.10.c**). When the loading position is moved and re-loaded on the middle bearing pad, new diagonal cracks occur in the corbel, propagating from the position of the new bearing pad to the sloping end of the corbel.

6.4.3. Crack patterns after failure

Fig.6.11, **Fig.6.12**, and **Fig.6.13** show the crack patterns of the experimental specimens, compared with the numerical models at failure. The displacement of the models is enlarged by 10 times. Simulation results can predict the crack patterns at failure as well as those of experimental results.

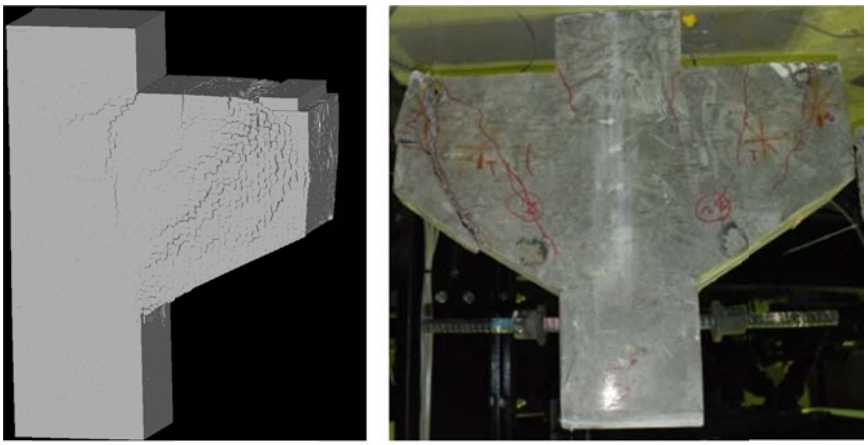

(a) Prediction **(b)** Observation

Fig.6.11 Failure pattern of corbel EC

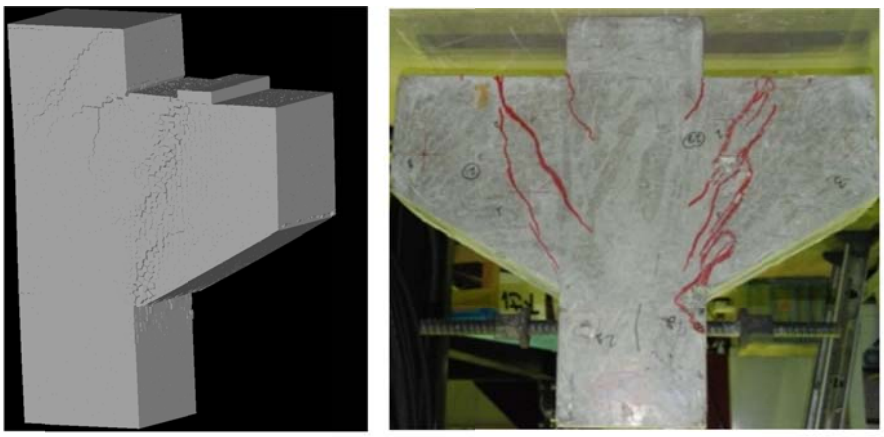

(a) Prediction **(b)** Observation

Fig.6.12 Failure pattern of corbel MC

Based on the crack pattern of corbel EC, flexural cracks, anchorage splitting cracks, and diagonal cracks propagating from the position of the bearing pad to the sloping end of the corbel occur in the numerical models and experimental specimens. In case of corbel MC, flexural cracks and diagonal cracks, propagating from the position of the bearing pad to the sloping end of the corbel occur in both numerical models and experimental specimens. Furthermore, flexural cracks, anchorage splitting cracks, anchorage splitting cracks, previous and new diagonal cracks occur in both numerical models and experimental specimens in case of corbel RCC.

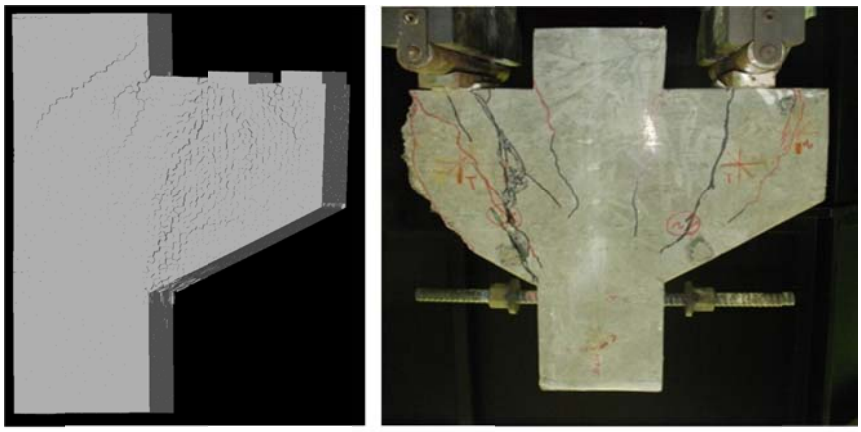

(a) Prediction (b) Observation

Fig.6.13 Failure pattern of corbel RCC

6.5 CONCLUSIONS

1. Based on the experimental results, the capacity of the corbel is reduced by approximately 45% of reduction ratio when the load is applied on the edge of the corbel. On the other hand, when a corbel failed by an anchorage splitting failure is re-loaded on the straight portion on the flexural reinforcements of the corbel, the corbel is still able to resist the load. It was observed that the residual capacity of the corbel is still very large, i.e. 95%. The option to move the bearing pad to the straight portion of flexural reinforcements of the corbel can be a simple way for recovering the capacity of a corbel failed by the local failure. However, the condition in construction site should be considered in practice.
2. Different failure pattern can be simulated due to different position of bearing pad by RBSM. The analysis could explain well the failure mechanism due to different position of bearing pad.

REFERENCES

Subcommittee on English Version of Standard Specifications for Concrete Structures., "Standard Specification for Concrete Structures "Design"," *Japan Society of Civil Engineers (JSCE)*, December 2010.

Kriz, L. B., Raths, C.H., "Connections in Precast Concrete Institute-Strength of Corbels," *Journal of Prestressed Concrete Institute*, Vol.10, No.1, February 1965, p.p. 16-61.

Ikuta, K.; Nagai, K.; Hayashi, D., "Numerical Simulation of Beam-Column Join with

Simple Reinforcement Arrangement by Three-dimensional RBSM," *International Symposium of New Technologies for Urban Safety Mega Cities in Asia (USMCA)*, 2012.

Kawai, T., "*New Discrete Models and Their Application to Seismic Response Analysis of Structure*," Nuclear Engineering and Design, 48, 207-229. 1978.

Nagai, K.; Sato, Y.; Ueda, T., "Mesoscopic Simulation of Failure of Mortar and Concrete by 3D RBSM," *J. Adv. Conc. Technol.*, 3(3), 385-402. 2005.

Chapter SEVEN

SIMULATION OF BEAM COLUMN JOINT WITH COMPLEX ARRANGMENT OF REINFORCEMENT BARS

7.1 INTRODUCTION

Reinforcement congestion, at a beam column joint, can cause difficulties during compaction of concrete, resulting poor quality of construction. To reduce the reinforcement congestion in a beam column joint, a comprehensive study of the behavior of a beam column joint is needed. However, the behavior of a beam column joint has not been clarified well. Many aspects are involved in a relatively small dimension of beam column joint.

In order to study the behavior of a beam column joint, there are 2 alternatives, i.e. experimental works and computational numerical simulations. Through experimental works, the real load-displacement relationship and surface cracks can be obtained easily. However, the internal cracks and the internal stress are difficult to be observed. Our research group has conducted a meso-scale simulation of reinforced concrete members by a 3-dimensional discrete element analysis, called RBSM. The study on a reinforced concrete member at the meso-scale, in which the local re-bar arrangement is considered by modeling the rib of re-bar, is useful for the precise evaluation of its behavior, since at this level, cracks occur as the result of the interlock mechanism between concrete and re-bar. Moreover, Ikuta *et al.* (2012) successfully simulated different crack patterns with different bending radius of re-bars of L-shaped beam column joint with simple arrangement of re-bars by RBSM. Meanwhile, the applicability of RBSM in modeling a beam column joint with a complex reinforcement arrangement has not been investigated. In this study, by modelling a complex reinforcement arrangement, the applicability of RBSM in predicting the beam column joint failure is investigated. Thus, the simulation results are compared with the experimental observations.

7.2 DETAIL OF NUMERICAL SIMULATION

7.2.1 Numerical models

Simulation was conducted for an experiment of a beam column joint, done by Japan Railway. Dimensions, reinforcements, and material properties of numerical model and experimental specimen are the same. **Table 7.1** shows the dimension and material properties of the beam column joint. **Fig. 7.1** shows the geometry of the numerical

Table 7.1 Dimension and material properties of numerical model

Model	Dimension			Number of Element	Concrete		Reinforcements	
	Width mm	Height mm	Length mm		Compressive Strength MPa	Tensile Strength(JSCE) MPa	Modulus of Elasticity MPa	Yield Stress MPa
1	400	1500	1900	690741	21.1	1.75	190000	365

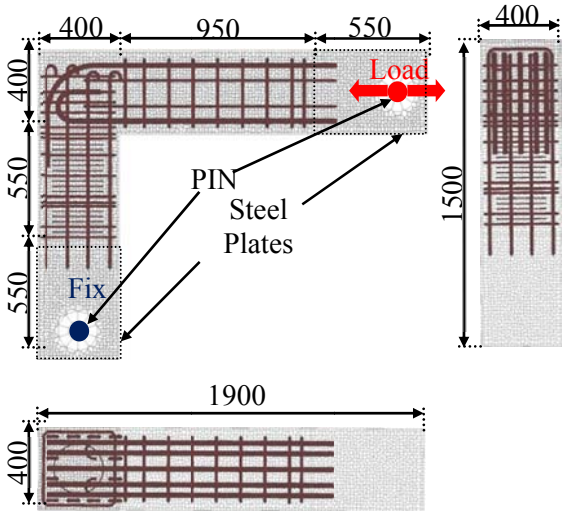

Fig. 7.1 Geometry and boundary condition of numerical model (Units: mm)

model. 690741 elements were used to model the beam column joint. As the comparison, **Fig. 7.2** shows the detail of the experimental specimen.

7.2.2 Boundary conditions

Fig. 7.3 shows the boundary condition of the numerical model. Steel plates were modeled located at the end of the beam and the column. The stiffness of the steel plates

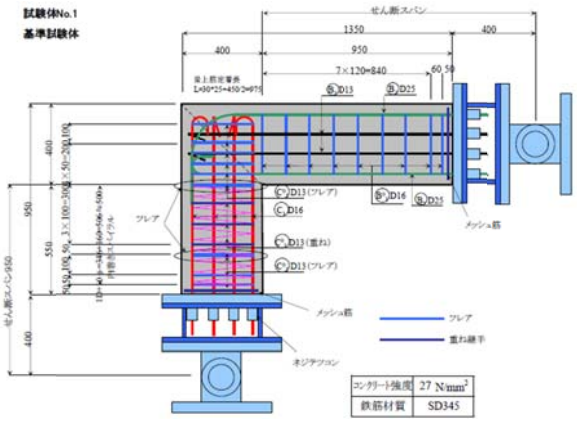

Fig. 7.2 Detail of experimental specimen

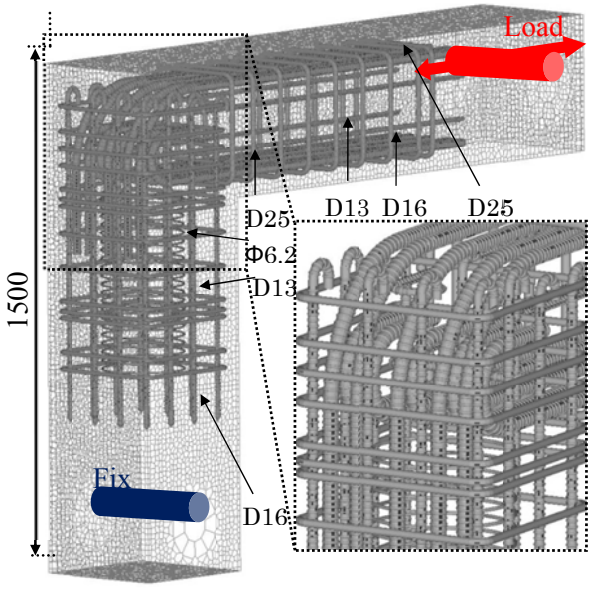

Fig. 7.3 Boundary condition of numerical model

was assumed rigid enough, so that the deformation of the steel plates will be prevented. In order to model the hinged condition, a pin element is introduced, located in the steel plates. Furthermore, in a pin element, forces are transferred only through normal springs of the pin element. Cyclic load of displacement control, pull load and push load alternately, was applied to the pin, located at the end of the beam. **Fig. 7.4** shows the experimental setup.

Fig. 7.4 Experimental setup

Table 7.2 Maximum load of the experimental specimen and numerical model

Case	Experiment(P_{exp})	Simulation(P_{ana})	P_{exp}/P_{ana}
Open	160.3 kN	114.2 kN	71%
Close	272.3 kN	217.9 kN	75%

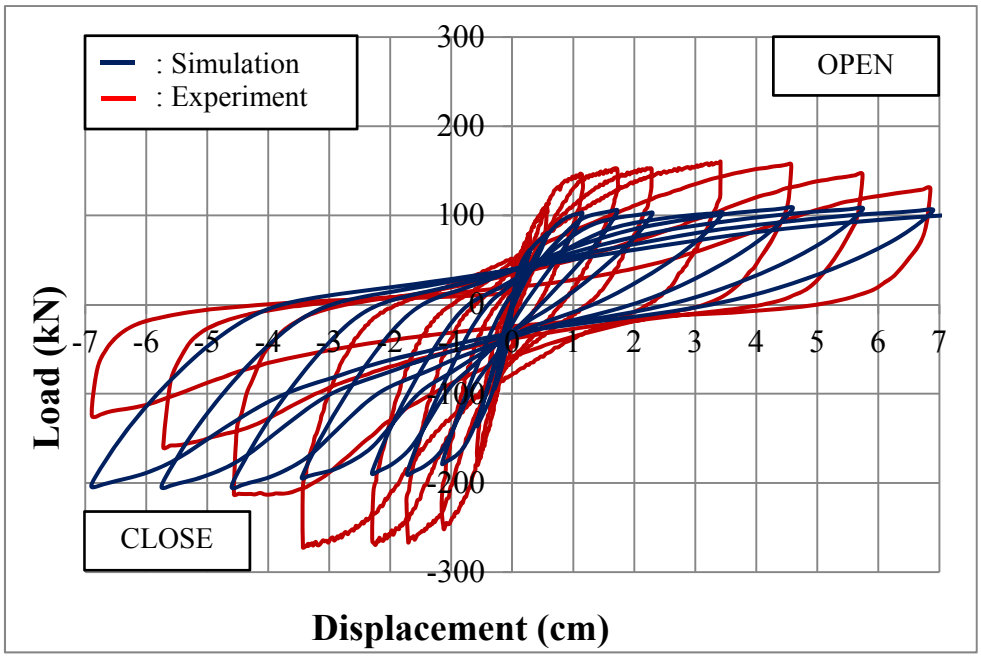

Fig. 7.5 Load-displacement relationship

7.3 RESULTS AND DISCUSSION

7.3.1 Load-displacement relationships

Fig. 7.5 shows the load-displacement relationship of simulation result, compared with the experimental observation. **Table 7.2** shows the maximum load of the experimental specimen and numerical model. The load and the displacement of the load-displacement relationship of numerical model were determined based on the load and the displacement which were applied to the pin, located at the end of the beam. The maximum loads of numerical model are roughly the same as those of experimental specimen, i.e. approximately 25-29% difference.

Both experimental and simulation results show that the maximum load of open case is lower than that of close case. Furthermore, the failure behavior of the beam column joint will be described below.

7.3.2 Internal cracks

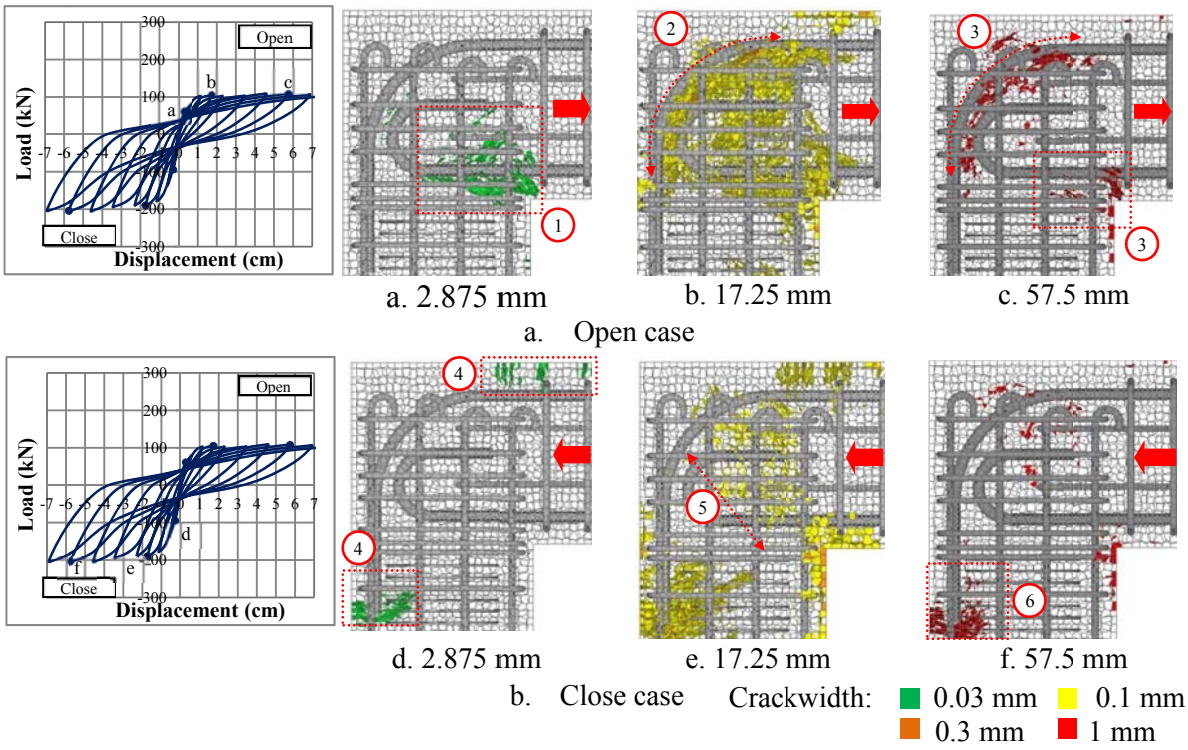

Fig. 7.6 Internal cracks

Fig. 7.6.a shows the internal cracks of the beam column joint in case of open case. When the load is relatively small, at displacement of 2.875mm, flexural cracks occur on the re-entrant corner of beam column joint (1). As the load increases, at displacement of 17.25 mm, typical diagonal cracks, roughly parallel to the bending portion of the anchorages, occur (2). At displacement of 57.5 mm, large width of cracks occurs parallel to the bending portion of the anchorages and on the re-entrant corner of beam column joint (3). **Fig. 7.6.b** shows the internal cracks of the beam column joint in case of close case. When the load is relatively small, at displacement of 2.875 mm, flexural cracks occur outside the bending portion of the bar anchorages and at the end of the anchorages (4).

As the load increases, at displacement of 17.25 mm, typical diagonal cracks, roughly perpendicular to the bending portion of the anchorages occur (5). At displacement of 57.5 mm, large width of cracks occurs at the end of the anchorages (6). Based on this observation, it can be concluded that the anchorage of beam reinforcements influences the behavior of beam column joint.

7.3.3 Internal stress

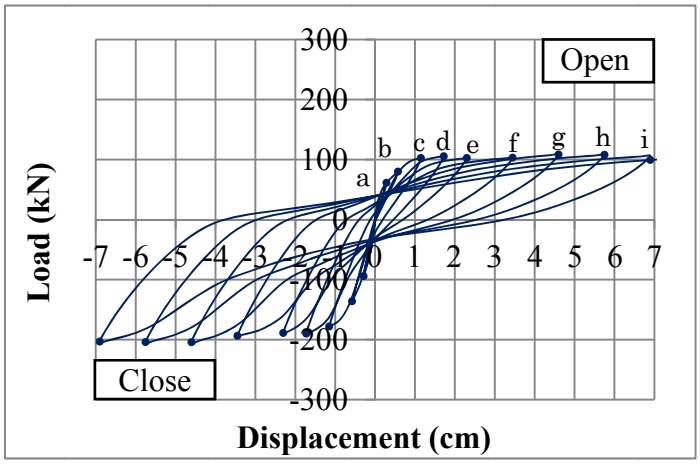

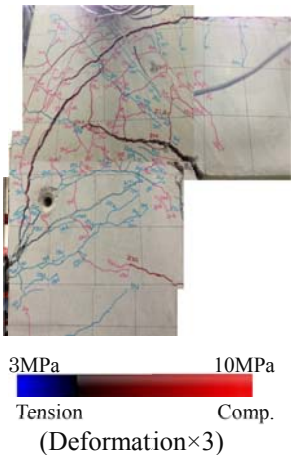

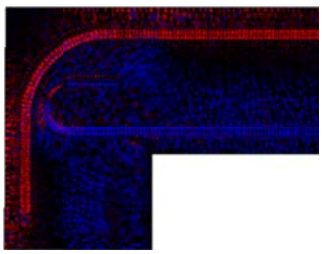

(a) Disp. 2.875 mm

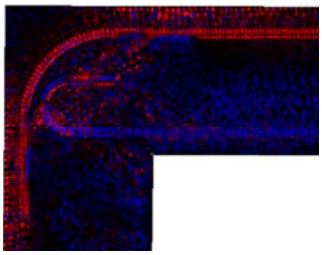

(b) Disp. 5.75 mm

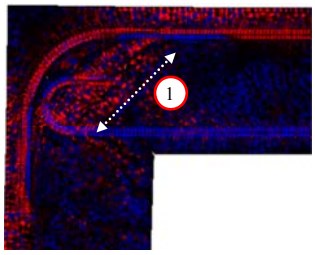

(c) Disp. 11.5 mm

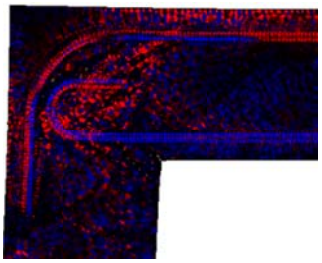

(d) Disp. 17.25 mm

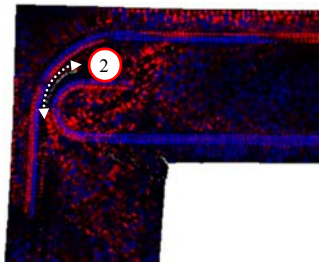

(e) Disp. 23 mm

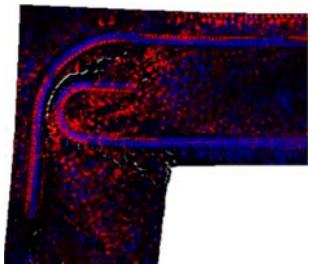

(f) Disp. 34.5 mm

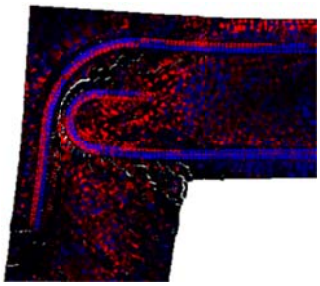

(g) Disp. 46 mm

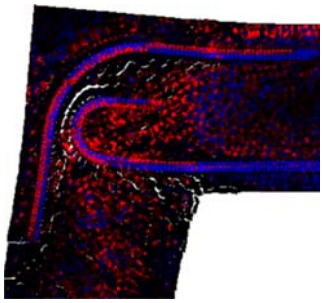

(h) Disp. 57.5 mm

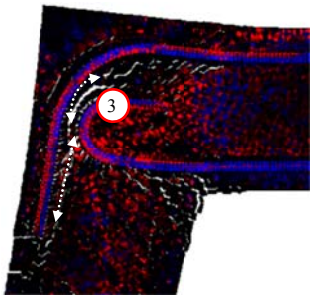

(i) Disp. 69 mm

Fig. 7.7 Internal stresses of open case

Fig. 7.7 shows the internal stresses of beam column joint when is loaded by a moment

that tends to open the beam column joint. Simulation results predict that complicated stresses, i.e. local compressive and tensile stresses, developed inside a beam column joint with complex arrangement of reinforcement bars.

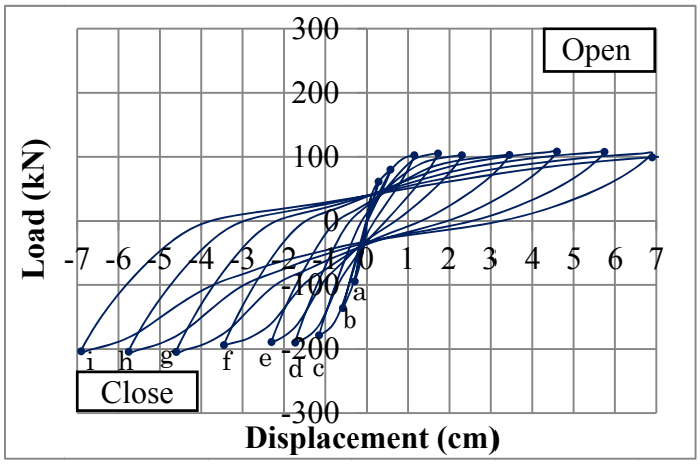

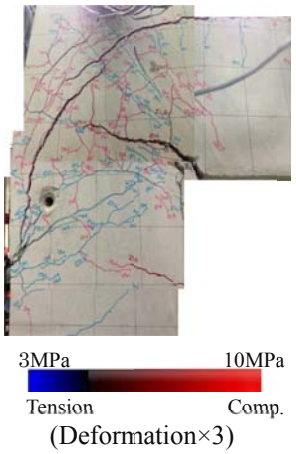

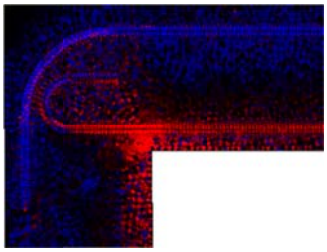

(a) Disp. 2.875 mm

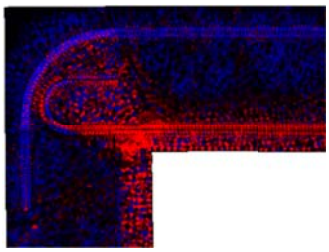

(b) Disp. 5.75 mm

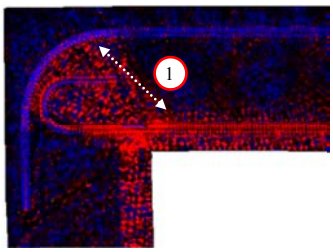

(c) Disp. 11.5 mm

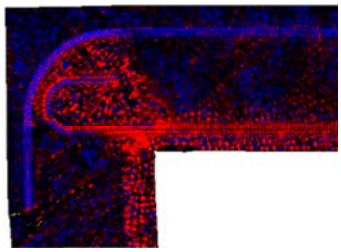

(d) Disp. 17.25 mm

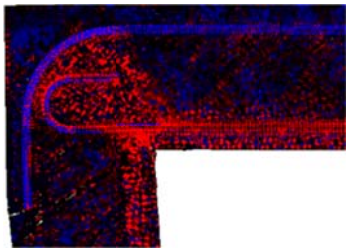

(e) Disp. 23 mm

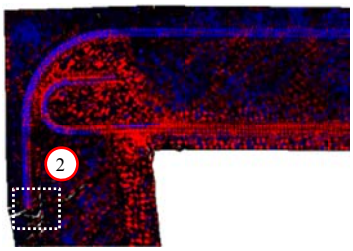

(f) Disp. 34.5 mm

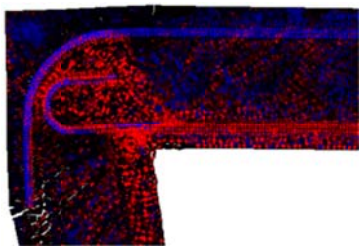

(g) Disp. 46 mm

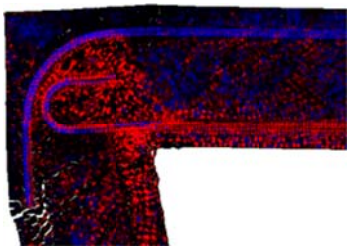

(h) Disp. 57.5 mm

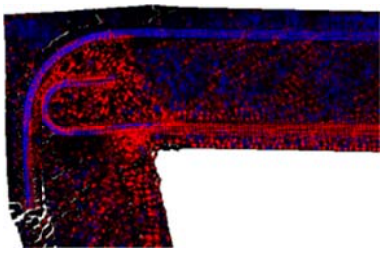

(i) Disp. 69 mm

Fig. 7.8 Internal stresses of close case

Furthermore, based on the internal stresses of the reinforcement bars, compressive stresses and tensile stresses also may occur in one reinforcement bar and simulation can predicts these behaviours.

When the displacement is relatively small, compressive stresses which are parallel to the bending portion of the anchorage bars, develop in a beam column joint (1). As the load increases, cracks that are parallel to the bending portion of the anchorages occur in the beam column joint (2). As cracks at the end of the anchorages open easier, these parallel cracks can open easily without any restrictions and are connected (3).

Fig. 7.9 shows the internal stresses of beam column joint when is loaded by a moment that tends to close the beam column joint. Diagonal compressive stresses which are perpendicular to the bending portion of the anchorages occur in the beam column joint (1). When the diagonal stresses exceed the capacity, some local cracks will occur that causes the diagonal cracks perpendicular to the bending portion of the anchorages. In addition, cracks are open easily at the end of the anchorage, because the weak region between concrete and reinforcement bar (2).

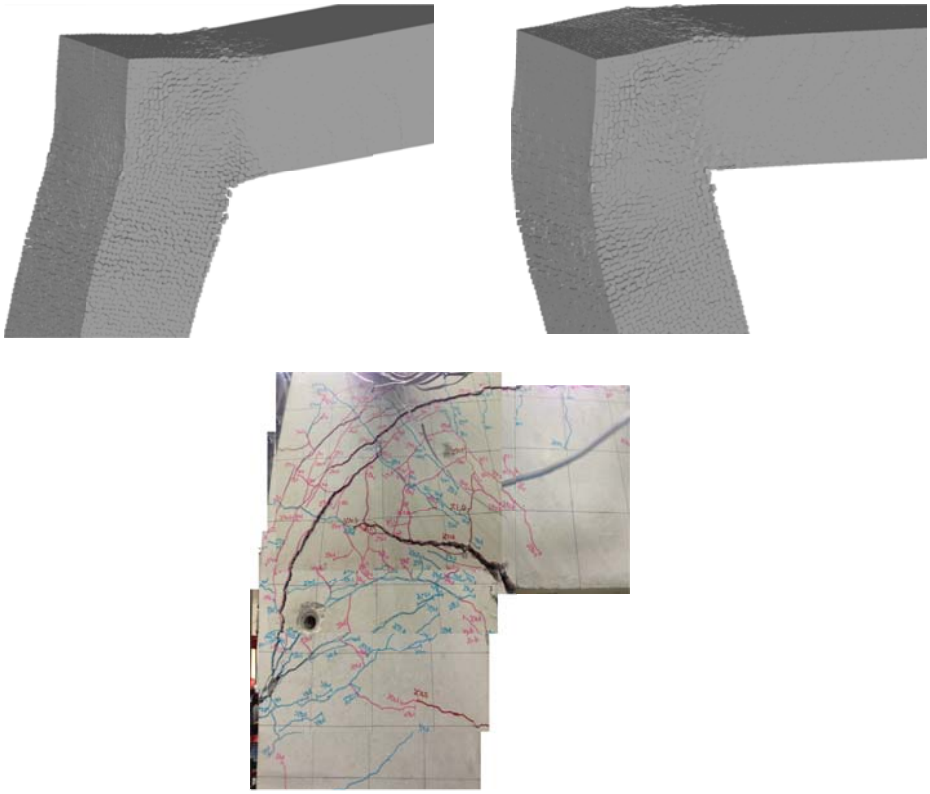

Fig. 7.9 Surface cracks (Deformation×3)

7.3.4 Surface cracks

Fig. 7.7 shows the surface cracks of the numerical model, compared with experimental specimen at failure. Large width of cracks occurs parallel to the bending portion of the anchorages and on the re-entrant corner of beam column joint in case of open case. On the other hand, large width of cracks occurs at the end of the anchorages in case of close case. The experimental specimen shows the same behavior.

CONCLUSIONS

1 Same tendency of load-displacement relationship with experiment was predicted. Maximum load in open case is lower than that of in close case

2 Different failure patterns can be predicted by RBSM due to different loading conditions. When the beam column joint is loaded to a moment that tends to close the beam column joint, cracks which are perpendicular to the bending portion of the anchorages occur that is caused by the diagonal compressive stresses perpendicular to the bending portion of the anchorages. In addition, since the interface between concrete and reinforcement bar is a weak region, this region can open easily when the beam column joint is loaded under this close moment. On the other hand, when the beam column joint is loaded to a moment that tends to open the beam column joint, cracks parallel to the bending portion of the anchorages occur. Since cracks at the end of the anchorages open easily due to the close moment, these parallel cracks can open easily without any restriction. Compressive stresses which are parallel to the bending portion of anchorages also occur under this open moment.

3 Simulation results predict that complicated stresses occur in a beam column joint with complex arrangement of reinforcement bars.

REFERENCES

Ikuta K., Hayashi D., & Nagai K., "Numerical simulation of beam column joint with simple reinforcement arrangement by three-dimensional RBSM," *ICUS Report Serial*, No.65, 2012, pp.173-180.

Kawai T., "New discrete models and their application to seismic response analysis of structure," *Nuclear Engineering and Design*, 48, 1978, 207-229.

Nagai K., Sato Y., & Ueda T., "Mesoscopic simulation of failure of mortar and concrete by 3D RBSM," *Journal of Advanced Concrete Technology*, Vol.3, No.3, 2005, pp. 385-442.

Chapter EIGHT

SIMULATION OF BEAM COLUMN JOINT WITH MECHANICAL ANCHORAGE

8.1 INTRODUCTION

Reinforcement congestion in a beam column joint can cause difficulties during compaction and, consequently, a poor quality of concrete is obtained. One way to reduce the reinforcement congestion is by using mechanical anchorage by introducing a simpler anchorage and a shorter length of the anchorage (see **Fig. 8.1**.). However, the use of the mechanical anchorage is still limited in the reinforced concrete members with thin concrete cover because the performance has not been well understood (JSCE 2007).

When the mechanical anchorages are applied, the reinforcement arrangement becomes simpler, but local failure occurs in the beam column joint due to the stress concentration from the anchorages plates, resulting brittle failure (Yoshimura *et al.* 2007) when the beam column joint is loaded by a moment that tends to close the beam column joint. In order to strengthen this anchorage system, additional local reinforcement bars should be added along the anchorages. Many experiments were necessary in order to find a rational way strengthening this anchorage system. However, a rational method to strengthen the mechanical anchorage system has not been found since the internal stress condition and the internal cracking pattern have not been well understood. Finally, it was concluded that the safest way to use this anchorage system is by adding concrete block at the top of beam column joint. However, the additional concrete block at the top beam column joint sometimes cannot be applied at the construction site. Simulation can be a beneficial tool to reveal the failure process of the beam column joint with mechanical anchorages in order to find a rational method to strengthen this system in the future.

Fig. 8.1 Mechanical anchorage

In this study, a meso-scale analysis of reinforced concrete member by 3D discrete element analysis, called 3D RBSM, was conducted. The study by 3D meso-scale discrete analysis is useful since the reinforcement arrangement can be modeled in an accurate manner, i.e. the rib of a reinforcement bar and the 3D model of a reinforcement bar, local failure can be predicted precisely as the result of the discontinous deformation of concrete and the the interaction of concrete and a reinforcement bar at meso-scale level, and cracks can be introduced directly as the displacement between 2 elements. Moreover, Wang *et al.* (2014) successfully simulated different crack patterns due to different anchorage systems of knee-joint by 3D RBSM. Eventually, the purpose is to investigate the effect of the local reinforcement arrangement, especially the arrangement of stirrups along the anchorage, on the failure process of beam column joints by 3D discrete model, through the comparison with experimental results. Capacity, cracking pattern, and local internal stress condition of simulation results will be investigated. In addition, by revealing the failure process will be proposed by the simulation considering the local stress and the crack propagation.

8.2 OVERVIEW OF EXPERIMENTAL STUDIES BY YOKOHAMA NATIONAL UNIVERSITY

Yokohama National University in Japan conducted many experiments in order to find the best location of local reinforcements in a beam column joint with mechanical anchorages through the studies done by Kiyohara *et al.* (2011), Kato *et al.* (2011), and Yoshimura *et al.* (2012). **Figs 8.2**, **8.3**, **and 8.4** shows the experimental specimens that were conducted Kiyohara *et al.* (2011), Kato *et al.* (2011), and Yoshimura *et al.* (2012)m respectively. Experimental results showed that just by changing the local arrangement of reinforcement bars affects the local failure significantly.

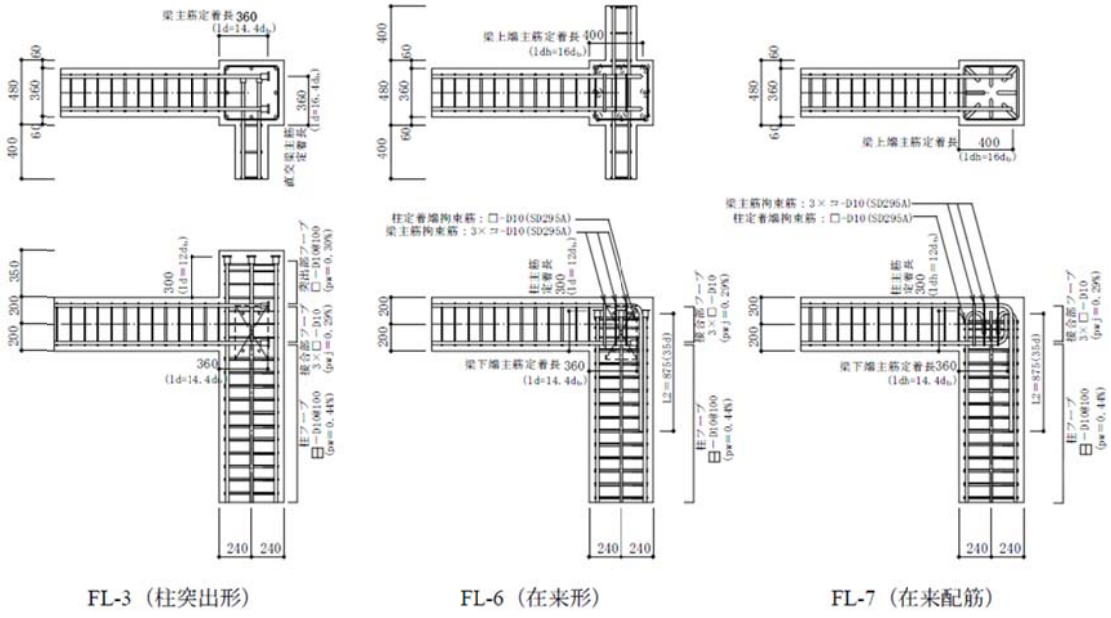

Fig. 8.2 Experimental specimens (Kiyohara *et al.* 2011**)**

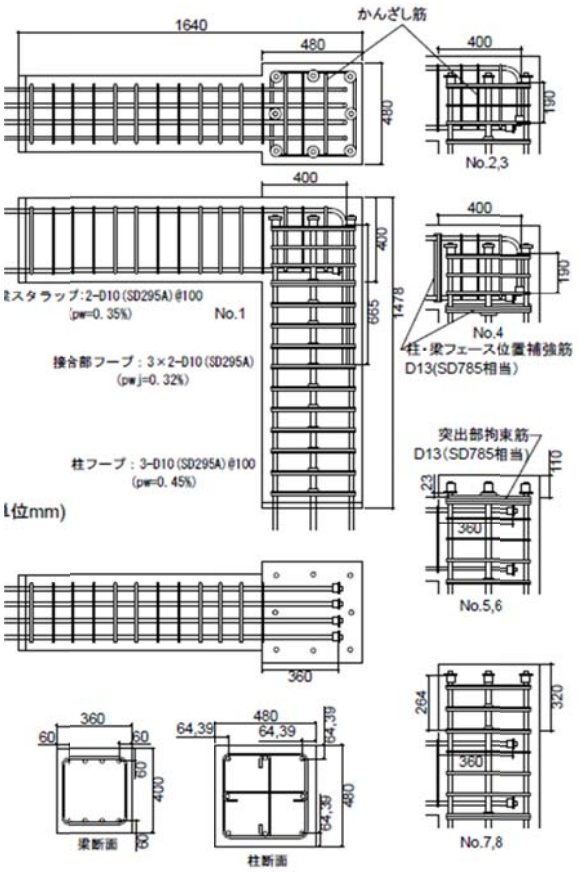

Fig. 8.3 Experimental specimens (Kato *et al.* 2011)

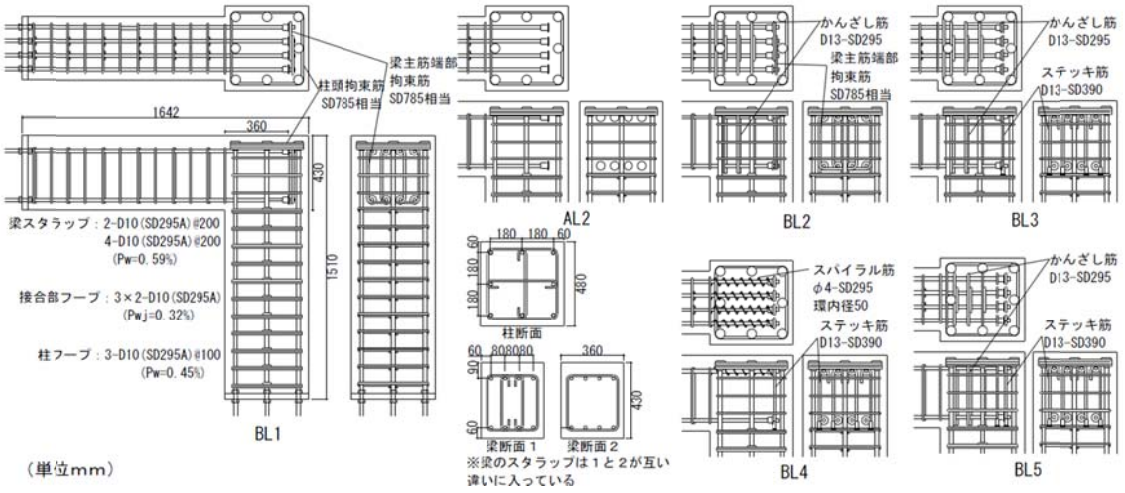

Fig. 8.4 Experimental specimens (Yoshimura *et al.* 2012)

8.3 DETAIL OF NUMERICAL SIMULATION

8.3.1 Numerical models

Three numerical models with different stirrups arrangement and one numerical model with additional concrete block at the top of beam column joints were simulated. Three numerical models were conducted for experiments, carried out by Yoshimura *et al.* (2012) and one numerical model was conducted for experiments done by Kato *et al.* (2011). In this study, the effect of the stirrups arrangement along the anchorage and additional concrete block at the top of beam column joint is the main focus.

Table 8.1 Detail of numerical models

Case	Parameter	Material Properties of Concrete			Number of elements	Maximum Load	
		Compressive f'_c (MPa)	Tensile f_t (MPa)	Elasticity E_s (MPa)		ANA (kN)	EXP (kN)
AL2	No stirrups	30.8	2.43	27900	756638	85.0	94.5
BL1	One stirrup (at the anchorage plates)	33.2	2.58	24200	766375	113.8	120.3
BL2	Four stirrups (at the anchorage plates and along the anchorage)	33.5	3.09	25800	805706	122.3	135.1
FL5	Additional concrete block	34.2	2.86	28600	778079	112.0	118.8

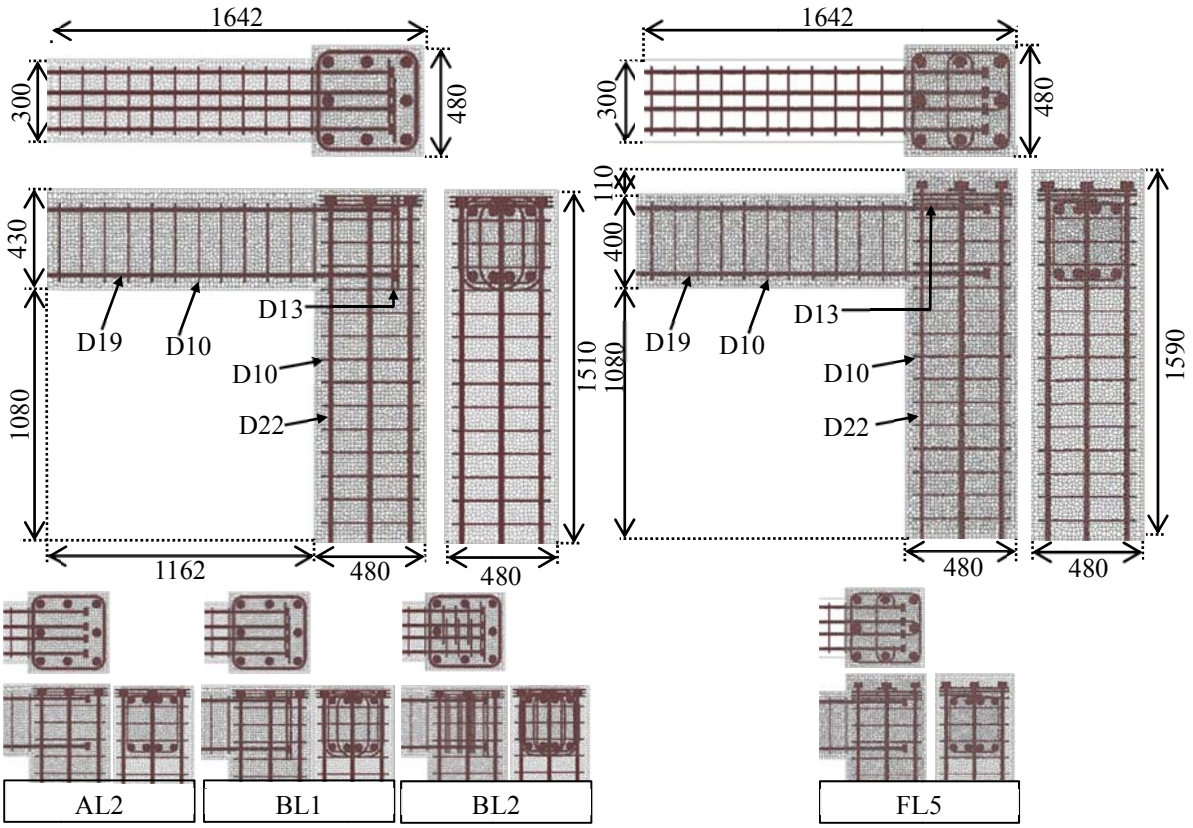

Fig. 8.5 Geometry of numerical models (Units: mm)

Numerical models are listed in **Table 8.1**. For the recognition of the variables in each model, the numerical models have the same notations with the experimental specimens. AL2 signifies that no stirrup was provided along the anchorage, BL1 signifies that stirrups were provided only at the position of the anchorage plates, and BL2 signifies that four stirrups were provided at the position of the anchorage plates and along the anchorage. FL5 signifies that concrete block is added at the top of the beam column joint.

8.3.2 Geometry of numerical models

Fig. 8.5 shows the geometry of the numerical models. The same dimensions, as the experimental specimens, were modeled. As the comparison, the detail of experimental specimens, conducted by Yoshimura *et al.* (2012) and Kato *et al.* (2011), is shown in **Figs. 8.6** and **8.7**, respectively. The reinforcement arrangement of numerical models was modeled as the same as that of experimental specimens. Deformed bars of 19 mm and 22 mm were used as the main reinforcement of column and beam, respectively. For the simplification of the model and in order to reduce the computational time, plain bar was

used for modeling all stirrups. Plain bars of 10 mm were used as the stirrups of both column and beam. Meanwhile, since local reinforcement arrangement affects the macroscopic behavior significantly, deformed bars of 13 mm were used as the stirrups at the position of anchorage plates and along the anchorage in the beam column joint. Material properties of reinforcement bars of each model are shown in **Table 8.2**. The material properties of numerical models are the same as those of experimental specimens.

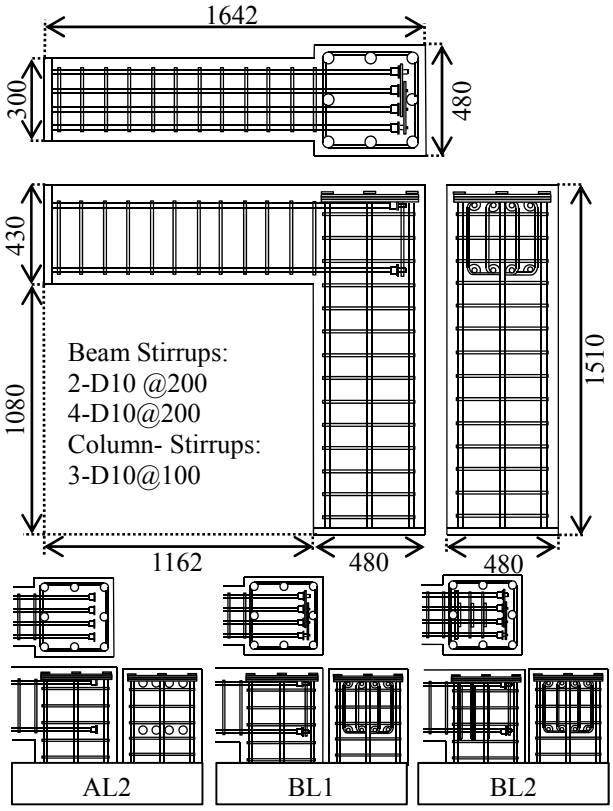

Fig. 8.6 Geometry of experimental specimens (Units: mm) (Yoshimura *et al.* 2011)

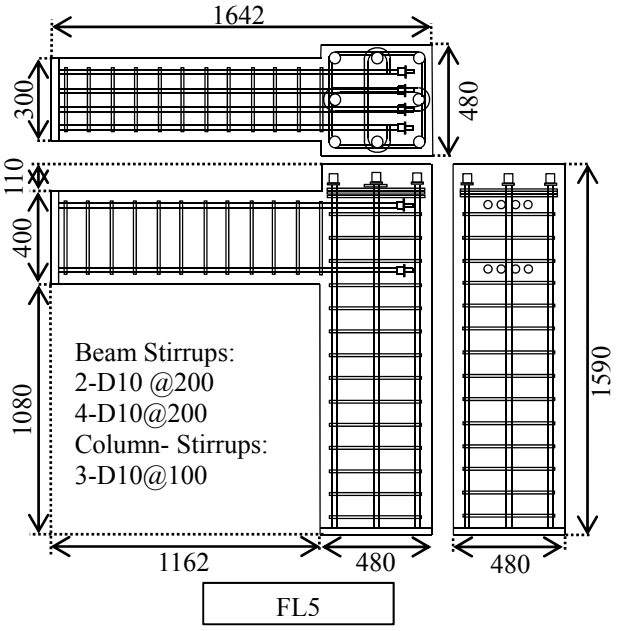

Fig. 8.7 Geometry of experimental specimens (Units: mm) (Kato *et al.* 2011)

Table 8.2 Material properties of reinforcement bars

Re-bars	Function	Numerical Model	Yield Strength MPa	Modulus of Elasticity
		MPa		
D22	Main reinforcement of column	AL2	377	183000
		BL1-BL2	392	193000
		FL5	395	196000
D19	Main reinforcement of beam	AL2	435	184000
		BL1-BL2	458	199000
		FL5	445	197000
D13	Stirrups at the anchorage plates	BL1-BL2	806	193000
D13	Stirrups along the anchorage	BL1-BL2	368	197000
D10	Stirrups of beam and column	AL2	363	203000
		BL1-BL2	368	197000
		FL5	368	183000

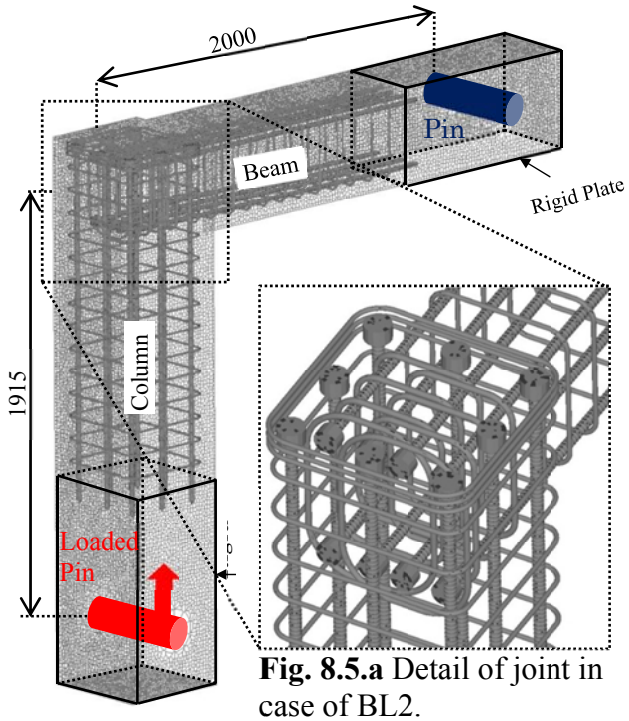

Fig. 8.5.a Detail of joint in case of BL2.

Fig. 8.8 Boundary condition (Units: mm)

8.3.3 Boundary conditions

Boundary conditions of numerical models are shown in **Fig. 8.8** As the comparison, the detail of the experimental setup is shown in **Fig. 8.9** Steel plates were modeled located at the end of the beam and the column. The stiffness of the steel plates was assumed rigid enough, so that deformation of the steel plates will be prevented. In order to model the hinged condition, a pin element is introduced, located in the steel plates. Furthermore, in a pin element, forces are transferred only through normal springs of the pin element.

Cyclic load was applied to the experimental specimens. However, since brittle failure was observed only when the beam column joint was loaded by a moment that tends to close the beam column joint and the stirrups arrangement may affect significantly on the anchorage performance under this load, only push load case will be discussed in this study. Monotonically displacement controlled was applied to the pin located at the end of the column and fix condition was assumed at the pin, located at the end of the beam. The displacement increases 0.1 mm for each step of load, and 1000 steps were applied.

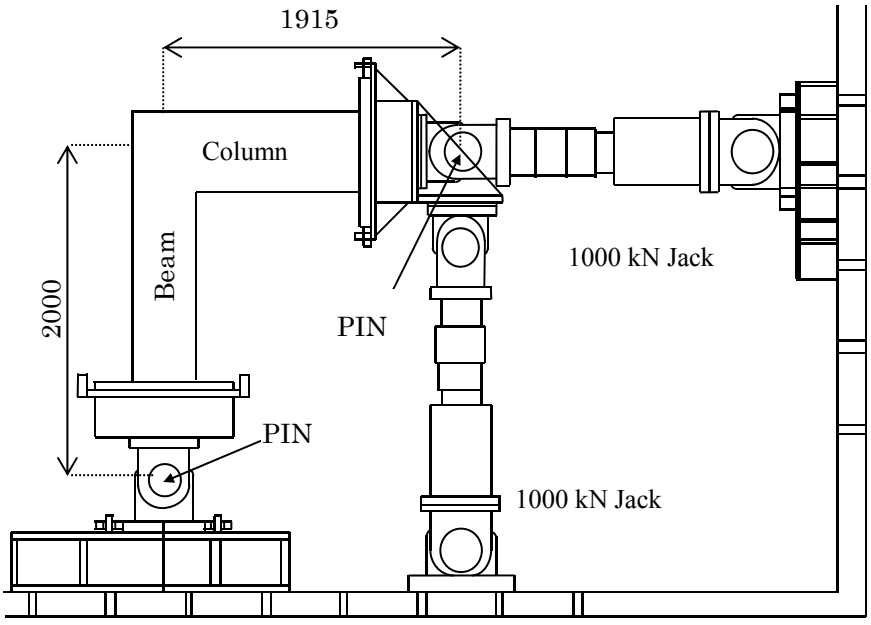

Fig. 8.9 Experimental setup (Units: mm)

8.4 RESULTS AND DISCUSSION

8.4.1 Load-displacement relationships

Load-displacement relationships of experimental specimens are compared with those of numerical models, in case of AL2, BL1, BL2, and FL5. **Fig. 8.10** and **Fig. 8.11** show the load-displacement relationships of experimental specimens and numerical models, respectively, in case of AL2, BL1, BL2, and FL5. The load of load-displacement relationships, both experimental specimens and numerical models, was determined based on the load which was applied to the pin, located at the end of the column. Meanwhile, the displacement of load-displacement relationships, both experimental specimens and numerical models, was calculated based on the drift angle. **Table 8.1** shows the maximum loads of experimental specimens and numerical models.

The maximum loads of numerical models were roughly the same as those of experimental specimens, i.e. approximately 5-10% difference. In case of AL2, the simulation underestimated by 10%, in case of BL1, the simulation underestimated by 5%, in case of BL2, the simulation underestimated by 10%, and in case of FL5, the simulation underestimated by 5%. Thus, the maximum loads of numerical models coincide well with those of experimental specimens.

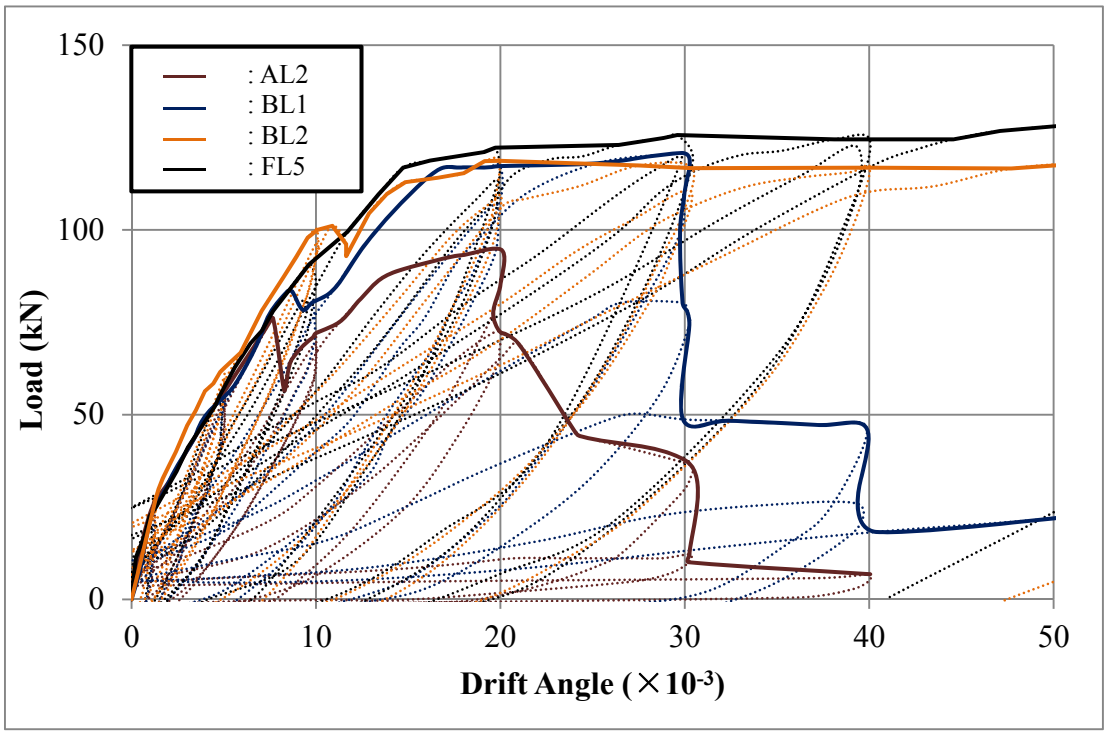

Fig. 8.10 Load-displacement relationships of experimental specimens

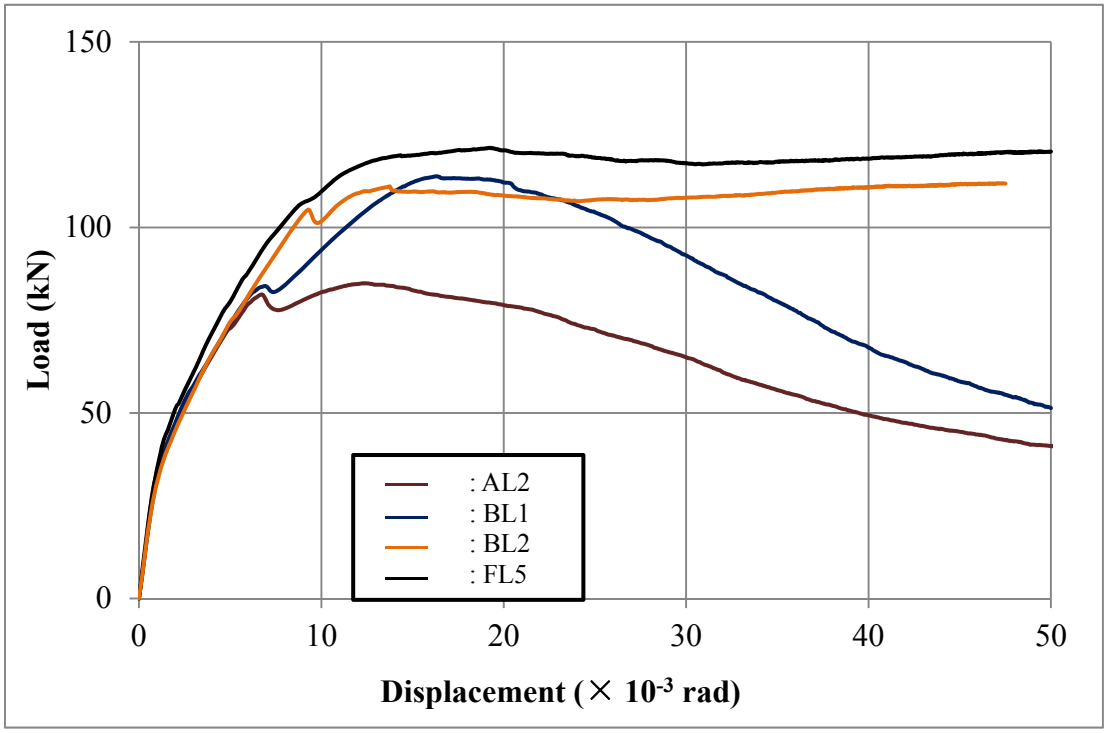

Fig. 8.11 Load-displacement relationships of numerical models

Based on the load-displacement relationship of simulation results, the same tendency as the experimental results was predicted. The maximum load of BL1 is higher than that of AL2. The maximum load of FL5 is higher than that of BL1. The maximum load of BL2 is higher than that of FL5. Simulation results predict that the load decreases significantly after the maximum load in case of AL2 and BL1. Meanwhile, in case of BL2 and FL5 the load does not decrease significantly.

In case of AL2, BL1, FL5, the load slightly dropped before the peak load approximately at the displacement of 6-10 x 10^{-3} rad. In case of AL2, the load dropped earlier than BL1 and FL5. Furthermore, in case of BL1, the load dropped earlier than FL5. The same tendency as experimental results was predicted.

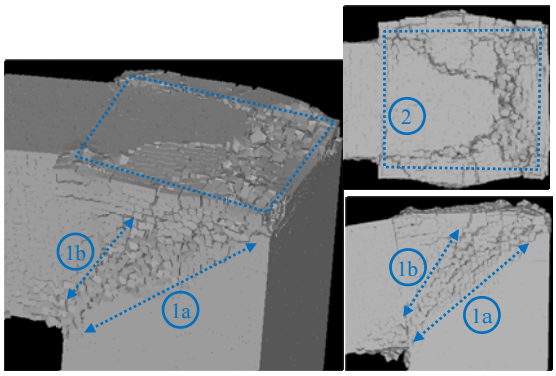

a. Predicted failure pattern of AL2 (Deformation×3)

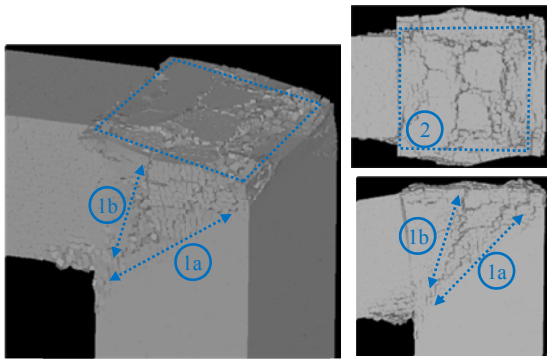

b. Predicted failure pattern of AL2 (Deformation×3)

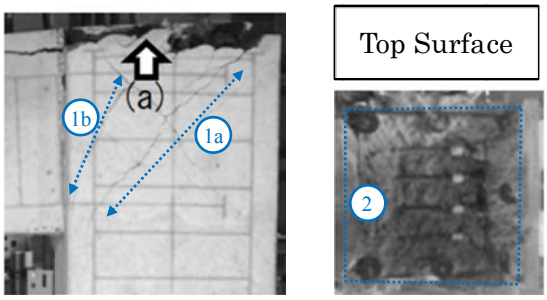

c. Observed failure pattern of AL2

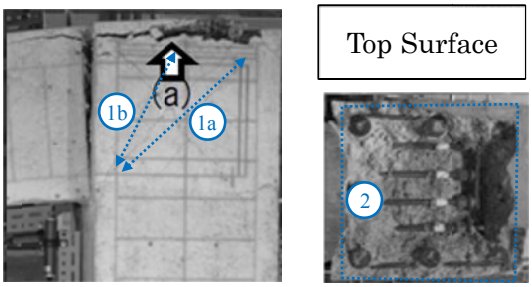

d. Observed failure pattern of BL1

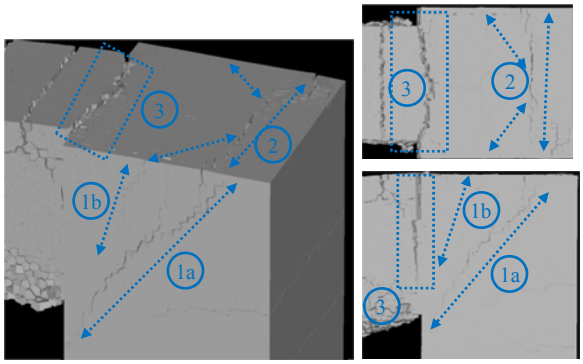

e. Predicted failure pattern of BL2 (Deformation×3)

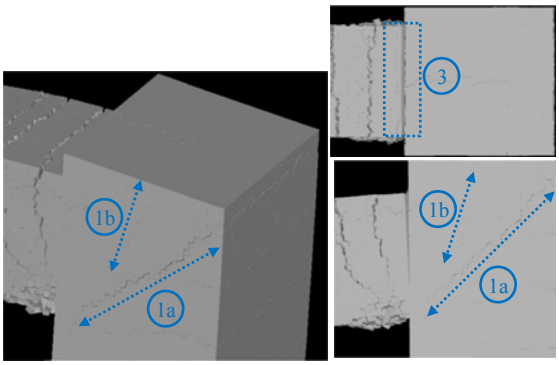

f. Predicted failure pattern of FL5 (Deformation×3)

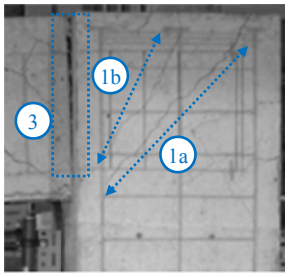

g. Observed failure pattern of BL2

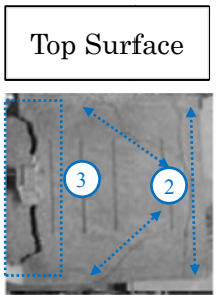

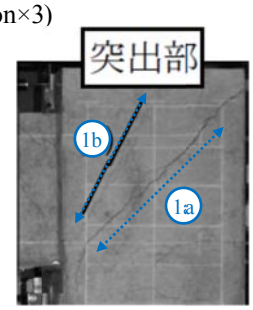

h. Observed failure pattern of FL5

Fig. 8.12 Surface cracks after failure

8.4.2 Surface cracks after failure

Surface cracks of experimental specimens are compared with those of numerical models, in case of AL2, BL1, and BL2. **Fig. 8.12** shows surface cracks of both numerical models and experimental specimens after failure. Generally, the crack patterns of numerical models are roughly the same of those of experimental specimens.

In all cases, simulation results predicted that diagonal cracks, propagating from the anchorage plates of top longitudinal bars of beam to the corner beam column joint ((1a)) and from the anchorage plates of middle longitudinal bars of the column to the corner of beam column joint ((1b)), occurred in the numerical models. As the comparison, the same cracks were observed in the experimental specimens.

In case of AL2 and BL1, simulation results predicted that damage occurred at the top surface of numerical models which indicated the anchorage failure in the beam column joint ((2)).However, the spalling of concrete at the top surface of numerical models, could not be simulated as well as experimental specimens so that simulation could not simulate well the sudden drop in capacity after exceeding the maximum load.

In case of BL2, the simulation result predicted that cracks, along the end of anchorage plates and propagating from the anchorage plates of top longitudinal bars of the beam to the side of the specimen, occurred at the top surface of numerical model ((2)). Fewer cracks were predicted at the top surface of beam column joint in case of FL5. Meanwhile, the width of the flexural crack of BL2 and FL5 was predicted larger than that of AL2 and BL1 that indicated the flexural failure in the beam column joint. The same cracks were also observed in the experimental specimens ((3)).

8.4.3 Internal stress

Fig. 8.13 shows the internal stress distribution of numerical models at the displacement of 0.006-0.01 rad, before slight drop of load is predicted. As described before, the occurrence of the slight drop of load was earlier in case AL2 and BL1. Based in the internal stress distribution in beam column joints, the compressive stresses along the development length of BL2 and FL5 are larger than AL2 and BL1 ((1)). Meanwhile there is no significance difference of stress distribution along the development length between AL2 and BL1. Based on these behaviors, it is confirmed based on the simulation results that in case of BL1 and FL5, the occurrence of the slight drop of load is delayed because of the increase of the bond performance along the development

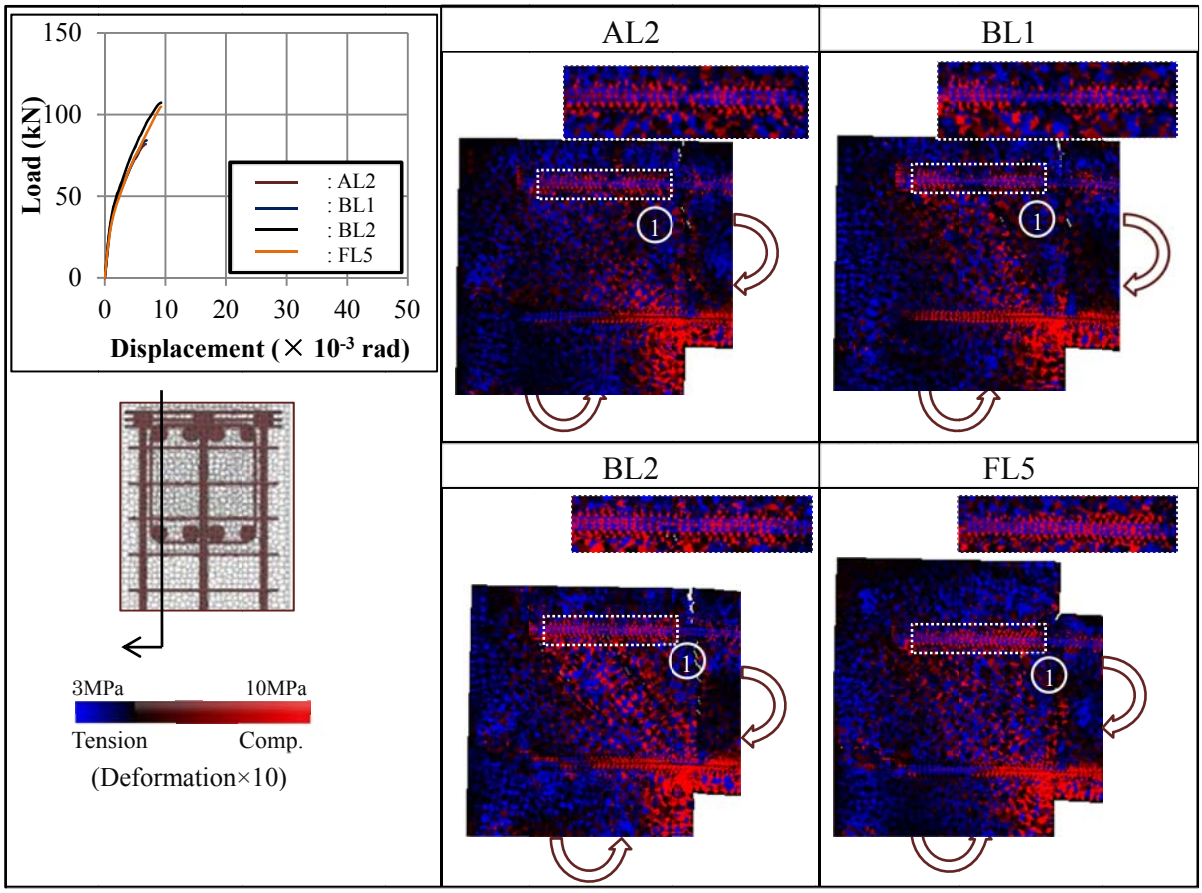

Fig. 8.13 Internal stress of AL2, BL1, BL2 and FL5 at the displacement of 6-10× 10^{-3} rad

length of anchorages which is caused by stirrups and addition concrete block at the top of beam column joint

Fig. 8.14 shows the internal stress distribution of numerical models at the displacement of 0.015 rad. It is confirmed based on the simulation results that diagonal cracks caused the slight drop of load. Since the width of diagonal cracks of BL2 is small, there is no slight drop of load. As the displacement increases, the load increases again after the maximum load. In addition, cracks were also predicted along the end of the anchorage plates, because the interface between anchorages plates and concrete is weak in tension. These cracks, i.e. diagonal cracks and cracks along the anchorages are connected together that cause the major cracks in beam column joint (②). As the results, when diagonal cracks open wider, cracks along the anchorage plates also open wider. In case of FL5, these cracks propagate to the additional concrete block (③).

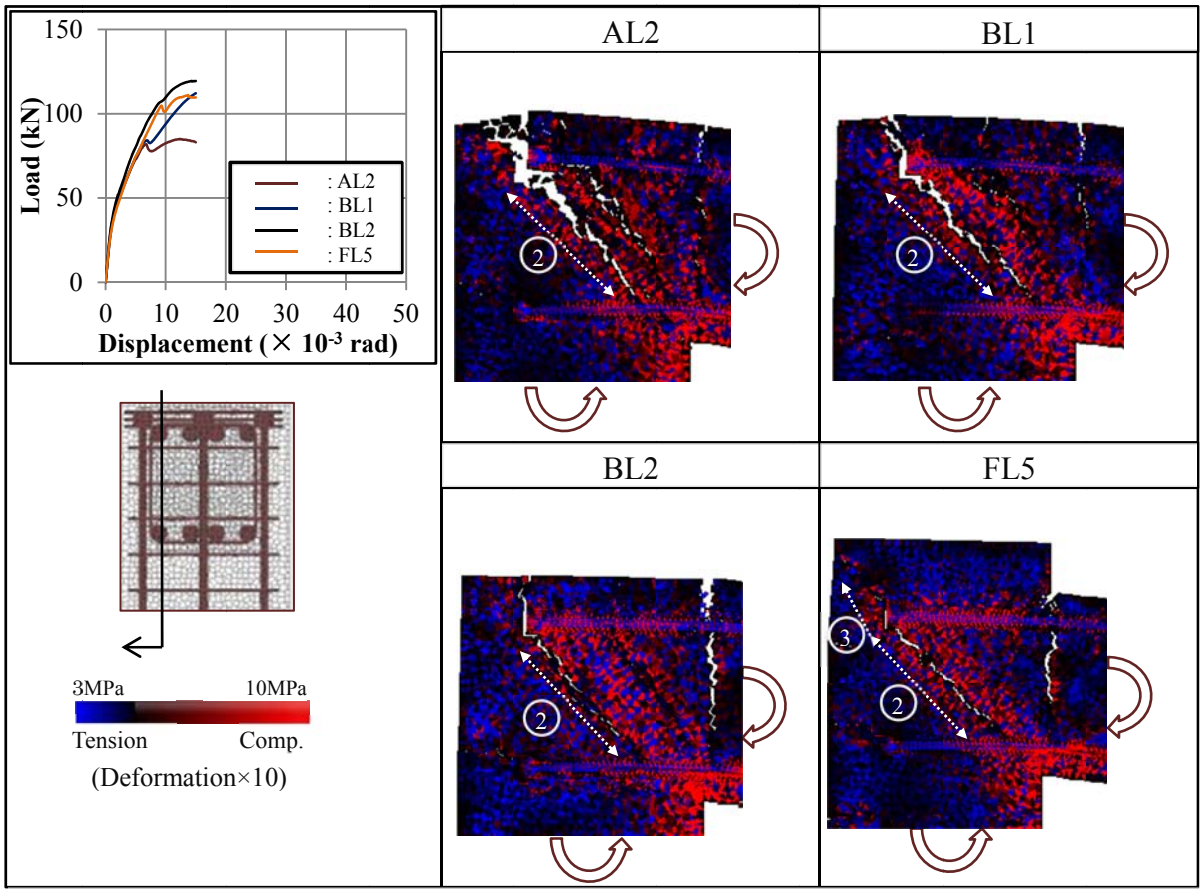

Fig. 8.14 Internal stress of AL2, BL1, BL2 and FL5 at the displacement of 15× 10^{-3} rad

Fig. 8.15 shows the internal stress distribution of numerical models at the displacement of 0.025 rad. Based in the stress distribution in the beam column joints, because of no restriction along the anchorages, diagonal cracks open easier in case of AL2 and BL1. As the results, diagonal compressive stresses are difficult to exist that causes the load decreases significantly after exceeding the maxim load. Meanwhile, because the restriction along the anchorages, diagonal compressive stresses still exist in the beam column joint that causes the load does not decreases significantly. The same behavior was predicted in case of FL5. The additional concrete block and reinforcement arrangement inside the concrete block at the top of the beam column joint prevent cracks to penetrate to the surface of the beam column joint. As the result, the diagonal cracks cannot open easier and diagonal compressive stresses still exist in the beam column joint.

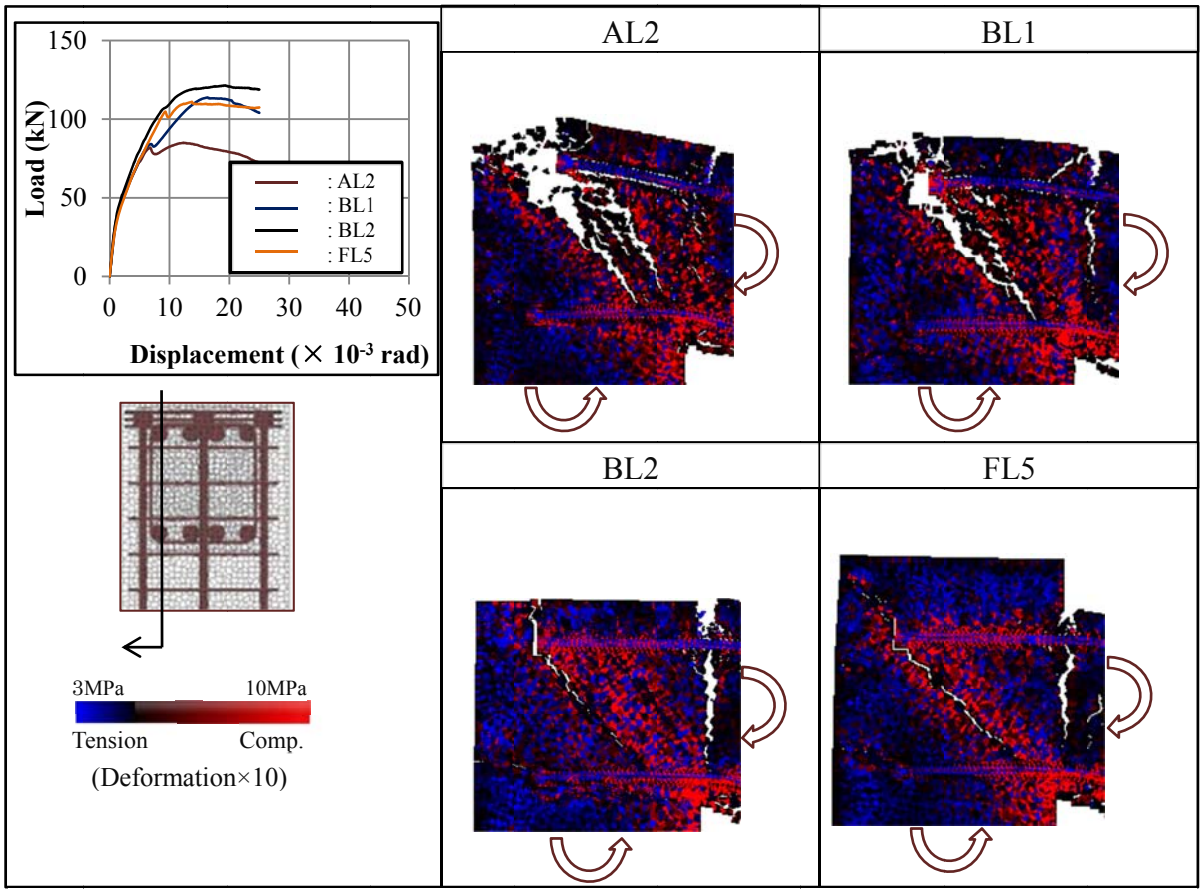

Fig. 8.15 Internal stress of AL2, BL1, BL2 and FL5 at the displacement of 25× 10^{-3} rad

8.4.4 Internal stress cracks

Fig. 8.16 shows the internal stress and internal cracks of numerical models at the displacement of 0.05 rad. As described before, diagonal cracks open easily in case of AL2 and BL1. As the diagonal cracks opened easily, cracks at the top surface of the beam column joint opened that caused damage. Furthermore, these cracks are connected each other. In case of BL2, the confinement provided by stirrups along the anchorages prevents diagonal cracks to open wider so that cracks at the top surface of beam column joint are difficult to open. In case of FL5, additional concrete block and reinforcement arrangement inside the concrete block at the top surface of beam column joint prevent cracks to penetrate to the top surface of beam column joint.

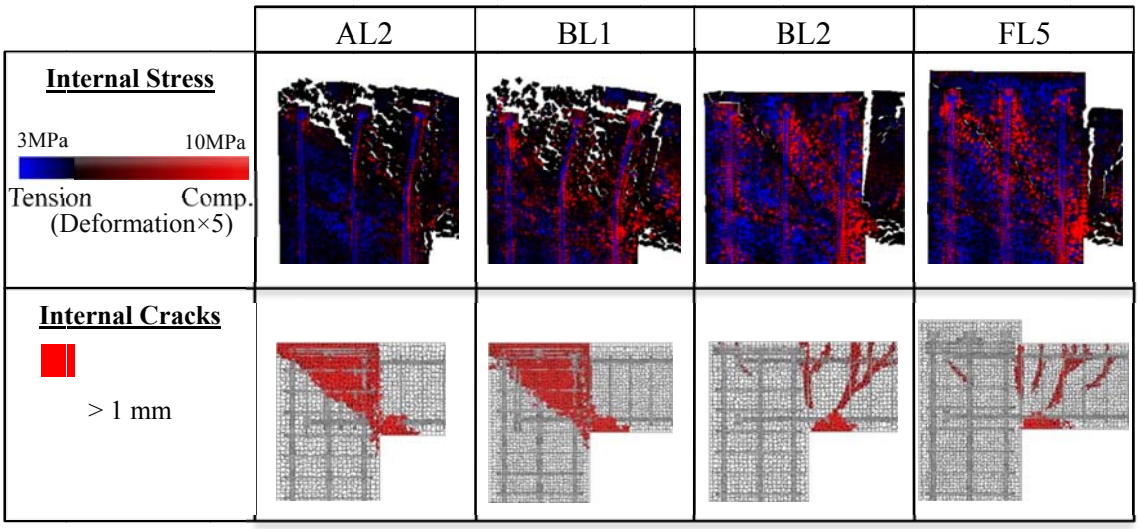

Fig. 8.16 Internal stress and internal cracks of numerical models at displacement of $50x10^{-3}$ rad

Fig. 8.17 shows the failure process of the beam column joint with mechanical anchorages. Based on the study of the internal study of the simulation results, the failure processes of beam column joint with mechanical anchorages can be revealed as below.

1. Bond works along the development length of the anchorages. Bond can be increased by the stirrups placed along the development length and concrete block at the top surface of beam column joints.
2. Diagonal cracks propagate
3. Cracks propagate to the surface of beam column joint. The cracks propagation can be restricted by the concrete block and reinforcement arrangement inside the concrete block.
4. Diagonal cracks open. It can be restricted by placing stirrup along the development length.

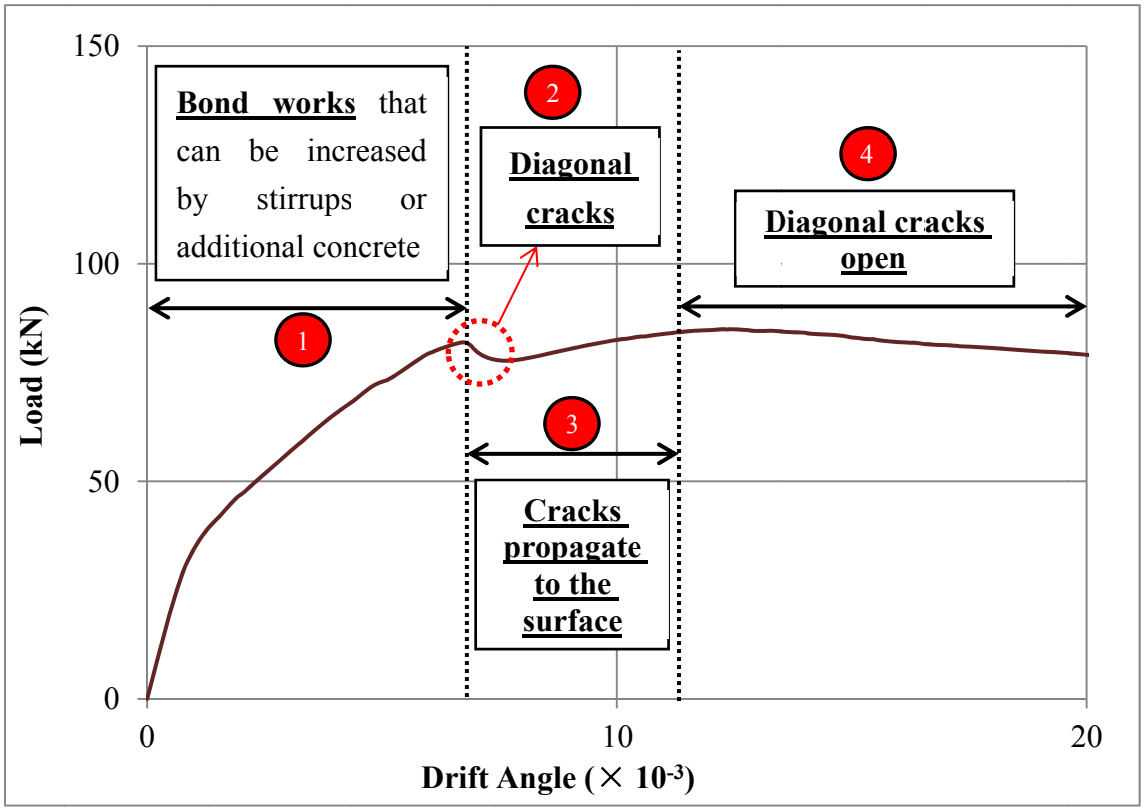

Fig. 8.17 Failure process of beam column joint with mechanical anchorages based on the simulation results.

8.4.5 Strain Profile

Fig. 8.19 shows the strain measurement of simulation results compared with the experimental results. **Fig. 8.18** shows the point measurement of the strain.

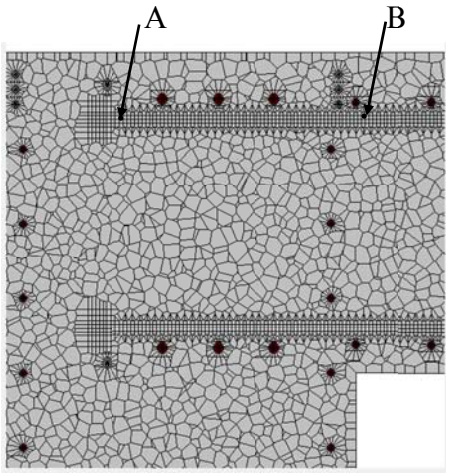

Fig. 8.18 Point measurement of strain

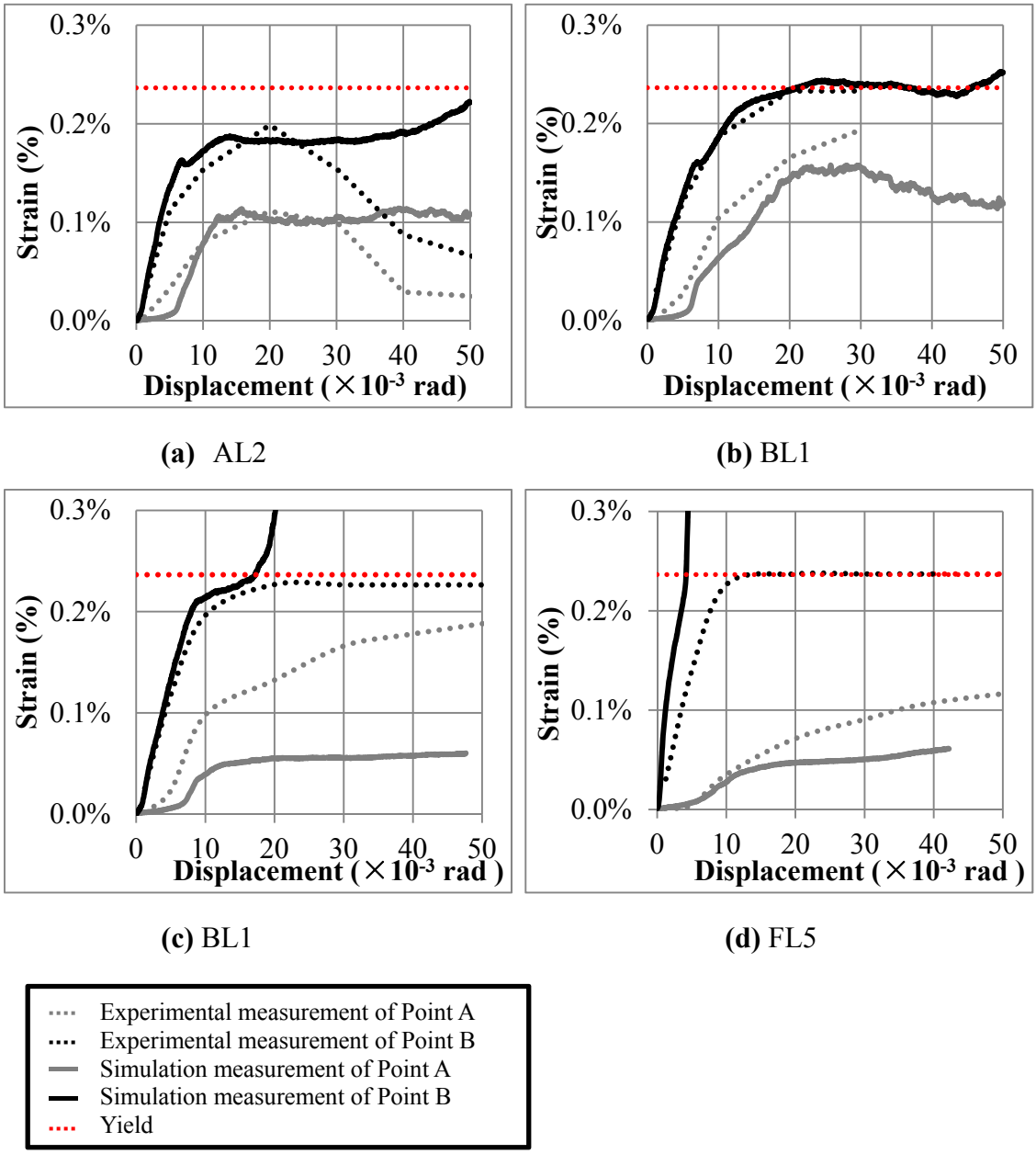

Fig. 8.19 Strain measurements of simulation results and experimental results

Simulation results show in a good agreement with the experimental results. Simulation results predict that the strain at point A is lower than that of point B, because of the bond along the development length. Simulation results and experimental results show that in case of AL2, the reinforcement bars do not yield either at the point A or point B. Meanwhile, other cases show that the reinforcement bars yield at the point A. Based on the simulation results, in case of BL1 and FL5 (flexural failure cases), after reinforcement bar yields, the strain jumps dramatically to the strain hardening region.

8.5 EFFECT OF MODELING RIB OF STIRRUPS IN THE BEAM COLUMN JOINT PORTION

As described before, the diagonal cracks affect significantly the behavior of beam column joint with mechanical anchorages. To confirm this behavior, parametric studies are conducted that stirrups in the beam column joint portion are modeled with plain reinforcement bars. It is well understood that in case of plain reinforcement bars, slip occur easily between concrete and a reinforcement bar because the bond is determined only by the friction between the concrete and reinforcement bar. If the slip occurs easily, diagonal cracks can open easier. The simulation was conducted for BL1 and BL2.

Fig. 8.20 shows load-displacement relationships of BL1 and BL2 with different types of stirrups. In case of BL1, the load-displacement relationships change significantly. Furthermore, the capacity of BL1 will be lower if stirrups inside the beam column joint were modeled as the plain bars. The load drops slightly at the same displacement. It indicates that the bonds between concrete and reinforcement bar are similar in both cases and diagonal cracks occur at the same displacement. As the displacement increases, the load increases in both cases. However, if stirrups inside the beam column joint are modeled as the deformed bars, the load increases more than plain bars case.

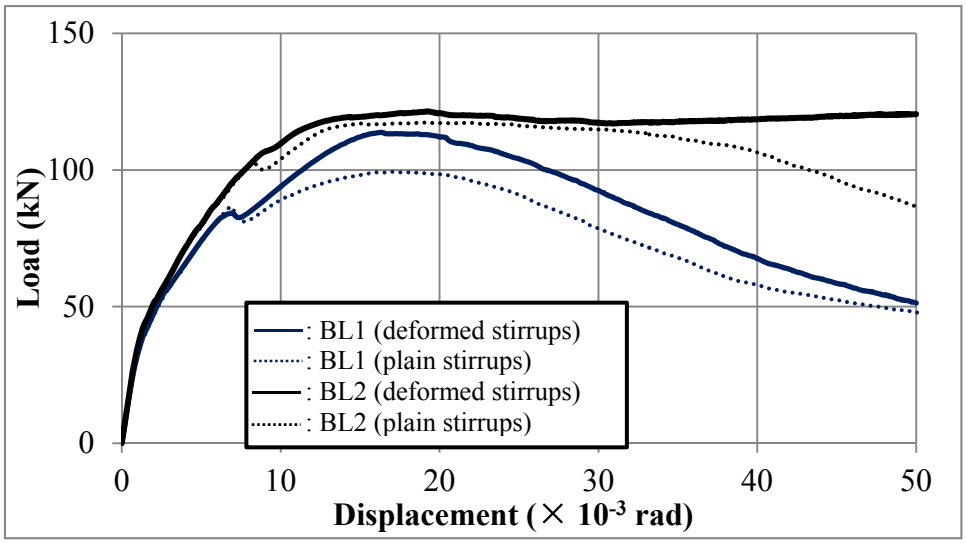

Fig. 8.20 Load-displacement relationships of BL1 and BL2 with different types of stirrups

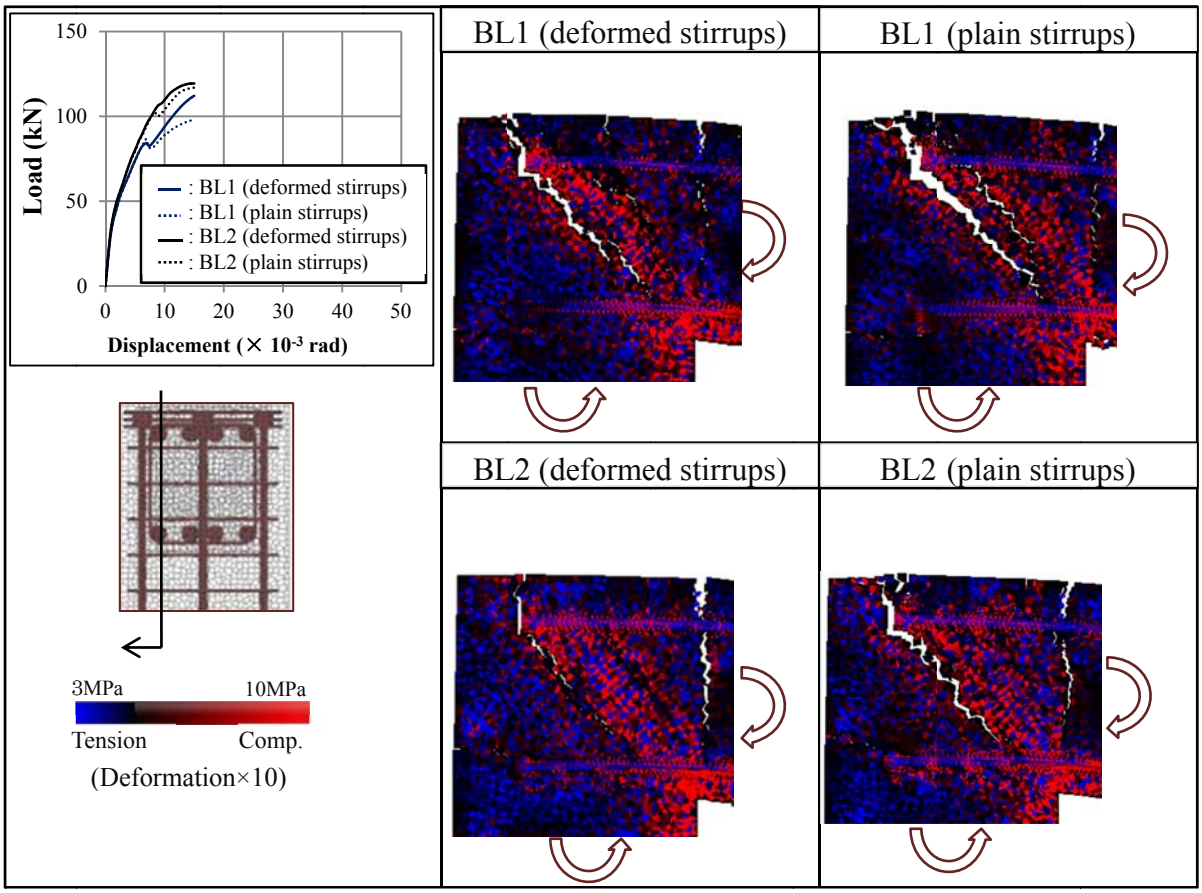

Fig. 8.21 Internal stresses of BL1 and BL2 with different types of stirrups at the displacement of 15× 10^{-3} rad

In case of BL2, the load drops slightly before the maximum load if stirrups inside the beam column joint are modeled as the plain bars. It indicates that the diagonal cracks open wider than the deformed bars case. As the displacement increases, the load increases at the same level. After exceeding the maximum load, the load drops at the displacement of 0.035 rad if plain bars were used as the stirrups inside the beam column joint. It indicates that the diagonal cracks open easier if stirrups were modeled as the plain bars. Furthermore, slip occurs easily if plain bars are used as the stirrups.

Fig.8.21 shows the internal stress distribution inside the beam column joints of BL1 and BL2 in case of plain bar stirrups and deformed bar stirrups. The width of diagonal cracks in case of plain bar stirrups is bigger than in case of deformed bar stirrups both BL1 and BL2. Thus, it can be concluded that if plain bars are used as the stirrups in the beam column joint, slip occur easily so that diagonal cracks can open easily. Furthermore, there are two functions of stirrups in the beam column joints, i.e. to give the confinement effect in the beam column joint and to restrict the opening of diagonal cracks.

8.6 EFFECT OF MODELING STRAIN HARDENING REGION OF STEEL ELEMENTS

In this chapter, the effect of modeling train hardening region of steel elements on the beam column joint behavior is investigated. As described in the previous section, if the strain hardening region is not modeled, the strain will jump dramatically after yield has occurred and it may affect the behavior inside the beam column joint. The simulation was conducted for BL1.

Fig. 8.22 shows the load displacement relationships of the numerical models. There is no significance different of load-displacement relationships in case of BL1 with and without modeling the strain hardening region.

Fig. 8.23 shows the strain measurement along the anchorage of BL1 with and without modeling the strain hardening region. Before the reinforcement bars yield, strain profile of BL1 without strain hardening region is same as that of BL1 with strain hardening region. After the reinforcement bars yield, there is no significant different of strain profile along the anchorages inside the beam column joint. Furthermore, at the location where the reinforcement bars yield, the strain jumps dramatically in case of BL1 without modeling strain hardening region. As the load increases more, the strain localization occurs at the location where the yield occurs and there is still no difference of strain profile along the anchorages inside the beam column joint.

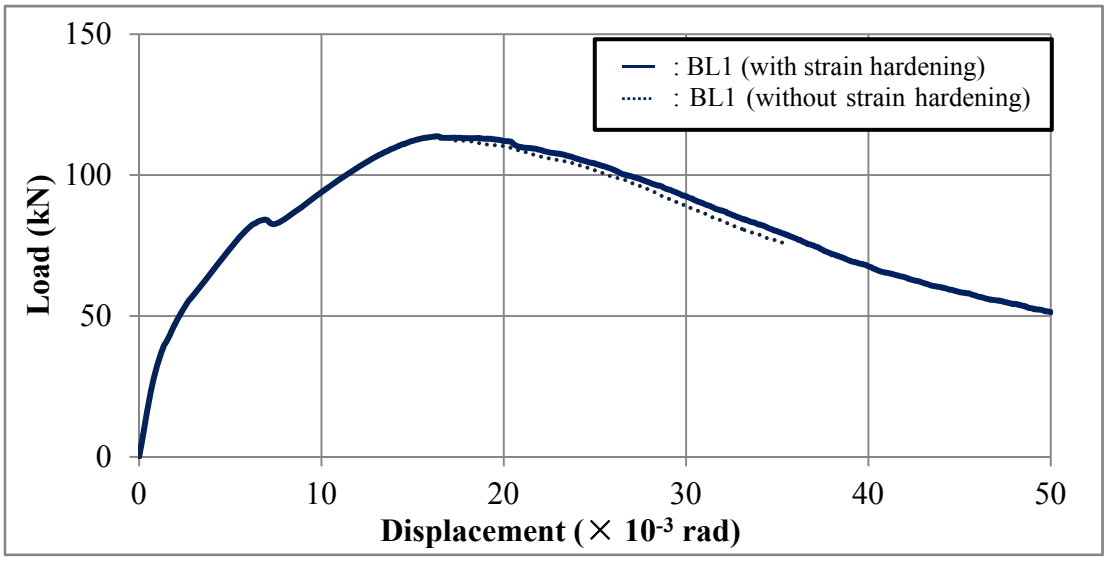

Fig. 8.22 Load-displacement relationships of numerical models with and without strain hardening region

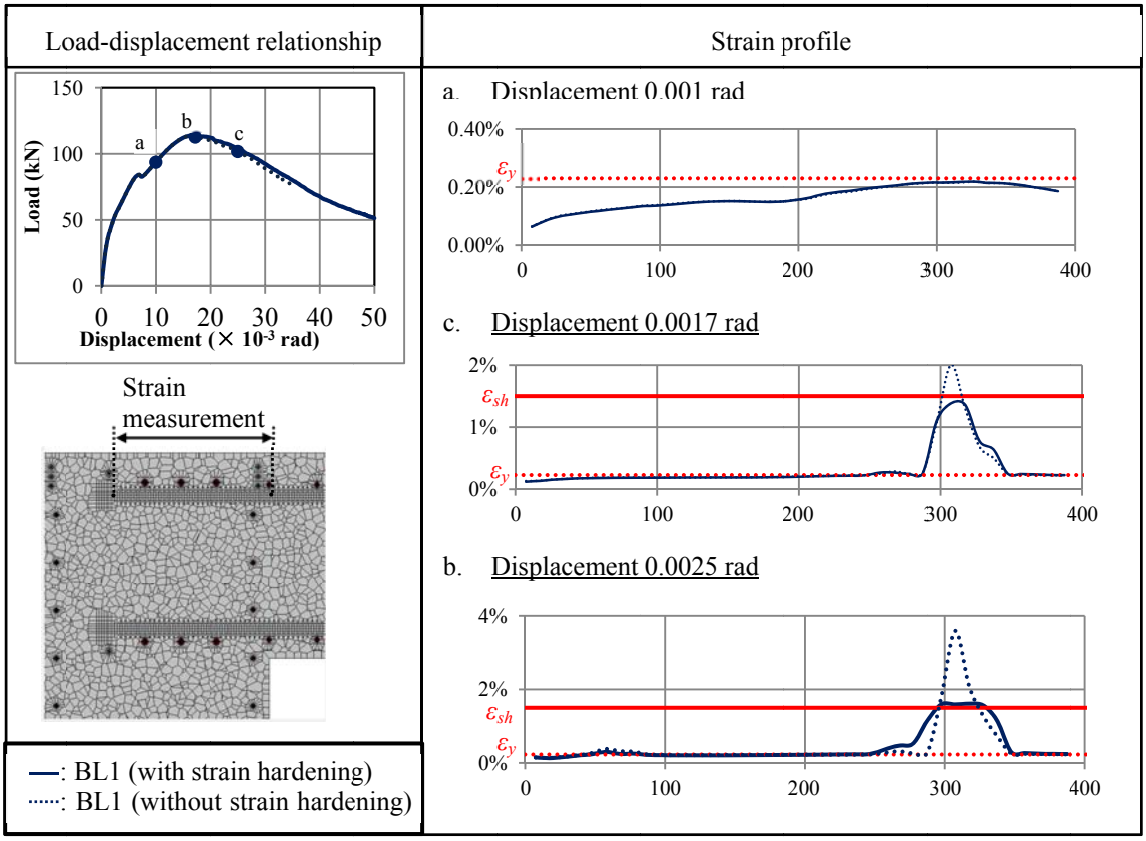

Fig. 8.23 Strain measurement along the anchorage with and without strain hardening region

8.7 CONCLUSIONS

Through the 3D RBSM meso-scale simulations on beam column joint with mechanical anchorages in this study, the following conclusions are made.

1. RBSM can simulate the different failure pattern due to different local stirrups arrangement. Based on the simulation results, the increase of the capacity of BL2 is due to the increase if bond performance along the development length of anchorages and confining diagonal stresses caused by stirrups.
2. It is confirmed based on the simulation results that when stirrups are provided along the anchorage stirrups can restrict the opening of diagonal cracks. Therefore diagonal compressive stresses still remain and avoid the cracking near the anchorages. As the result, flexural failure occurs.
3. The failure process of beam column joints with mechanical anchorages has been revealed through the study of internal stress and crack pattern of RBSM, i.e. bond works along the development length, diagonal cracks occur, cracks propagate to the surface of beam column joint, and diagonal cracks open.

4. Based on simulation results, it is proposed that there are 2 scenarios to strengthen the beam column joint with mechanical anchorages. First is to restrict the opening of diagonal cracks in beam column joints. Second scenario is to restrict the crack penetration to the surface of the beam column joint so that diagonal cracks are difficult to open.
5. Based on the parametric study of the types of stirrups inside the beam column joint, there are two functions of stirrups inside the beam column joint. First function is to provide the confinement effect and another function is to restrict the diagonal cracks in the beam column joints.

REFERENCES

Japan Society of Civil Engineers., "Recommendations for Design, Fabrication and Evaluation of Anchorages and Joints in Reinforcement Bars," *Concrete Library 128*, 2007. (in Japanese)

Kato, F., Kiyohara, T., Tasai, A., and Kusunoki, K., "Experimental Study of Knee Joints with Mechanical Anchorage," *Proceedings of Japan Concrete Institute*, 33(2), 2011. (in Japanese)

Kawai, T., "*New Discrete Models and Their Application to Seismic Response Analysis of Structure*," Nuclear Engineering and Design, 48, 207-229. 1978.

Nagai, K.; Sato, Y.; Ueda, T., "Mesoscopic Simulation of Failure of Mortar and Concrete by 3D RBSM," *J. Adv. Conc. Technol.*, 3(3), 385-402. 2005.

Nagai, K., Hayashi, D., and Eddy, L., "Numerical Simulation of Failure of Anchorage with Shifted Mechanical Anchorage Bars by 3D Discrete Model," *J. Adv. in Structural Engineering* 117:861-870. 2014.

Wang, T., Eddy,L., and Nagai, K., "Numerical Simulation of Failure of Beam Column Joints with Mechanical Anchorage by 3D Discrete Analysis," *6th Asia-Pacific Young Researchers and Graduates Symposium*.2014.

Yoshimura, M., Kiyohara, T., Tasai, A., and Kusunoki, K., "Experimental Study of Performance Improvement of Knee Joints with Mechanical Anchorage," *Proceedings of Japan Concrete Institute*, Vol.34, No.2, 2012. (in Japanese)

Chapter NINE

SUMMARY AND CONCLUSION

In this study, numerical simulations of failures of beam column joints by 3D RBSM are conducted. In this chapter, contents of the study, achievements and tasks for the future are summarized with respect of each chapter.

In Chapter 1, background, literature review, purpose, research significance and strategies are described.
Because of the demanding in the specification, reinforcement congestion occurs in beam column joint that can increase construction time and cause difficulties during compaction. As the result, a poor quality of concrete is obtained. Meanwhile, the anchorage specification was developed based on the simple arrangement of reinforcement bars and has not been changed for many years. The reduction of reinforcement congestion is possible based on the mechanism in the congested joint. Based on the experimental works, it is not easy to understand the behavior because complex cracks occur in the beam column joint due to the complex arrangement of reinforcement and loading history.

Mechanical anchorage can be the way to reduce the reinforcement congestion in the beam column joint. However, if it is placed near the surface of the beam column joint, local cracks will occur because of the local stress from the mechanical anchorages. To avoid this failure, additional reinforcement bars should be placed along the anchorages. Furthermore, many experiments are necessary to find the best or rational way to strengthen this system. It takes time and inefficient.

Numerical simulation can be a beneficial way to understand the behavior through the study of the internal stress and internal cracks. Meso scale analysis is proposed in this study because cracks propagate in 3D domain, the 3D shape of a reinforcement bar is modeled directly, including the rib of the reinforcement bar, cracks occur because of the discontinuous of concrete and interaction between concrete and reinforcement bar at meso scale level, and cracks can be simulated directly.

In chapter 2, the method of analysis is explained. In RBSM, a reinforced concrete

member is meshed into rigid bodies. Each rigid body consists of 6 degrees of freedom and connects to another rigid body by 3 springs. In order to prevent cracks propagate in non-arbitrary direction, random mesh is used for the concrete elements. In this chapter, the decision to choose 10x10x10 – 20x20x20 mm^3 of mesh size is described because the limitation of this study is only for normal concrete. Furthermore, in the normal concrete, cracks propagate between aggregates and don't penetrate into the aggregate. In order to represent the real cracking pattern in the normal concrete that is determined based on the aggregate size and location, 10x10x10 – 20x20x20 mm^3 of mesh size is decided. Based on this mesh size, the constitutive models are decided. For different types of concrete, for example high strength concrete and fiber reinforced mortar, different mesh size and constitutive models should be applied and these types of concrete are not applicable in this study.

In this chapter, various shapes of reinforcement bars are introduced in order to simulate the same model and reinforcement arrangement of the beam column joint with complex arrangement of reinforcement bars as the real condition

In chapter 3, a unified constitutive model for spring at the selected mesh size is proposed because in the past studies, the simulations were conducted for simple pull out tests of reinforced concrete members. The constitutive models were determined in such a way to represent the material behavior in macro-scale. The bi-linear model for tension softening of concrete elements, new failure criterion of concrete elements, and strain hardening region for steel elements are proposed in this study.

For the normal spring of concrete, in compression zone it behaves elastically. After the tensile stress exceeds the tensile strength of concrete, it has the softening part. An elasto plastic model is assumed for the shear spring of concrete, where the tau max is calculated based on the relationship of shear stress and normal stress. For normal spring of steel elements, its behavior is the same as the real stress-strain relationship of steel. In order to consider the interface between concrete and reinforcement bar as a weak region, the tensile strength of interface elements is reduced by half of that of concrete elements.

To develop the constitutive models for the simulation, simulations of concrete at material scale were conducted, which are described in Chapter 4. Uniaxial compressive and tensile loading and biaxial compressive loading were applied to the concrete models. By setting different tensile strength of normal springs, different uniaxial compressive

and tensile strength are obtained at macro scale. Based on the new failure criterion of concrete, the simulation results show that the relationship of uniaxial compressive and tensile strength is in a good agreement with JSCE equation. In the biaxial compression test, the simulation is little overestimate but still with the same tendency as the experimental results that the compressive strength under biaxial compressive loading is higher than that of uniaxial compressive loading.

In this chapter, parametric studies are also conducted. By varying the failure criterion of concrete, the failure criterion of concrete affects significantly the behavior of concrete under both uniaxial and biaxial compressive loading. However, it doesn't affect the behavior of concrete under uniaxial tensile loading. Meanwhile, the tension softening of concrete affects the softening of concrete both under uniaxial compression and tensile loading.

In order to check the applicability of simulation system to simulate the bond between concrete and a reinforcement bar, tension stiffening simulations were conducted with different yield strength of a reinforcement bar in Chapter 5. Simulation results are presented by load-displacement relationship, average stress-strain of the reinforcement bar, and average stress-strain of concrete. Based on the simulation results, as the load increases, cracks can propagate gradually because bond between concrete and reinforcement bar is simulated well. Furthermore, simulation results show that the yielding point of average stress-train of reinforcement bar is lower than that of bare bar which is a good agreement with the experimental results. In addition, the simulation results also predict that the average stress-train of reinforcement bar in case of low yield strength is lower than that of in case of high yield strength. In this chapter also, parametric studies of the tensile strength of the interface elements were conducted. The simulation results show that the tensile strength of the interface elements affects slightly the stiffness of the reinforced concrete member and increase the concrete strength in the average stress-strain relationship of concrete. The effect of modeling strain hardening region is explained in this chapter that the strain localization after the reinforcement bar yields will not occur.

By this well-developed simulation system, some achievements have been obtained. In chapter 6, by this simulation system, how the local cracking occurred in the corbel that has wrong detailing of loading position has been understood because the local shape of the reinforcement bar is modeled directly. Simulation results show different capacity

between wrong detailing and correct detailing because of this local failure. Furthermore, by this simulation, how to repair the damage corbel by simulating directly the damage corbel has been proposed. After the failure occurs in the corbel, the loading position is moved into the middle and applied it. The simulation results show that the capacity can be recovered. This kind of residual performance can be simulated.

In chapter 7, by this well-developed simulation system, how each rebar contributes to the complex cracks in the beam column joint with complex arrangement of reinforcement bars can be understood because the local shape of the reinforcement bars is modeled directly.

In chapter 8, as described before, mechanical anchorage can be the way to reduce the reinforcement congestion in the beam column joint. To strengthen this system, additional reinforcement bars should be placed along the anchorage and the best or rational way has not been proposed yet. Based on the experimental works, by placing the stirrups along the development length and additional concrete block at the top surface of beam column joints are the example ways to achieve the flexural failures. By the simulation, the mechanism to strengthen this system has been understood through the study of internal stress and internal crack pattern. Simulation results show the same tendency as the experimental results in term of load-displacement relationships. The failure behavior of simulation results is also the same as that of experimental results. Based on the study of the internal stress of beam column joint with mechanical anchorages by simulation, the failure processes have been understood. First, bond works along the development length of the anchorages. Second, diagonal cracks occur in the beam column joint. Third, cracks propagate to the surface of the beam column joint. Finally, the diagonal cracks open. Furthermore, based on the simulation results, it has been understood, the mechanism of stirrups along the development length is by restricting directly the opening of diagonal cracks. Meanwhile, additional concrete block and reinforcement arrangement on the top surface of beam column joint restrict the cracks propagation to the surface of the beam column joints.

Appendix A

FINITE ELEMENT ANALYSIS OF BEAM COLUMN JOINT WITH COMPLEX ARRANGEMENT OF REINFORCEMENT BARS

A.1 INTRODUCTION

By finite element analysis, Salem *et al.* (2004) simulated well the bond behavior of ribbed reinforcement bars. However, the three dimensional arrangement of reinforcement bars was not modeled and the applicability of the finite element analysis in predicting the failure behavior of a beam column joint with complex arrangement of reinforcement bars has not been investigated. In this chapter, by modeling directly a complex arrangement of reinforcement bars, the applicability of the finite element analysis in predicting the beam column joint failure will be studied. The simulation was carried out by 3D finite element analysis, COM3, developed by The University of Tokyo. In COM3, a three dimensional reinforced concrete member is meshed into solid elements. Furthermore, in this study, a beam column joint was meshed into plain concrete elements and steel elements. Details of the material models are discussed in the references (Maekawa *et.al.* (2003)).

A.2 DETAIL OF NUMERICAL SIMULATION

A.3.1 Numerical model

In order to study the behavior of a beam column joint with complex arrangement of reinforcement bars, the finite element analysis was conducted for an experiment of a beam column joint, done by Japan Railway. Since the purpose of this research is to study the behavior of a beam column joint with complex arrangement of reinforcement bars, the dimensions, the reinforcement bars, including bending portion of the reinforcement bars, and the boundary condition were modeled in an accurate manner. Three dimensional shape of a reinforcement bar was modeled. However, for the simplification of the analysis model, the shape of a reinforcement bar is rectangular, with the same area as the circular shape of the actual reinforcement bar. Furthermore, the dimensions, the reinforcement bars of the beam column joint, and the boundary conditions of the analysis model, will be described below.

A.3.2 Geometry of numerical model

The dimensions of the analysis model are shown in **Fig. A.1**. Further, the material properties of the concrete and reinforcement bars are shown in **Table A.1**. 67314 elements are used to model the beam column joint. The size of elements in the beam column joint portion is approximately 1 cm^3.

Table A.1 Material properties

Material	Modulus of Elasticity (MPa)	Compressive Strength (MPa)	Tensile Strength (MPa)	Modulus of Elasticity (MPa)	Yield Strength (MPa)
Concrete	22000	21.1	1.75		
D25 (Beam Longitudinal Bar)				190000	383
D13 (Beam Longitudinal Bar)				190000	362
D16 (Beam Transversal Bar)				190000	368
D16 (Column Longitudinal Bar)				190000	365
D13(Column Transversal Bar)				190000	362

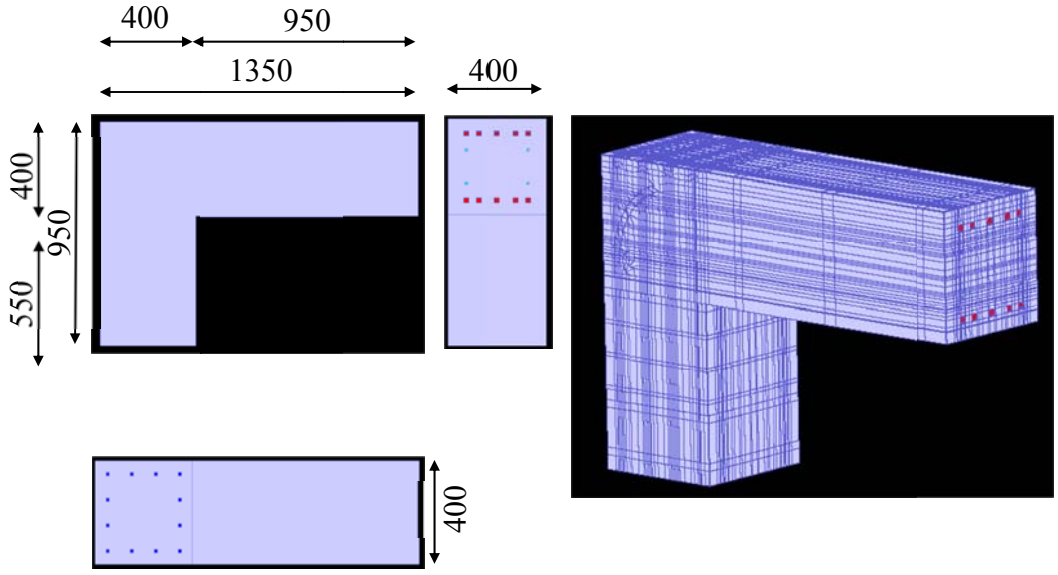

Fig. A.1 Analysis model (Units: mm)

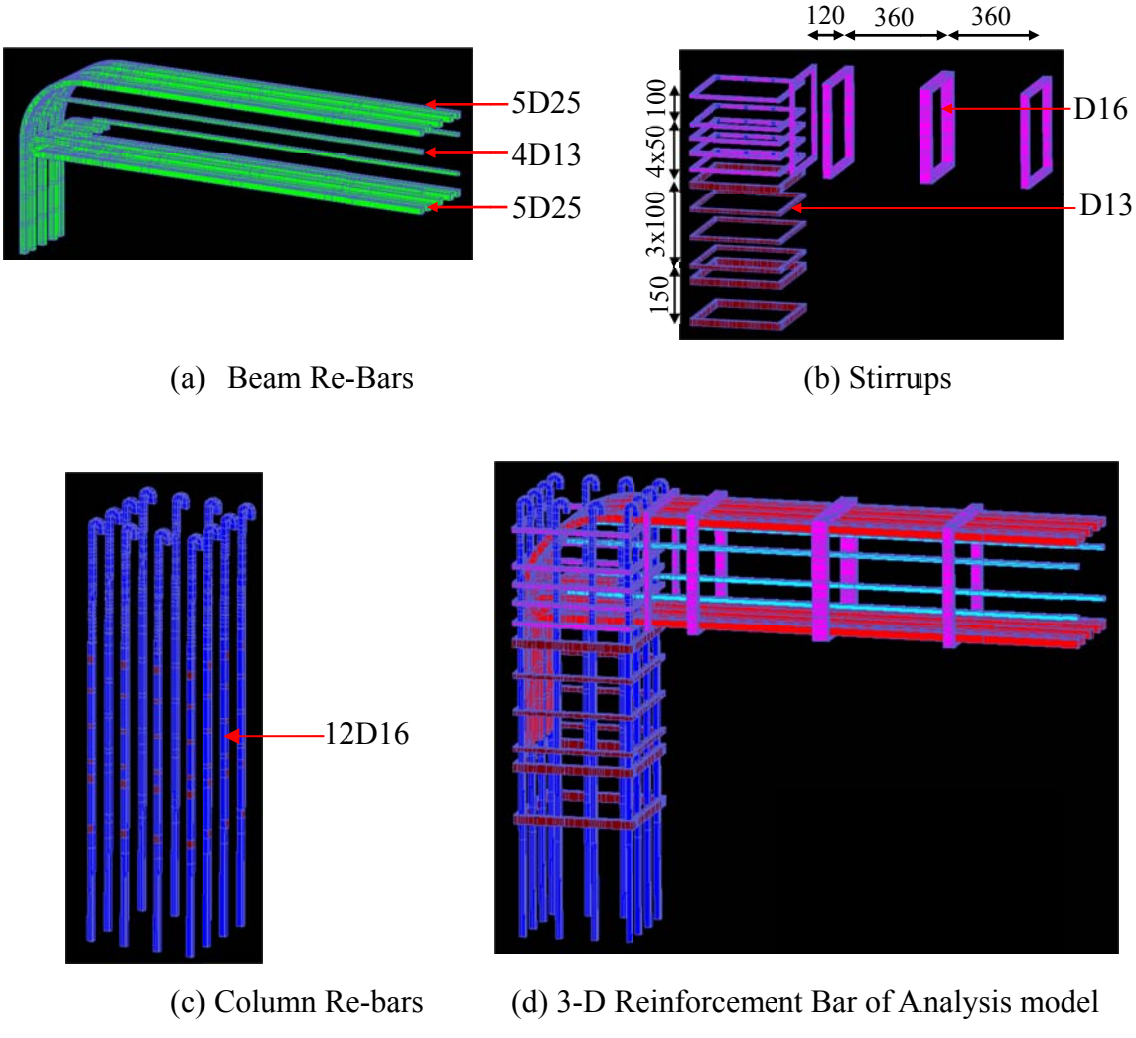

(a) Beam Re-Bars (b) Stirrups

(c) Column Re-bars (d) 3-D Reinforcement Bar of Analysis model

Fig. A.2 Reinforcement bars of the analysis model

For the meshing simplification purpose in the numerical simulation, the shape of a reinforcement bar is a rectangular where its area is the same as the actual reinforcement bar. On the other hand, spiral stirrups of the column were simplified by increasing the yield strength of the tied stirrups of the column, and tied stirrups of the beam were simplified by enlarging the area of the tied stirrups of the beam. The bending portion of hooked bar anchorages, located in the beam column joint was modeled in an accurate manner. **Fig. A.2** shows the reinforcement bars of the analysis model.

A.3.3 Boundary condition

Fig. A.3 shows the detail of the frame loading of the analysis model, which represents the frame loading in the experimental set-up (**Fig. A.4**). Fix condition in all direction is assumed as the boundary condition at the bottom of the steel frames. There are 3 hinges

that are modeled as the boundary condition. To allow the rotation, a pin, located in the middle of steel plates, is introduced as the connection between steel plates (**Fig. A.5**). Furthermore, an interface element is introduced between the pin and the steel plates, with a small value of shear stiffness, so that no shear force is transferred between the steel plates and the pin.

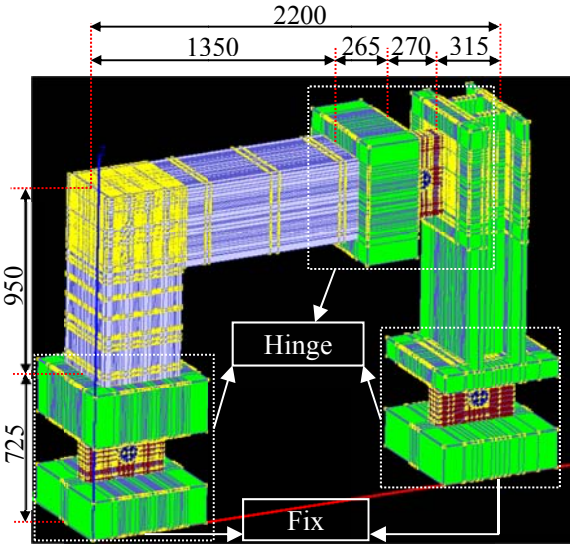

Fig. A.3 Boundary condition of numerical model

Fig. A.4 Experimental setup

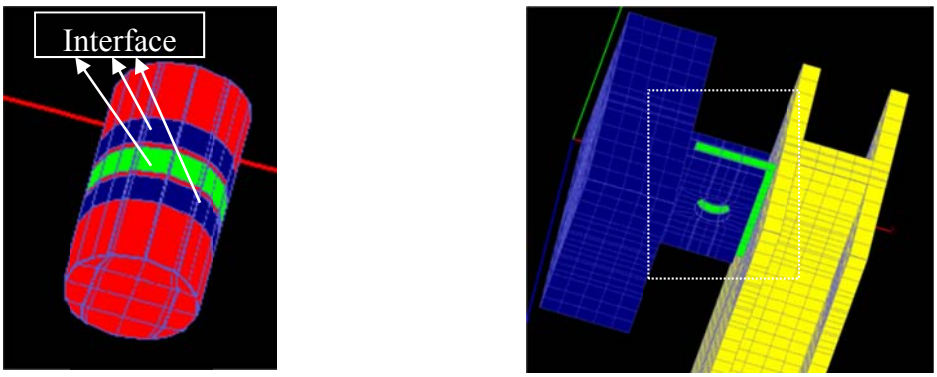

(a) Pin

(b) Hinge

Fig. A.5 Detail of hinge

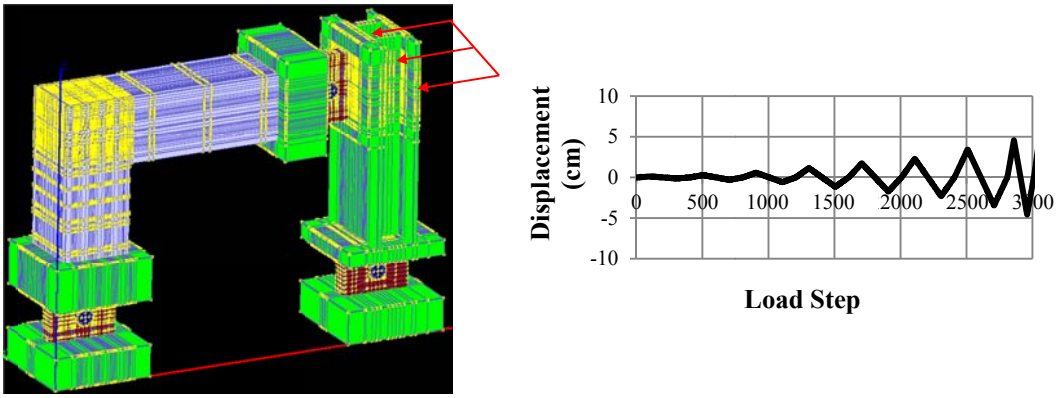

Fig. A.6 Load pattern of cyclic load

Cyclic load of displacement control, pull load and push load alternately, is applied to the steel frame, located at the end of the beam. In addition, the applied load, pull load and push load, is intended to examine the behavior of the beam column joint for a moment that tends to open and close the right angle, respectively. The same load pattern as the experiment is used in the simulation. **Fig. A.6** shows the load pattern of the cyclic load.

A.3 SIMULATION RESULTS

A.3.1 Load-displacement relationships

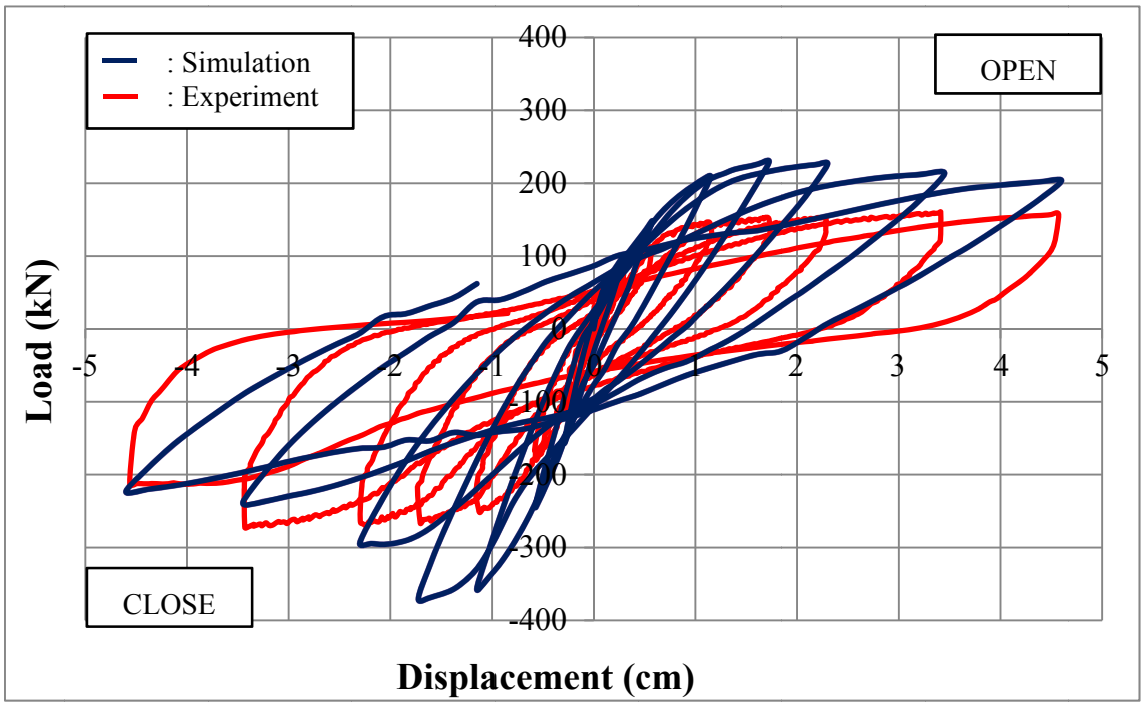

Fig. A.7 Load-displacement relationship

Table A.1 Maximum load of the experimental specimen and numerical model

Case	Experiment(P_{exp})	Simulation(P_{ana})	P_{ana}/P_{exp}
Open	160.3 kN	229 kN	70%
Close	272.3 kN	370 kN	73%

Fig. A.7 shows the load-displacement relationship of simulation result, compared with that of experimental result. **Table A.1** shows the maximum load of the experimental specimen and numerical model. The load and the displacement of the load-displacement relationship of numerical model were determined based on the load and the displacement applied to the steel frame located at the end of the beam. The maximum loads of numerical model are roughly the same as those of experimental specimen, i.e. approximately 27-30% difference.

Both experimental and simulation results show that the maximum load of open case is lower than that of close case. In open case, the simulation predicts that the maximum load of the beam column joint is 229 kN at the displacement of 1.725 cm. Meanwhile, in close case, the simulation predicts that the maximum load of the beam column joint is 370 kN at the displacement of 1.725 cm. Simulation results predict that the maximum loads of both cases occur earlier compared with the experimental results. After exceeding the maximum load, simulation results show that the load decreases significantly in close case and the load does decrease significantly in open case. The same tendency as the experimental results was predicted. Anchorage failure causes the drop of capacity after exceeding the maximum load in close case. Furthermore, to observe the failure behaviour of the beam column joint by numerical simulation, the crack patterns of the beam column joint are described below.

A.3.2 Crack patterns

In this study, the crack pattern obtained by the simulation is described below. The cracks are not associated with the discrete cracks, but represent the smeared cracks. Furthermore, the cracks depend on the magnitudes of strains and element sizes.

A.3.2.1 Crack pattern in close case

Fig. A.8 shows the crack patterns of the numerical model at the displacement of 0.288 cm, 1.15 cm, and 1.75 cm in close case.

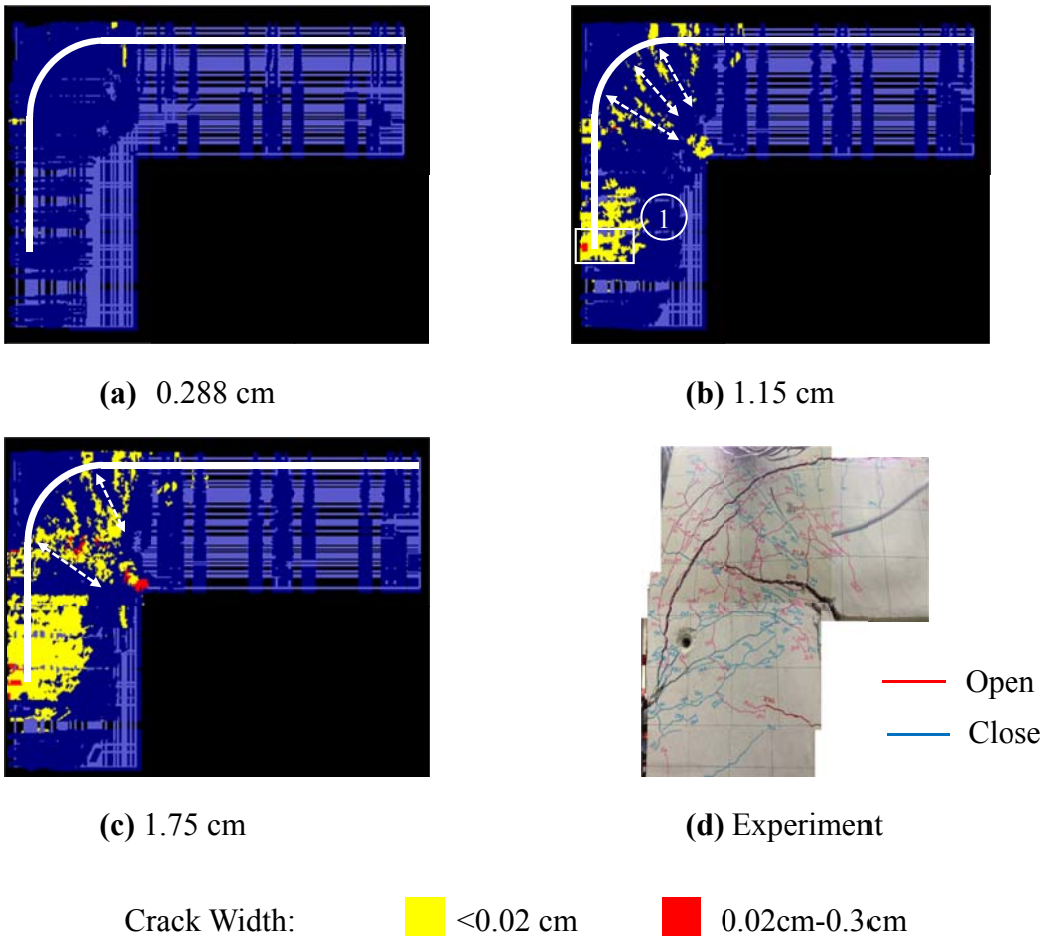

(a) 0.288 cm **(b)** 1.15 cm

(c) 1.75 cm **(d)** Experiment

Fig. A.8 Crack patterns of the numerical model compared with experimental specimen in close case

When the applied load is relatively small, at the displacement of 0.288 cm, flexural cracks occur outside the bending portion of the anchorages, inside the beam column joint portion. As the load increases, i.e. at the displacement of 1.15 cm, cracks occur inside the bending portion of the anchorages. Furthermore, diagonal cracks, which are roughly perpendicular to the bending portion of the anchorages, occur. Before the load reaches the maximum load, large width of cracks occur at the end of the anchorages (1), and may indicate the beginning of the anchorage failure. At the displacement of the maximum load, i.e. 1.75 cm, more cracks occur inside the bending portion of the anchorages. The same tendency of crack patterns was observed between the finite element analysis and the experimental work. Diagonal cracks which are roughly perpendicular to the bending portion of anchorages also occurred inside the bending portion of anchorages in the experimental specimens.

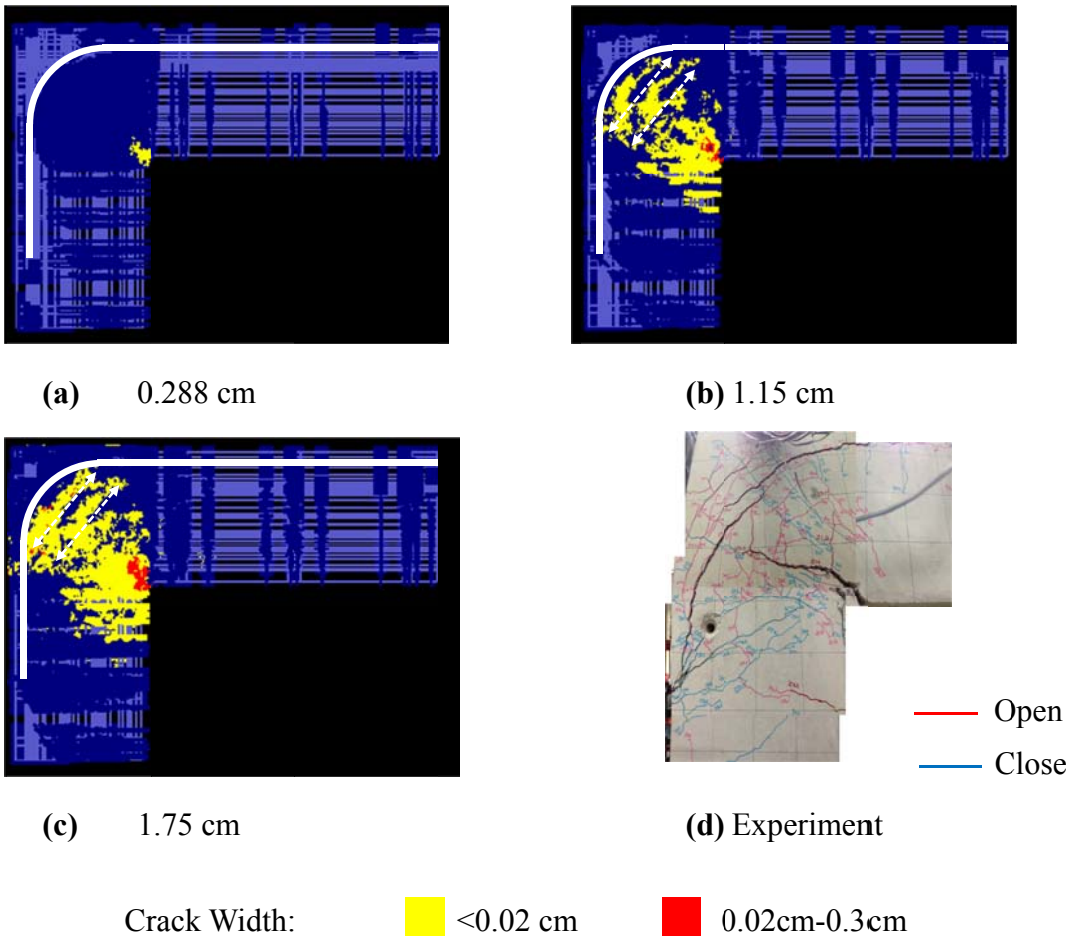

Fig. A.9 Crack patterns of the numerical model compared with experimental specimen in open case

A.3.2.2 Crack pattern in open case

Fig. A.9 shows the crack pattern of the analysis model at the displacement of 0.288 cm, 1.15 cm, and 1.75 cm, under the opening load. When the applied load is relatively small, at the displacement of 0.288 cm, flexural cracks occur on the re-entrant corner of the beam column joint. As the load increases, i.e. at the displacement of 1.15 cm, cracks occur inside the bending portion of the anchorages. Furthermore, diagonal cracks, which are roughly perpendicular to the cracks formed in close case, occur. At the displacement of the maximum load, i.e. 1.75 cm, more cracks occur inside the bending portion of the anchorages. Based on the experimental result, typical diagonal cracks, which are roughly perpendicular to the cracks formed in close case, also occurred inside the bending portion of the anchorages of beam column joints.

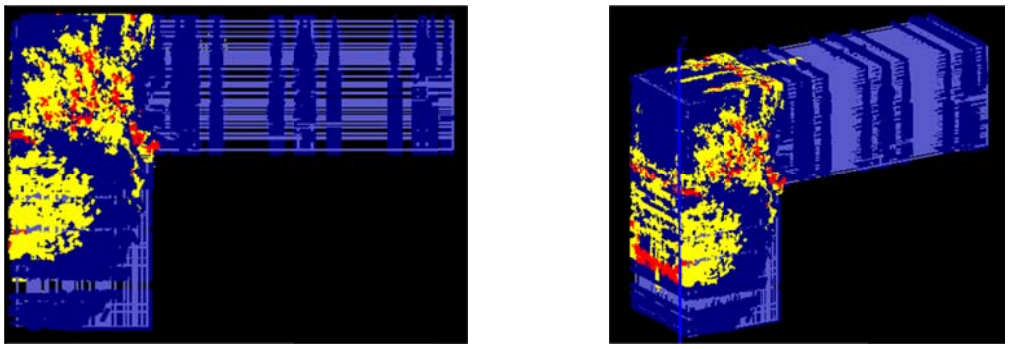

(a) Cracks of Front's Surface **(b)** Cracks of 3-D Model

Crack Width: <0.02 cm 0.02cm-0.3cm

Fig. A.10 Crack patterns of the numerical model at final step of load

A.3.2.3 Crack pattern at displacement of 2.3 cm in close case

Fig. A.10 shows crack patterns at the displacement of 2.3 cm in close case. Complicated cracks occur inside the beam column joint portion of the numerical model, after loaded by several loads of the open load and the closing load. However, the behavior of the beam column joint is difficult to be observed by finite element analysis, when the complicated cracks occur inside the beam column joint portion.

A.4 CONCLUSIONS

Based on the results of the numerical study of the behavior of a beam column joint with complex arrangement of reinforcement bars by finite element analysis, the following conclusions are made.

1. Finite element analysis could simulate the global behavior of a beam column joint with complex arrangement of reinforcement bars.
2. When the push load was applied (close-mode), after the load exceeds the maximum load, the load decreases significantly because of the failure of the anchorages. Diagonal cracks, which are roughly perpendicular to the bending portion of anchorages, occur. These typical diagonal cracks were also observed in the experimental specimens.
3. When the pull load was applied (open-mode), after the load exceeds the maximum load, the load does not decrease significantly as cracks propagated inside the beam column-joint portion. Diagonal cracks, which are roughly

perpendicular to the cracks formed under the close load, occur. These typical diagonal cracks were also observed in the experimental specimens.

4. The behavior of the beam column joint is difficult to be observed by finite element analysis, after complicated cracks occur inside the beam column joint portion.

REFERENCES

Salem, H., and Maekawa, K., "Pre- and Postyield Finite Element Method Simulation of Bond of Ribbed Reinforcement Bars," *Journal of Structural Engineering* 130:671-680. 2004.

Maekawa, K., Pimanmas, A., and Okamura, H., "Nonlinear Mechanics of Reinforced Concrete," *Spon Press Taylor & Francis Group*, London and New York, 2003.